Driving Techniques for High Power PZT Transducer Arrays

by

Tarren M J Smith

Thesis Presented for the Degree of

Magister Technologiae

in the Department of Electrical Engineering

Cape Peninsula University of Technology

November 2006

Declaration

This thesis is being submitted for the degree of Magister Technologiae in the Department of Electrical Engineering at the Cape Peninsula University of Technology.

I, Tarren Smith, declare that the work contained within this thesis is my own and has not been previously submitted for academic examination toward any qualification. The opinions expressed in this thesis are not necessarily those of the Cape Peninsula University of Technology.

.....

T M J Smith

November 2006

Acknowledgments

Firstly and foremost I would like to thank my supervisor Associate Professor Jevon Davies for all the time spent and effort exerted in his assistance with this study. He answered many questions and put up with much senseless rambling on numerous occasions. My gratitude also goes to Dr Aletta Van der Merwe and Mr Johannes Van Zyl for their assistance with mathematical calculations involved. Dr Ian de Vries was of great assistance where any hint of power electronics arose. Thank you too to all those at the CIR for creating a wonderful working environment and all the encouragement.

Finally I would like to thank my family for putting up with me during many months of answering, "it's going!" to their supportive question, "how is it going?" and supporting me unconditionally during that time.

This work was supported financially by the National Research Foundation (NRF) and the Cape Peninsula University of Technology.

Driving Techniques for High Power PZT Transducer Arrays

by

Tarren M. J. Smith

Submitted to the Department of Electrical Engineering
on March 19, 2007, in partial fulfillment of the
requirements for the degree of
Magister Technologiae

Synopsis

Because of the nature of piezoelectric ceramics and the physical construction of high power piezoelectric transducers, such devices are inherently non-linear and become unpredictable when driven at high power. To drive an ultrasonic transducer or an array thereof efficiently, specific resonant points are used. These points are characterised by the devices' mechanical modes of oscillation. At high electrical power levels, the resonance points of PZT transducers vary. The movement of the resonances points in the frequency domain, coupled with the transducers high Q, is severe enough to seriously hamper the devices' efficiency. The problem is specifically apparent when multiple transducer arrays are driven at power. The electrical fluctuations and interactions of the characteristics of separate transducers cause arrays to be driven efficiently at a single resonance point.

To efficiently drive an array of PZT transducers it is necessary to employ a suitable technique. Although several methods exist in the literature, each is designed for a specific configuration of transducers and dedicated matching circuitry. The fundamental flaw in most methods is that they are conceived with the assumption all PZT transducers are identical and can be driven as such. Inherent nonlinearities caused by poling and construction methods, result in each transducer to be slightly different causing a superposition of resonance frequencies for each transducer array.

Existing methods cannot be used to efficiently drive generic transducer arrays and a novel approach has been adopted to accommodate transducer nonlinearities. This novel approach can be described as a culmination of two driving techniques and has been named, Swept Frequency Dwelling (SFD). This thesis examines five different driving techniques and quantifies their effectiveness by means of experimental evaluation proficiencies. The driving techniques are grouped into two categories - straight driving techniques and frequency sweeping techniques - which are compared and evaluated.

In conclusion, a novel method for driving ultrasonic transducer arrays was established with the aim of eliminating some detrimental effects of other driving techniques, while exploiting some of their positive attributes and was found to be effective.

Contents

List of Figures

Abbreviations and Symbols

Anglicised spelling has been used throughout this dissertation.

Abbreviations

BVD	Butterworth-Van Dyke
DC	Direct current
FM	Frequency modulation
OH	Free radicals
PLL	Phase locked loop
PZT	Lead zerconate titinate
Q	Quality factor
RMS	Root mean square
SFD	Swept frequency dwelling
SFM	Swept frequency modulation
VCO	Voltage controlled oscillator

Symbols

A	Area
C	Capacitance
c	Velocity of sound
F	Force
f_r	Fundamental resonant frequency of piezoelectric transducer
G	Conductance
I	Current
k	Polytropic index
L	Inductance
λ	Wavelength
ω	Angular frequency
ϕ	Phase
R	Resistance
ρ	Density
S	Susceptance
t	Time
Γ	Time constant
v	Velocity
X	Reactance
Y	Admittance
Z	Impedance
Z_0	Characteristic acoustic impedance

Chapter 1

Introduction

1.1 Transducer arrays

High power ultrasound has many applications from accelerated chemical and physiochemical reactions to changing reaction pathways and effectively cleaning intricate components [15]. These characteristics give power ultrasound potential for a wide range of applications in chemical and industrial processing industries [15]. In spite of these promising attributes, large-scale ultrasonic equipment is not reported to be in extensive use in industry [15]. One reason is the inefficiency of large-scale equipment, both electrically and acoustically [16][8].

A common process of creating large-scale ultrasonic cavitation is to use piezoelectric transducers connected in array topologies. PZT arrays are constructed by connecting single PZT transducers in parallel over the area of required cavitation. Two types of mass processing arrangements exist today in the form of batch and flow process treatment systems [15]. Batch treatment units include cleaning baths and tanks, both driven in one of two ways - an array of high power transducers is attached to the outside of a tank or submersible transducer assemblies are inserted into the tank (see Figure 1-1 A and B). Type A is usually constructed out of a material such as stainless steel, strong enough to withstand the violent vibrations of the directly coupled transducer array. Type B can be constructed of softer materials such as plastics, as the transducers are not directly attached to this bath.

Heating systems are often added to cleaning bath applications to accelerate the chemical and cleaning processes [15]. Flow process systems consist of a flow loop and an ultrasonic reactor. Ultrasonic energy is applied to the system using in-line ultrasonic generators, through which the medium is pumped (see Figure 1-1 C).

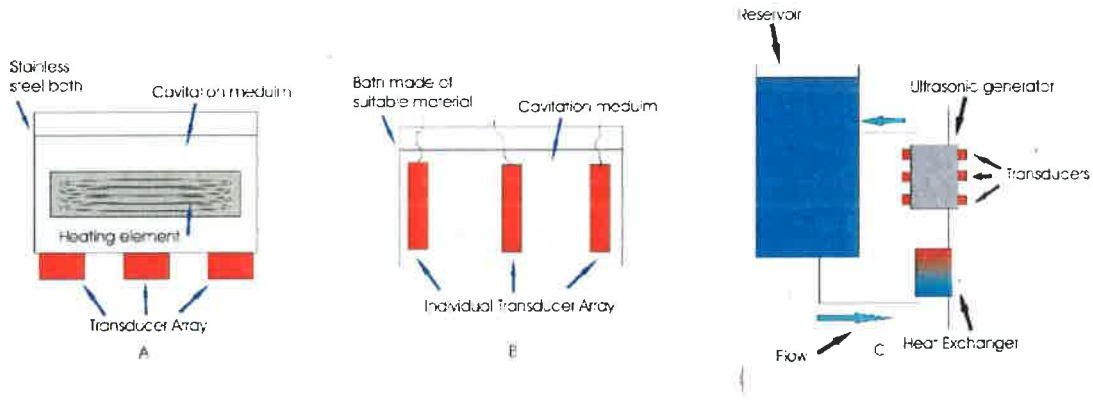

Figure 1-1: Three different types of cavitation vessels utilising ultrasonic transducer arrays. Figure 1-1a shows a cavitation bath with the array connected to its base, figure 1-1b is a bath with a submerged transducer array and figure 1-1c shows a flow type processing system

Manufacturers of cavitation vessels have two fundamental engineering goals:

- To distribute the cavitation activity evenly within the volume of the vessel and,
- ensure optimal electroacoustic efficiency.

  Often these goals are difficult to achieve because of the shifting resonance frequencies of PZT ultrasonic transducers at high power [24].

Frequency shifting of the resonance points during operation can be caused by factors such as temperature, frequency pulling between the transducers in the array, acoustic interaction from the liquid, loading of the transducers and mechanical resonance modes within the liquid [2].

Frequency pulling, resulting from direct mechanical coupling of the stainless steel with the transducers, occurs in all arrays where transducers are fixed to the same surface.

This happens when two or more resonance frequencies of the transducer array interact with one another causing one (or more) of the frequencies to change its Q and resonance frequency [24]. This phenomenon causes certain transducers in the array to operate off their designed resonance points, often reducing the electroacoustic efficiency of the cavitation cell.

One of the primary concerns in the design of a system that delivers an even acoustic field at high power is the occurrence of standing waves. Nodes and antinodes are created when pressure waves are applied to a medium of different acoustic impedance from that in which they are moving, causing a reflected wave to return along the same path, but in an opposite direction. When an equilibrium state is reached nodes and antinodes form [13]. Standing waves are particularly apparent in applications such as cleaning baths where a pressure wave originates in a liquid, moves through the liquid to air where a reflected wave is formed.

Many PZT systems suffer from induced mechanical noise (e.g. from the cavitation) which is converted into electrical noise via the inverse piezoelectric effect, causing another difficulty in the drive circuitry.

In an effort to create a more even distribution of cavitation, different electrical driving techniques were devised to overcome certain shortfalls encountered by different users [21]. Driving techniques involve the control of the electrical driving signal, mainly by means of frequency variations to maintain a particular driving condition. The thesis of this study empirically compares the most common of these driving techniques in order to achieve optimal electroacoustic efficiency and acoustic distribution.

1.2 Transducer Nonlinearities

The electromechanical inefficiency in PZT transducers suffered when driving ultrasonic loads at high power, results in huge amounts of energy being wasted. This wasted energy takes the form of reactive power and mechanical movement in unwanted mechanical modes occurring in the transducer array [23].

To efficiently drive a mechanically coupled array of PZT transducers it was necessary to employ a suitable driving technique [7]. Although a variety of methods existed in the literature, each was designed for a specific configuration of transducers and dedicated matching circuitry sometimes used. The fundamental flaw in most methods was their design was achieved on the assumption that all PZT transducers behaved identically and could be driven as such. Inherent nonlinearities resulted in each transducer being slightly different from any other causing a superposition of resonance frequencies for each transducer array [1].

To ideally drive a PZT array, two criteria needed to be addressed. Electrically, each transducer needed to be driven and tracked at its resonance point ensuring maximum electrical power dissipation.

Acoustically, an even acoustic field needed to be generated inside the liquid volume. This is a field without any local nodes or antinodes resulting in an even spread of cavitation activity inside the vessel.

There are three primary methods in which PZT transducer arrays are driven in industry.

- Straight frequency drive;
- frequency locking and tracking and,
- frequency sweeping.

In the first case, an ultrasonic load is driven at a constant frequency. This frequency is usually the specified centre frequency of the transducer devices or the resonance frequency of the unit in which the cavitation is to be created. No feedback was implemented and, therefore, the system was inefficient because of the dynamics of the PZT transducer array [23].

Frequency locking and tracking use a form of feedback to influence a systems driving frequency. The feedback is typically quantified using power, admittance or phase. Self-oscillating systems may be classified in the phase locking category. Locking methods of driving ultrasonic transducers are considered superior to straight frequency driving techniques in that the dynamic resonance frequency is tracked at all times [7].

Frequency sweeping was devised to eliminate the problem of standing waves and their resultant uneven acoustic power distribution [21]. In this method a frequency range was chosen and swept at a predetermined rate. The standing waves were effectively made to move in three-dimensional space causing the nodes and antinodes to move. This movement resulted in the regions of high and low acoustic power shifting within the vessel, causing a more even spread of cavitation over time. In a transducer array where many transducers are used, the resonant point of each transducer was excited as the frequency bandwidth was swept.

The aim of this study was to evaluate existing driving techniques used on multiple transducer arrays with the specific aim of optimising the acoustic distribution inside the cavitation vessel and the electrical power versus the acoustic power yield.

Three tests were conducted on a test rig with each of the driving methods resulting in an empirical analysis of both the acoustic power and its distribution in the vessel.

The results of these tests were used to evaluate the driving techniques in both the electrical and acoustic domains.

Furthermore, the key issues surrounding multiple transducer array driving methods were identified. Five different driving techniques were evaluated, four of which were found to have serious shortcomings in driving multiple ultrasonic PZT arrays.

A novel, hybrid driving system was successfully developed. The technique was designed to achieve more even resultant acoustic field distribution than other driving techniques and optimal electrical power distribution over the separate transducers forming the array.

1.3 Scope and Limitations

This study considered only high power, ultrasonic transducers of the Tonpilz type driven by sinusoidal waves.

The test rig used consisted of a parallel configuration of six Tonpilz PZT transducers attached to the outside base of an open top stainless steel bath.

No temperature or pressure related effects were considered. The only liquid used was distilled water at a temperature in the range between 19°C and 26°C. The pressure exerted on the liquid during the tests was ambient atmospheric pressure.

Cavitation behaviour and its effects were considered in a limited way and were used as quantification tools for the evaluation of the amount of cavitation occurring.

Liquid modelling was ignored.

This study was limited to considering only electrical driving topologies and evaluating their acoustic effects in the test rig.

Chapter 2

History

Ultrasound can be widely classified as the frequency range above the limit of human hearing; usually this begins at 20 kHz. To produce ultrasound an active transducer was required, the most common of which being made using piezoelectric or magnetostrictive materials.

Pierre and Jacques Curie observed the first visible piezoelectric effect in quartz in 1880 [10]. Subsequent to this discovery, Lippmann mathematically deduced the opposite effect in that movement could be obtained when a voltage was applied to the surface of a piezoelectric material [26]. The word "piezo" is derived from the Greek word "pizein" meaning "to press". The basis of early experimentation was performed on quartz crystal and many early transducers were constructed from this material.

Today, mainly two compounds are used in high power piezoelectric ceramics - barium titanate and lead zirconate titanate (PZT) [24]. One major advantage of these ceramics is their characteristics may be altered during the manufacturing process with chemical additives [24]. Many different piezoelectric ultrasonic transducers are used in a variety of applications.

2.1 High Power PZT Ultrasonic Transducers

High power, ultrasonic transducers are designed and built for specific applications. Varieties include the horn, disc, sonotroid and tonpilz type transducers [10]. Horn transducers are used when high intensity ultrasound is required in localised areas. Sonotroids are used in flow processing systems where these submersible transducers are placed in pipelines creating a low intensity of ultrasound in large areas through which liquid flows. Tonpilz transducers are used in cavitation cells and flow process chambers where sound is transmitted from the outside of a vessel to its inside.

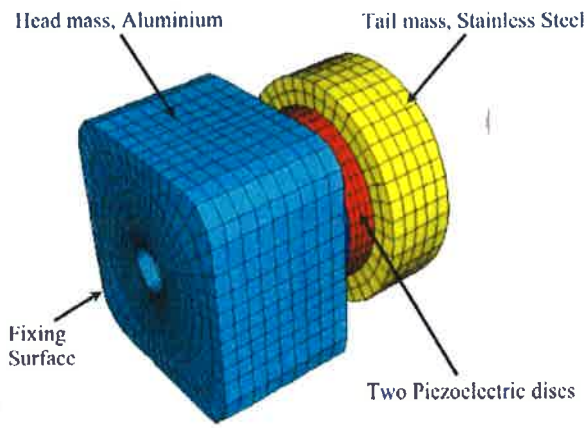

Figure 2-1: A Tonpilz Transducer showing its basic construction and main components

The construction of a tonpilz transducer is physically simple, comprising of two solid pieces of metal sandwiching one or more piezoelectric discs (see Figure 2-1). Although such transducers are physically simple to bolt together, the flexing of the metal and the modes of the system when made to vibrate vigorously are mathematically complex. Presently, much of the mathematics in transducer design is calculated using Finite Element Modelling systems [10]. The active component of the transducer consists of one or more piezoelectric ceramic compounds, usually in the shape of disks with central holes, sandwiched between two pieces of metal. A bolt is used to squeeze the components together. The metal used in the construction usually consists of a head mass having a lower Youngs Modulus (or a more elestic property) than the tail mass.

The two masses, as well as the elasticity of the materials determine the natural oscillation frequency of the transducer [10].

The word Tonpilz is derived from two German words, "ton" meaning sound and "pilz" meaning mushroom. The name originates from the physical appearance of the device vaguely resembling a mushroom with a capability to produce sound by physically shaking.

2.1.1 The Electro-acoustic Transducer Model

A model developed by Warren Mason [17] can be used to analyse a piezoelectric transducer operating over a narrow frequency band (see Figure 2-2). Mason's model consisted of two mechanical ports coupled to an ideal electromechanical transformer. The transformer ratio represented the coupling between the electrical and mechanical systems. On the electrical port, E was related to the current I through E = ZI, where Z was the electrical impedance. On the mechanical or acoustic port the force, F, was related to the velocity v where F = vZ_0 (Z_0 is the characteristic acoustic impedance and $Z_0 \propto \rho A v$). ρ represented the density, A the area of the piezoelectric transducer and v the velocity of sound in the piezoelectric ceramic. The two equations for the two port network were defined as [17]:

$$F = NE + Z_0 v \tag{2.1}$$

$$I = Y_b - Nv \tag{2.2}$$

The circuit elements for Mason's equivalent electromechanical circuit are shown in Figure 2-2 (1) and may be defined by the following set of equations:

$$Z_T = jZ_0 \tan(\frac{kt}{2}) \tag{2.3}$$

$$Z_S = j\frac{Z_0}{\sin(kt)} \tag{2.4}$$

Where:

k = wave number $=\frac{2\pi}{\lambda}$ or $\frac{\omega}{v}$;λ is the wavelength and ω is the angular frequency

Z_0 = the characteristic acoustic impedance

t= the thickness of the transducer

The electrical capacitance and the electromechanical transformer ratio are calculated using the following equations:

$$C_o = \frac{\varepsilon^s A}{t} \tag{2.5}$$

$$N = h_x C_0 \tag{2.6}$$

Where:

ε^s= Clamped permittivity

h_x = Piezoelectric constant

The negative capacitor, $-C_0$ (shown in Figure 2-2 (1))represents the excitation of the piezoelectric transducer when an electrical field is applied that is parallel to the wave propagation direction.

If an open circuit was created on one side of the equivalent circuit and a load applied to the other side, the transmission line could be reduced into a lumped network resulting in the simplified Figure 2-2 (2). The ideal transformer coupled the electrical terminals on the primary side and the mechanical arm on the secondary side.

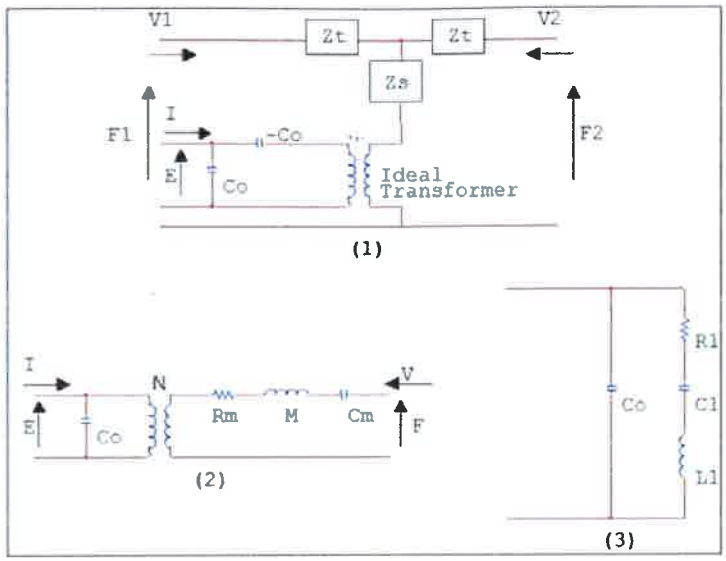

Figure 2-2: The equivalent circuit for a PZT transducer. (1) shows Mason's transmission line model. (2) is the simplified circuit where the oscillator is free on one side and drives a load on the other. (3) The Butterworth-Van Dyke one port equivalent circuit, valid only in the vicinity of a single resonance

C_0 represents the capacitance of the piezoelectric ceramic as well as the capacitance of the cables. The series motional branch consists of C_m (the compliance of the oscillating body), M the motional inductance giving a measure of mass and R_m, the mechanical energy lost because of the mechanical impedance.

When the admittance spectrum was examined the real and imaginary components of a piezoelectric transducer could be evaluated. An admittance vector diagram (Figure 2-3) was acquired when a unit voltage was swept across a predetermined frequency bandwidth while the current was monitored. The conductance of the system was represented on the abscissa in Figure 2-3 and shows its real part. The imaginary part of the diagram, susceptance, is depicted on the ordinate.

A vector diagram resulting in a circular pattern in the complex admittance plane, as shown in Figure 2-3 is often referred to as a transadmittance circle [17]. This circle represents the electrical characteristics of a single piezoelectric transducer over a predetermined frequency range. The vector diagram illustrates the piezoelectric response.

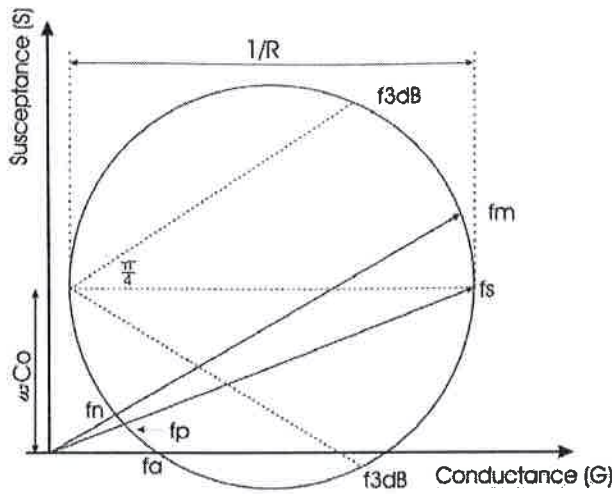

Figure 2-3: The transadmittance circle representing the BVD model of a PZT transducer

Each circle represents a unique resonance and its size represents its magnitude and quality factor. The vertical offset of the plot was created by the clamped capacitance C_0. The transducer diameter $\frac{1}{R}$ can be seen as the absolute admittance difference. The half power points, f_{3dB}, are shown at the intersection of the circle and line at $\frac{\pi}{4}$ from the horizontal diameter.

The following equations can be used to calculate the three parameters, R, L and C, of the PZT transducer from the transadmittance circle:

The admittance Y of the electrical circuit of the PZT transducer:

$$Y = \frac{R}{R^2 + X^2} + j[\omega C_0 - \frac{X}{R^2 + X^2}] \tag{2.7}$$

X, the reactance is given by:

$$X = \omega_s L - \frac{1}{\omega_s C} \tag{2.8}$$

The electromechanical coupling (k_{eff}) of the transducer can be calculated using the series (fs) and parallel (fp) points on the vector diagram:

$$k_{eff} = \sqrt{1 - \frac{f_s^2}{f_p^2}} \approx \sqrt{1 - \frac{f_m^2}{f_n^2}} \tag{2.9}$$

The mechanical quality factor Q_m can be measured using the series resonance fs and half power point Δf_{3dB}.

$$Q_m = \frac{f_s}{\Delta f_{3dB}} \tag{2.10}$$

Or, using the absolute admittance curve:

$$Q_m \approx [\frac{\omega_m}{2(\omega_n - \omega_m)}][\frac{|Y_{fm}|}{|Y_{fn}|}] \tag{2.11}$$

The fundamental PZT transducer parameters (Figure 2-2 (3)), R, L, C and Co can now be calculated as follows:

$$L = \frac{Q_m R}{\omega_m} \tag{2.12}$$

$$C = \frac{1}{\omega_m Q_m R} \tag{2.13}$$

$$R = \frac{1}{|Y_{fm} - Y_{fn}|} \tag{2.14}$$

The electrical capacitance can easily be measured directly or determined using the electromechanical coupling factor, k_{eff}:

$$C_0 = C(\frac{1}{k_{eff}^2} - 1) \tag{2.15}$$

These values correspond to the Butterworth-Van Dyke (BVD) circuit Figure 2-2 (3). It must be noted this model is only valid at frequencies near the fundamental resonance frequency of the device.

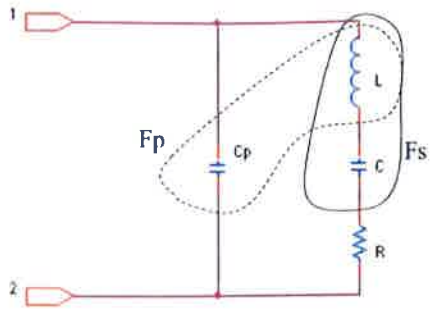

Figure 2-4: The equivalent transducer circuit showing the electrical and mechanical resonant components. The electrical resonant component is represented by system Fp and the mechanical resonant component by system Fs

A Butterworth-Van Dyke electromechanical equivalent circuit for a piezoelectric transducer (Figure 2-4) can be used to illustrate what happens at the characteristic resonance points of the PZT transducer (these resonance points, Fs and Fp, can be seen in the admittance plot shown in Figure 2-5).

Each resonance was characterised by a mechanical resonant system and an electrical resonant system. The two systems are marked in figure 2-4. The electrical resonance occured between the parallel capacitor, Cp, representing the static electrical capacitance of the PZT disks and the inductor, L, representing the mechanical mass of the transducer (Figure 2-4). Mechanical resonance occured between the inductor L and the capacitor C representing the mechanical capacitance and the mass of the transducer. It can be seen in Figure 2-4 that such resonant systems differ in that the electrical system is a parallel resonant system (Fp) and the mechanical system series resonant (Fs). These systems caused the characteristic resonant admittance peaks depicted in Figure 2-5.

Figure 2-6 shows the admittance vector plot of a PZT transducer measured in the frequency bandwidth between 20 and 45kHz. The fundamental resonance of the device is included in this bandwidth and is depicted by the largest circle. Every circle represents a resonance mode. Figure 2-5 shows the absolute admittance versus the frequency measurement of the same transducer.

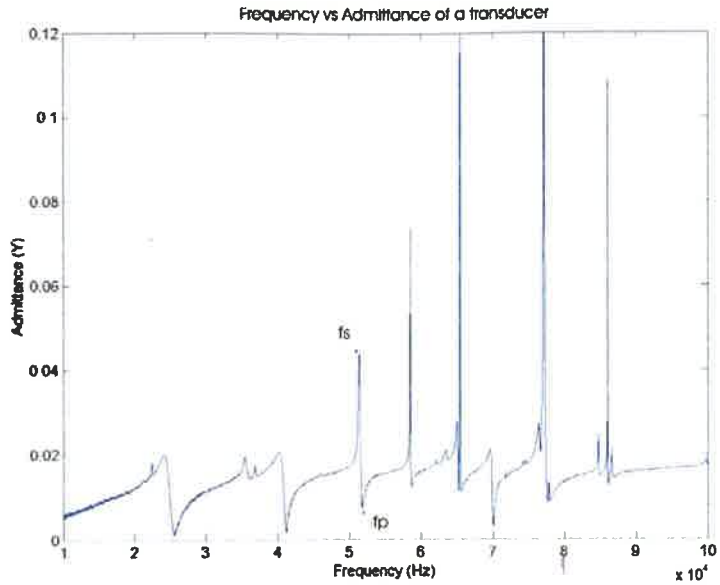

Figure 2-5: The result of a measured tonpilz transducer showing many resonance points and their narrow bandwidth properties

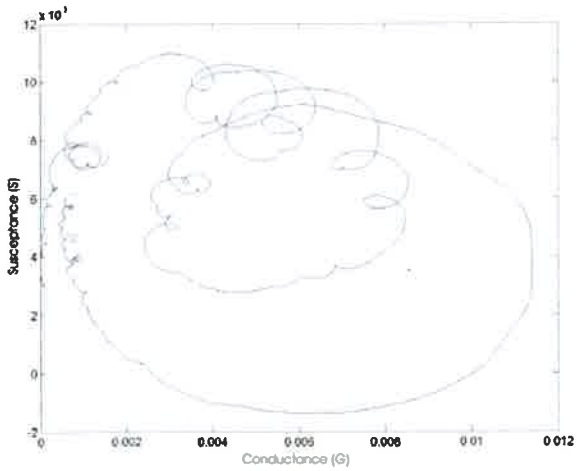

Figure 2-6: The transadmittance circle of the ultrasonic bath in the frequency bandwidth between 20kHz and 45kHz

Many resonance modes can be seen in both the admittance plot and the transadmittance circle showing the Q and resonant frequency of each point.

Most transducers are designed to operate at one resonance frequency as this excites the required mechanical oscillation mode. When a PZT transducer is driven at a mode for which it is not designed, unwanted mechanical resonances can be excited, physically damaging the device. These modes include sheering and torsional modes [10]. Most Tonpilz type transducers are designed to oscillate at their breathing mode in order to produce maximum mechanical movement in a longitudinal direction at their head surface.

2.2 Piezoelectric Transducer Arrays

Transducer arrays can be used when acoustic pressure is required over a large area. Electrically, these arrays are usually connected in parallel configurations to achieve a realistic input impedance, but, they are not driven efficiently because of fluctuation and interaction between the separate transducers. The result of the fluctuations cause an uneven spread of acoustic energy in the vessel and an uneven distribution of electrical power over the array.

Each of the six transducers used in the test rig carried similar admittance plots. When these transducers were attached to the bath, the admittance spectra changed because of the acoustic transformations and mechanical coupling. The changes in each transducer's admittance caused the resultant sum of the transducer array to peak at a point that did not coincide with any individual transducer resonance.

Figure 2-7 shows two plots representing the input admittance of the bath (lower) and the input admittance for each transducer superimposed on one another (upper). Transducer i is drastically different from the other devices because of inadequate acoustic coupling to the bath. This device was left in this way for the experimentation to create a more unpredictable load. A simple graph, such as Figure 2-7, might be used as a varification tool for the acoustic connections of the transducers to the bath during the manufacturing process.

From the two graphs it can be observed the net series or mechanical resonance point did not coincide with any of the individual resonance points of the transducers.

If the array was driven at its combined series resonance point, many individual transducers are not driven at their resonance frequency, resulting in an inefficient electro-mechanical system and ultimately little electrical power dissipation, resulting in little cavitation.

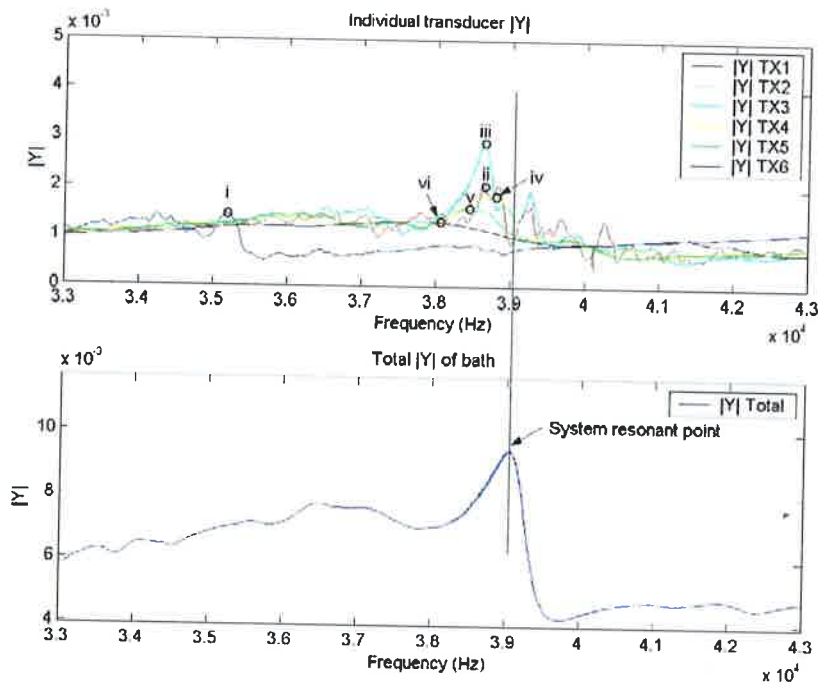

Figure 2-7: Points i, ii, iii, iv, v and vi represent the individual transducers' mechanical resonant points (Fs). Note the difference in frequency of each of these points and the resonant point of the entire system.

The variations in the admittance, resulting from differences in acoustic connections to the bath and mechanical coupling through the metal of the bath, could cause many unsatisfactory results in applications such as ultrasonic cleaning baths, where delicate instrumentation could be damaged or not cleaned effectively. Transducers can also be damaged through over-driving (too much electrical power), while others in the same array, however, dissipate minimal electrical power.

2.3 Methods Employed in Driving Ultrasonic Transducer Arrays

A method of frequency drive needed to be applied to a PZT transducer to achieve maximum efficiency both in the electrical and acoustic domains [7]. The driving method ensured that fluctuations in the values of the electromechanical model resulting from the changing PZT load did not disrupt the functionality of the array by driving transducers off their resonance points.

Existing methods of driving PZT arrays are discussed below.

2.3.1 Straight Driving

In this technique a frequency is chosen, the resonance frequency of the device and the transducer, or transducers, is driven at that frequency. There is no feedback so this technique is mainly used when wide bandwidth transducers are required. Straight driving is better implemented with horn-type transducers rather than tonpilz transducers as a horn type usually has a wider operating bandwidth.

Straight driving is sometimes used in conjunction with parallel or series compensation in the form of added inductors. Compensation simplifies the PZT load by eliminating either the series of parallel capacitance at a specific frequency. In most cases matching is seen to be sufficient but practically, this is not the case for PZT arrays [21].

2.3.2 Mode Locking Techniques

To overcome the problems with straight driving, mode locking driving techniques were devised so the operation of the transducer/s could be tracked in the frequency domain. Common locking mechanisms are phase locking, power and admittance locking. Phase locking can also include self-oscillation techniques and can be classified as phase locking systems locking at 0° phase angle between the voltage and current. All these techniques are tracked by means of feedback mechanisms. Tracking systems are well suited to single transducer applications but not suited to array topologies.

2.3.3 Frequency Modulation

Frequency sweeping systems are used in conjunction with transducer arrays. In this driving technique the transducers in an array are excited by a sinusoidal wave that sweeps through a specified frequency bandwidth (see Figure 2-8). The concept behind the technique was to excite the resonances of the separate transducers as the bandwidth was swept. This technique is used in industry by CAE Ultrasonics [9] who recommend modulating the modulation signal and claim a non-constant or modulated sweep rate resulting in varied spaces between the power pulses in the sweep cycle, avoiding a resonant condition at twice the sweep rate and potential damage during cleaning applications. This technique was not, however, assessed in this project.

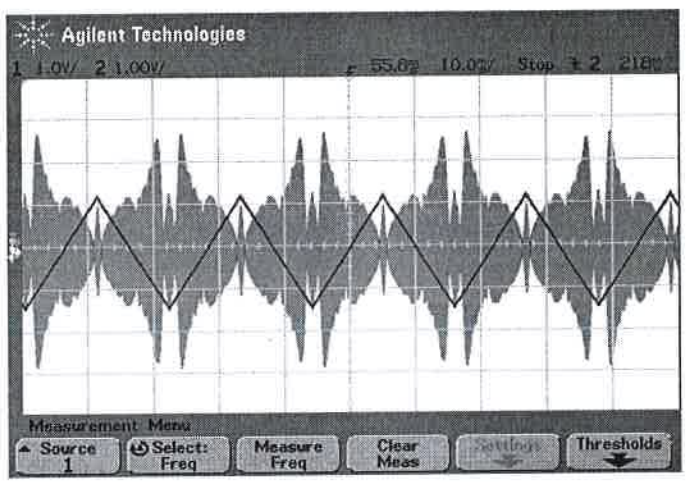

Figure 2-8: Conventional frequency modulation (triangle) signal and power delivery to a multiple transducer cleaning bath

A variation of this driving technique is to control the sweeping frequency with a sawtooth waveform. The frequency is made to increase at a linear rate to a maximum where it instantaneously reverts to its starting frequency. The sudden change in the driving frequency is said to excite harmonics in the system that could be detrimental to piezoelectric transducers [21]. As a result, the sawtooth type frequency control is not considered in this study. Figure 2-8 shows a typical frequency sweeping system.

Chapter 3

Construction of the Ultrasonic Cavitation Bath

Experimentation in this thesis called for the construction of a test rig as comparative studies of different driving systems were required. The rig had to meet the requirements of ease of access to the cavitation medium both visually and physically and represent a multiple PZT transducer array. A typical cavitation cleaning bath design was chosen comprising of an open topped stainless steel basin with an array of tonpilz transducers attached to the outer side of the bath's bottom.

A pressed stainless steel container with the capacity of 8l was availiable in the lab. The container resembled a typical industrial unit and was perfectly suited to the application. The rounded corners would cause random reflections of the pressure waves inside the liquid adding to the unpredictable resonant behaviour inside the volume of liquid. Being a test vessel, an unpredictable system was encouraged to best mimic a commercial unit.

3.1 The Number and Type of Tonpilz Transducers Required for the Bath

To determine the number of transducers required for the test bath, an average electrical power requirement needed to be determining. Specification sheets of high power cavitation baths were assessed which disclosed average power ratings for a bath of similar dimensions to be between 300W and 450W [23].

To avoid damage to the transducer, an over-specification was included and the transducer array made capable of handling a maximum electrical power rating of 600W. Six transducers, capable of handling 100W each, were used on the test bath.

The transducers were connected in parallel as a series connection would have required excessisively high driving voltages because of high electrical impedance. The transducers were equidistantly spaced along the bottom of the bath in an attempt to spread the acoustic power across the volume of liquid. Tonpilz transducers were chosen over single piezoelectric elements, as the tonpilz had a high Q and an ability to produce more acoustic power from its mechanical oscillation modes. Single element transducers are common in applications at frequencies greater than 1MHz [24] and could, therefore, not be used at the required operation frequency of about 50kHz. The proximity of the six devices would encourage coupling and interactions between the transducers leading to an unpredictable and difficult system to drive as the resonance frequencies would change at power [24].

3.2 Attaching the Tonpilz Transducers to the Bath

Typically, ultrasonic transducers are attached to baths by means of an adhesive. The adhesive used must withstand violent vibrations while converting mechanical energy from the transducer to acoustic energy in the medium. It also needed to be capable of transferring heat produced by the transducers into the cavitation bath in order to cool the devices. Consideration had to be made for the acoustic impedance of the glue and the acoustic transformation required.

The relevance of the matching influenced the amount of acoustic energy being transferred from the transducer to the liquid in the bath.

When an ultrasonic transducer is attached to a bath it is important to know the acoustic impedance of the transducer, the medium into which the energy is being transferred and the bonding material used. If there is poor acoustic transformation, acoustic energy will be lost at the join in the form of reflected and absorbed energy [20]. The acoustic impedance of any sound propagating system is the product of the density of the medium through which the sound is being propagated and the sound's velocity [20].

Mathematically:

$$Z_a = c\rho \tag{3.1}$$

Where:

Z_a =acoustic impedance ($\frac{kg}{m^2 s}$or Rayls)

ρ =mass density of medium ($\frac{kg}{m^3}$)

c = velocity of sound in medium ($\frac{m}{s}$)

And:

$$c = \sqrt{\frac{Y}{\rho}} \tag{3.2}$$

Where:

Y =Modulus of elasticity, Youngs Modulus (N/m^2)

Then substituting equation 3.2 into equation 3.1 yields:

$$Z_a = \sqrt{Y\rho} \tag{3.3}$$

To correctly match a transducer to the material to which it is being attached, the user must know the acoustic impedance of both mediums [20]. The matching allows maximum acoustic power to be transferred from the transmitter to the receiving medium.

In this case the transducer head was made of aluminium and the medium into which the sound needed to be transferred was water. If the length of the path of sound, however, is less than a quater of the wavelength of the propogating wave, the acoustic impedance is irrelevant. This means that any glue that is capable of transferring heat and the violent vibrations produced by the transducer is sufficient.

3.3 Input Admittance of the Test Bath

A transducer array was measured using an impedance analyser [HP4192A] in order to discover variations in characteristics of the array when the liquid load in the bath (water) was changed. Three plots of admittance verses frequency were completed at three different water levels, see Figure 3-1.

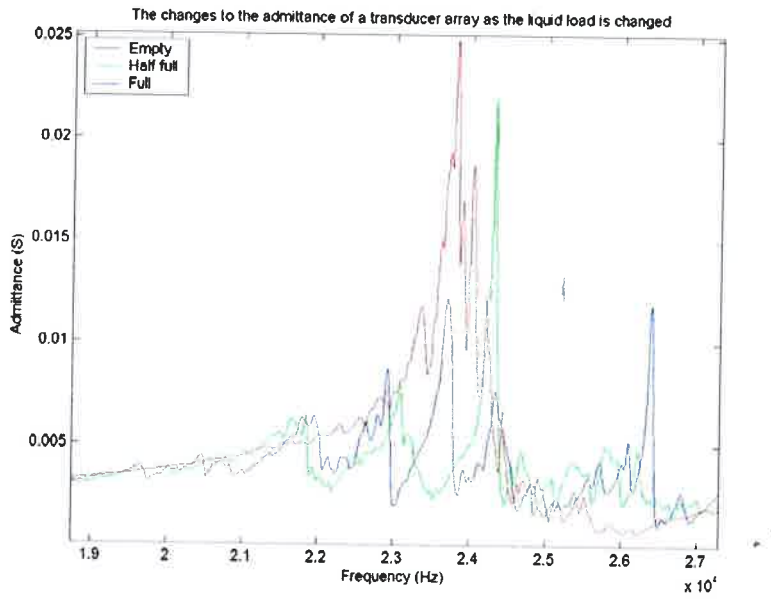

Figure 3-1: The plots above shows changes in the characteristics of the PZT array when different loading conditions were applied. The water level in a test bath is changed in three steps from empty to full. Note the shifts in the frequency domain and changes in the admittance amplitude

It can be seen from Figure 3-1 that the admittance plots of the bath changed as the load inside the bath was altered. Changes in the frequency, as well as admittance, can clearly be seen. This was expected as the volume and resonant geometry of the load changed, resulting in an altered admittance spectra of the array. R in this case (referring to Chapter 2, figure 2.4) becomes larger as the external load is increased, reducing the Q.

When referring to figure 3-1, it can be seen that the admittance drops as more liquid load is added to the bath.

3.4 The bath as a Resonant System

It is well documented that PZT transducers are difficult to drive because of their complex resonances and dynamic behaviour at both high power and under different loading conditions [24][7][10].

When an array of PZT transducers is driven at power into a liquid medium it becomes increasingly more unstable and its load characteristic becomes the summed complex result of the transducers (see figure 2.7), the resonant system of the liquid load volume itself and the physical bath.

Standing waves inside an ultrasonic chamber cause major problems when an even distribution of acoustic power is required. When a pressure wave is driven through a liquid a certain wavelength is created that is a function of the bulk modulus, frequency and density. When a constant drive at a specific frequency is generated, the pressure wave moves through the liquid, reflects at a point of density change (the liquid surface, for example) and propagates back through the liquid in the opposite direction. The two waves collide as they travel causing pressure variations in localised planes along the entire volume of liquid resulting in localised nodes and antinodes [28].

When the ultrasonic system was driven at low power a resonant system was set up from the standing waves and their interaction with the tank, themselves and any surface (see Figure 3-2). Three resultant mode conditions can occur when the pressure wave originating from any transducer interacts with the walls of the cell or the surface of the liquid, reflection, refraction and/or transmission [13]. A conversion of the wave from a longitudinal type to other forms such as Radial, Lamb, Rayleigh and Cylindrical waves also occurs. The complex result of the resonating system tended to be stable at low power but when cavitation is acquired the system became unpredictable and nonlinear [3]. This happened as the bubbles, or voids, occurring in a cavitating medium caused random reflections, refractions and transmissions of acoustic energy.

Attenuation (loss of acoustic energy) of the pressure wave also occured in the form of absorption (absorption occurs when acoustic energy is converted into thermal energy and other mechanisms that deflect or scatter acoustic energy out of the acoustic beam [13]).

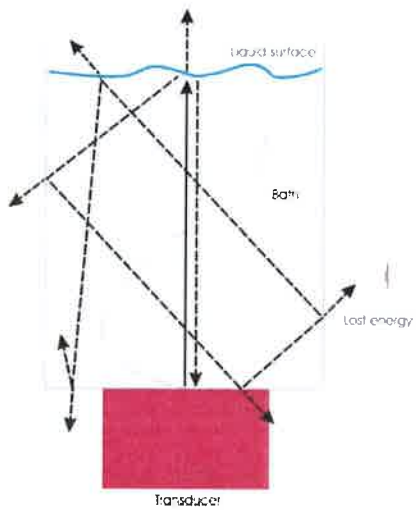

Figure 3-2: A simplified interpretation of acoustic power paths showing a standing wave as well as arrows representing the acoustic energy beeing reflected, refracted and/or transmitted

Acoustic energy was also lost due to streaming. Steaming is defined as currents that are set up in the vicinity of vibrating objects. Lord Rayleigh theorised streaming depended on the viscosity of the liquid and could be mathematically described as a second order, nonlinear system [22].

These reasons define the fact a cavitation cell is totally unpredictable and cannot be modelled in any simple way. This study will not involve the evaluation of the nonlinear and unpredictable cavitation system, but will concentrate on the electrical systems used to drive the vessel and attempt to identify and improve the acoustic yield and distribution of this complex system.

3.5 Evaluation of Test Bath Experimentation

The test bath was used to evaluate the electrical and acoustic effects on the liquid load in the bath for five electrical driving techniques. Evaluations of the techniques were performed by the three tests discussed in sections 3.5.1, 3.5.2 and 3.5.3. The test methods are described in this chapter to avoid later repetition.

3.5.1 Examining the Pressure Contour in the Liquid

The aim of this test, completed using a needle hydrophone, was to illustrate the low power acoustic distribution inside the bath. A needle hydrophone was used in conjunction with an X-Y plotter system. The probe was moved inside the cavitation medium in a grid pattern recording the average value of acoustic power at each point. A matrix of points could then be assembled using software to create a three-dimensional graph of the acoustic power distribution. The apparatus used in conjunction with Labview and Matlab will be discussed here.

An automated positioning device was constructed in order to move the needle hydrophone around the bath in small steps of a predetermined size. The requirements of the system were to move the hydrophone in the X-Y plane automatically, while a Z axis was manually adjustable, so enabling the hydrophone to be moved around the bath's three-dimensional volume.

An X-Y plotter was built using two stepper motors controlling the X and Y axes. The Z axis could be moved manually by sliding an aluminium tube inside a cylinder. The hydrophone assembly was fixed inside the moving aluminium tube. The stepper motors were geared so that each rotational step caused a movement of the device of 0.25mm. This accuracy was sufficient for the tests being performed as the wavelength in water at 40kHz was calculated to be in the region of 37.08mm, yielding a maximum resolution of 148 steps per wavelength.

A programme written in Labview (*see Appendix A*) and a high speed National Instruments data acquisition card (PCI-6221) was used to signal the stepper motor driving circuit and control the two stepper motors.

Apart from driving the motors, the programme also read analogue values from the needle hydrophone and calculated an RMS voltage proportional to the acoustic pressure. This value was stored to a file in tabular format, along with the X-Y position of the probe.

The user could specify the size of the rectangle to be scanned, the step size between scans and file name of the saved file. After information was entered the system showed the user the values being read and time remaining before completion of the scan.

Upon completion, a data file containing the average acoustic pressure at each point on the scanned grid was created. The data was manipulated in Matlab to form a visual three-dimensional contour graph display of the pressure profile inside the bath (*see Appendix B*). Figure 4.4 shows a typical contour graph.

3.5.2 Localised Cavitation Activity Test

This test assessed the localised cavitation inside the test bath. When the cavitation void collapsed, energy was released. This energy took the form of heat, pressure and chemical alteration on a molecular level (sonochemistry) [15].

The destructive power of cavitation was used to illustrate its distribution within a vessel. Aluminium foil proved ideal, as it is a soft metal in a thin layer ($10\mu m$), it disintegrates rapidly when exposed to the violent cavitation process. Pressure impacts of the collapsing voids created small pits marks visible to the naked eye, see Figure 3-3. Areas of foil could be decayed completely, forming holes.

During the test, a sheet of aluminium foil was placed inside the cavitation medium at a predetermined level. The level for the tests in this project was kept constant at 10mm from the bottom of the bath. Ultrasonic exposure was limited to a time duration of 1.5 minutes. This time was long enough to cause considerable damage to the foil at full power using the straight driving technique. After exposure the tinfoil was visually assessed. Image processing could be performed on the aluminum as an assessment tool of the destruction but would have been useful only for quantifying the gross amount of cavitation occurring in the vessel. Since chemical dosimetry was to be used, image analysis was not performed.

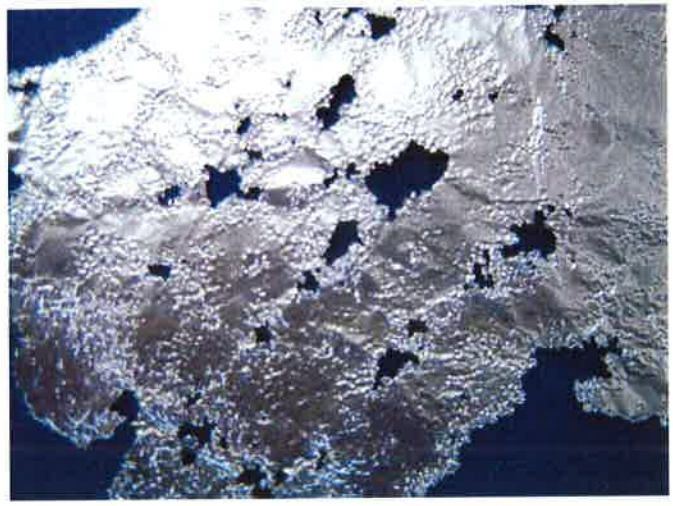

Figure 3-3: The result of cavitation exposure to a sheet of tinfoil. Note the small pit marks, severely damaged areas and regions where minimal cavitation activity occured showing an uneven cavitation distribution

The tinfoil test was used to ascertain the location and intensity of the points of high and low acoustic activity, rather than the gross amount of cavitation.

The result was the areas of foil under which intense cavitation occurred are destroyed, while the areas of minimal cavitation remained largely intact.

3.5.3 Chemical Dosimetry for the Quantification of Cavitation

Sonochemistry refers to chemical reactions catalysed by acoustic cavitation. It is estimated that temperatures of several thousand Kelvin and pressures of several hundred atmospheres are produced during the collapse of a transient void [14].

Under these conditions water molecules are split into free radicals that recombine to form hydrogen peroxide.

$$H_2O \rightarrow H + OH \tag{3.4}$$

$$2OH \rightarrow H_2O_2 \tag{3.5}$$

$$2OH \rightarrow O + H_2O \tag{3.6}$$

$$2O \rightarrow O_2 \tag{3.7}$$

$$\frac{1}{2}O_2 + 2H \rightarrow H_2O \tag{3.8}$$

The formation of hydrogen peroxide during cavitation could be used to provide quantitative data on transient cavitation. The quantity of hydrogen peroxide produced during sonication of a liquid can be determined using various techniques, one of which was documented by Weissler [12][11] and is, therefore, sometimes referred to as the Weissler Test. This could be related to the amount of transient cavitation occuring over a specified time period. One quantifying method was potassium iodide dosimetry. The hydrogen peroxide oxidises iodide to an I_3^- complex, iodine, (see equation 3.10). The amount of iodine released was determined by spectrophotometric analysis (OD_{352}, at a wavelength of 352nm) and used to calculate the amount of transient cavitation occurring in the liquid volume.

$$2KI + free\ radical \rightarrow I_2 + 2KOH \tag{3.9}$$

Where free radical = OH or O_2H

$$I_2 + I^- \leftrightarrow I_3^- \tag{3.10}$$

Verification of the test was performed by driving the bath at incremental electrical power levels of 50W steps.

A linear increase in cavitation production with increased electrical power was expected.

The chemical dosimetry results were assessed and are graphically represented in Figure 3-4. The graph shows a linear relationship between electrical power and OH produced with a correlation coefficient of 0.982 proving a just quantification method.

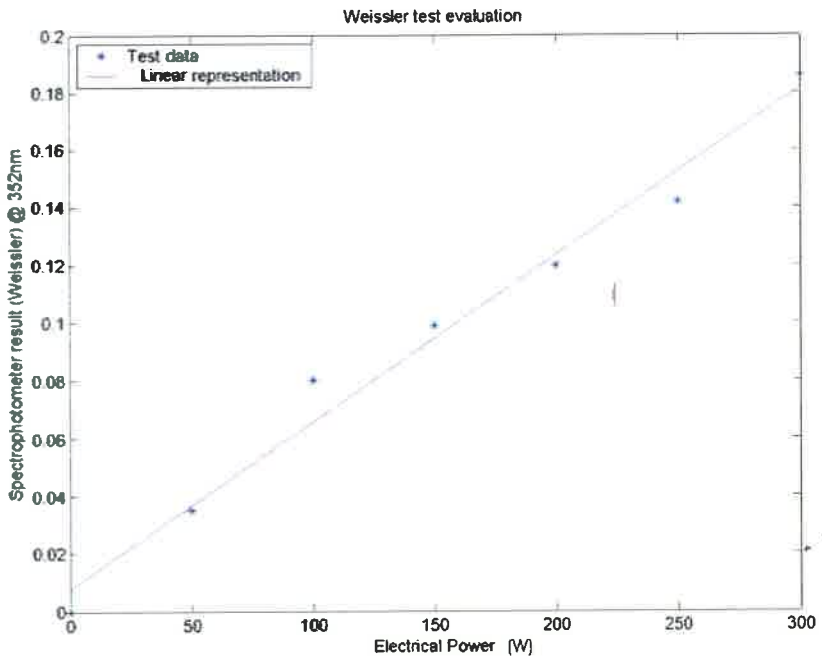

Figure 3-4: The varification of the Weissler Test. The bath was driven at 50W power increments from 0W to 300W RMS. A linear reponse was achieved confirming the Weissler Test's accuracy

Chapter 4

Straight Driving Techniques

4.1 Introduction

The resonant system of a PZT transducer is usually defined by a high quality factor and can be characterised by the graphs in Figure 4-1 [27].

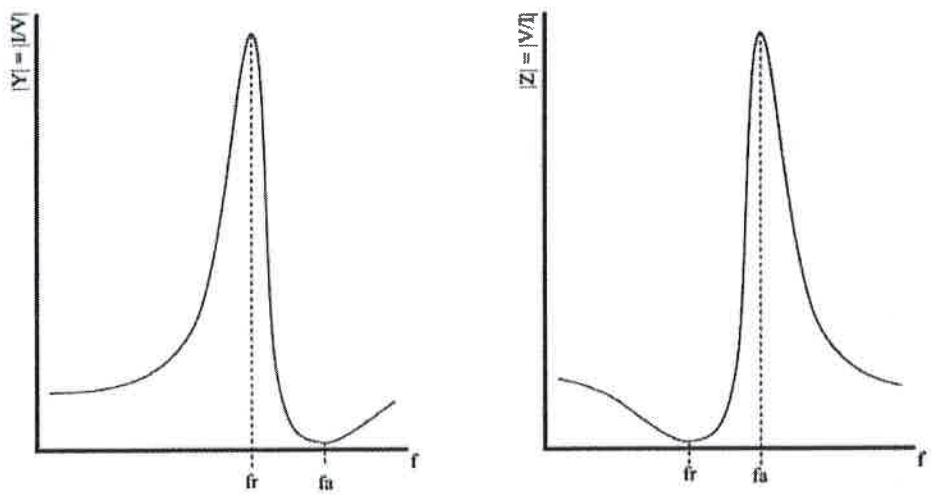

Figure 4-1: A visual description of the resonant characteristics of a typical PZT transducer. fr represents the series resonant frequency and fa represents the anti-resonant frequency;. fr can be seen as the series tuned mechanical resonant frequency

It was possible to determine the resonance point of the electro-mechanical series LCR (inductor/capacitor/resistor) system of the transducer model and drive it at that frequency. However, when PZT transducers driven at power were considered the resonance frequency shifted unpredictably [24] resulting in a pure straight driven system being inefficient both electrically and mechanically. Still, straight driving systems are used in industry [21] at a satisfactory level as the bandwidth of the load can be increased and the Q can be reduced by means of matching circuitry[4].

4.2 Inductor-Capacitor Resonant Circuits

When an LCR series circuit (or the electro-mechanical branch of the PZT transducer model) was driven at its resonance frequency, the current and voltage through the resistor were at maximum amplitude. The impedance of this system was then seen to be purely resistive and the phase angle between the current and voltage zero degrees. If the driving frequency was changed, the system would not act in its resonant mode, but become inefficient as reactive power was dissipated. The narrow bandwidth of most PZT transducers results in large changes in the phase and admittance of the load for small shifts in the frequency domain. The changes result in the system being inefficiently driven. As the mechanical loading of the transducer was increased the Q decreased and the bandwidth increased, making the system more compatible with straight driving techniques. High frequency transducers (above 100kHz) are more susceptible to straight driving techniques than low frequency transducers (20kHz to 100kHz) as the reduction in the Q and increased bandwidth is considerably more apparent in such transducers [4]. Coates *et al* [4] suggests using straight driving techniques in ultrasonic systems functioning above 100kHz, rather than systems functioning at lower frequencies.

4.3 Matching Networks

To simplify the electro-mechanical model of the PZT transducer, reactive components could be added to match the system at particular frequencies. Phillips [27] recommends electrically tuning PZT transducers in series or parallel topologies with a single inductor.

Figure 4-2 shows a series tuned circuit with an inductor added in series to a transducer. The mechanical capacitance (C) added to the static capacitance (C-static) and the new inductor (Ls, added inductor) are made to resonate at the anti-resonant frequency, fa. In this case, the anti-resonant frequency was used as at this frequency the impedance of the series tuned transducer was purely resistive [27]. This is the frequency at which the minimum admittance (Y) peak was found after fr (see Figure 4-1). The minimum admittance peak could be equated to the maximum impedance (Z) peak, because $Y = \frac{1}{Z}$

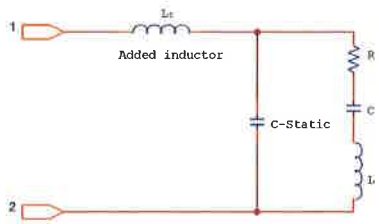

Figure 4-2: The series tuned transducer system showing the added series inductor (Ls). This inductor is calculated to resonate with the combined capacitance of C-static and C at the anti-resonant frequency of the system

The following equation (4.1) can be used to calculate the value of the required inductor for series tuning:

$$Ls = \frac{1}{(2\pi f_a)^2 C_{static}} \tag{4.1}$$

A parallel matched circuit is seen in Figure 4-3. This method matches the driving device to the load using an inductor added in parallel to the transducer. The added inductor, seen in figure 4-3, is tuned to the electrical 'static' capacitance (C_{static}) allowing the inverter to drive only the motional series tuned circuit (R, L and C).

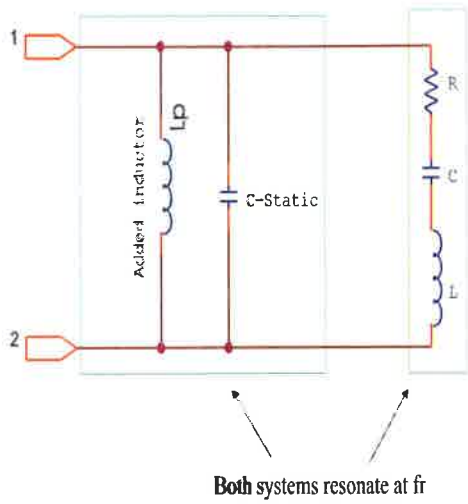

Figure 4-3: The parallel tuned PZT transducer showing the added inductor (Lp) and the two resonant systems. This method of tuning forces the driving power to be directed through the motional arm of the transducer ensuring the generation of acoustic power at the series resonant frequency (fr)

Equation 4.2, can be used to calculate the value of the inductor required for parallel tuning [27]:

$$Lp = \frac{1}{(2\pi f_r)^2 C_{static}} \tag{4.2}$$

This driving technique can be used only at the designed frequency, fr, [27] which by definition changes when the transducer is driven at power [24].

A third type of matching used is termed Q matching. This technique is mainly used when switching power amplifiers are utilised. The technique enables the user to change the Q of the PZT load and use it to filter the harmonics of the produced square wave. As Q matching is mainly considered for switching power amplifiers, a brief discussion was added as an appendix (see *Appendix C*), to this document.

4.3.1 Problems with Straight Driving

All matching systems rely on the addition of expensive reactive components and the common assumption is made that the fundamental resonance frequency of the system will always be identical. Unfortunately PZT transducers, cavitation and resultant energies make PZT systems nonconstant electrical loads. Matching can make the system appear more stable by increasing bandwidth but inevitably energy will be lost in the reactive form causing heat and an inefficient system as compensation is not made for the changes in the resonant frequency. For the tests in this project matching systems were not implemented as they are not suitable over the large bandwidths used in sweeping techniques. As sweeping systems were tested, additional external matching circuitry was not feasible.

4.4 Circuit Design and Analysis

The straight driving system was developed using a function generator and a power amplifier. The signal generator created a sinusoidal wave that was amplified and used to drive the transducer array directly. The frequency and amplitude of the drive signal could be changed by alteration of the function generator's output during testing procedures. No matching circuitry was used in tests conducted.

4.5 Test Procedures and Results

The straight driving technique was evaluated using acoustic scans, chemical dosimetry tests and the tinfoil test. The three tests were performed to create a benchmark to which the other driving techniques could be compared.

4.5.1 Acoustic Scan

Aim

The aim of this test was to evaluate the spread of acoustic energy inside the test rig by means of a graphical representation of the average pressure throughout a single level of the bath. This was used to determine the node and antinodal behaviour. The result could be evaluated by visual inspection and compared to scans of other driving techniques. This test was valid only at low power levels where cavitation did not occur, as the delicate hydrophone faced damage if exposed to a cavitation field.

Apparatus

- Needle hydrophone: An HP series high performance hydrophone measurement set from Precision Acoustic UK was used. A tip with a diameter of 0.5mm was used for the tests;

- the constructed XY plotter: Discussed in Chapter 3;
- a programme written in LABVIEW (7) and a National Instruments high speed data acquisition interface card (PCI-6221);
- the test bath, discussed in Chapter 3;
- Crest Audio Amplifier (CA6);
- function generator (Escort EFG-3210) and,
- 4l of distilled water.

Method

The XY plotter was positioned above the bath with the needle hydrophone tip set 50mm from the bottom of the bath. This level was chosen as it was about halfway between the liquid surface and the bottom. The bath was filled with 4l of distilled water. Labview was used as a tool to automate the scanning process. The user entered the length and width of the surface to scan as well as the step size between measurements. The step size used for the tests was set at 5mm. When the programme ran, the plotter moved to the required position, read a measurement from the hydrophone and saved its average acoustic pressure value to an array, along with the X and Y position of the tip. The movement of the probe followed a pattern of one length scan, followed by one width movement followed by a length scan in reverse. This was followed by another width scan until the entire surface was scanned at the required depth and readings saved (Labview programme, see *Appendix A*). The saved file was then manipulated in Matlab (see *Appendix B*) resulting in a three-dimensional surface plot of the power profile inside the vessel. The signal generator was used as a VCO to generate a sinusoidal wave which was amplified using the Crest Audio Amplifier to drive the transducer array directly.

Results

The acoustic field occurring during low power operation showed definite regions of high and low acoustic power levels, see Figure 4-4. Note specifically the two deep blue areas near the centre of the plot. These areas showed to be little affected by the acoustic field, whereas the regions in red were greatly affected.

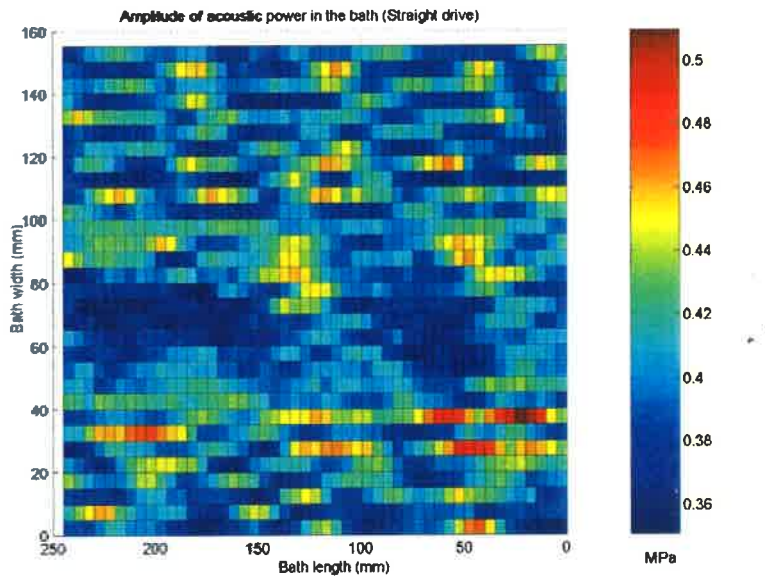

Figure 4-4: The result of the low powered acoustic scan. An uneven distribution of acoustic pressure can be seen indicating that straight driving is not the ideal driving method for high powered PZT arrays

Figure 4-4 shows that an even distribution of acoustic power was not achieved. This driving technique was therefore, not ideal for large application volumes where PZT transducer arrays are required.

4.5.2 Chemical Dosimetry

Aim

A chemical dosimetry test, sometimes referred to as the Weissler Test [12] can be performed to evaluate the amount of transient cavitation occurring inside a cavitation vessel. Later the result will be compared with the results from other driving techniques.

Apparatus

- The test bath, discussed in Chapter 3;
- Crest Audio Amplifier (CA6);
- function generator (Escort EFG-3210);
- spectrophotometer capable of measuring wavelengths of 352nm (Jenway 6300);
- cuvettes for spectrophotometer ($1000\mu l$);
- 4l of distilled water;
- ammonium hepthomolydate, catalytic agent ($((NH_4)^6MO_7(O_2)^44H_2O)$;
- potassium iodide (KI);
- 1ml Gilson pipette (P1000) and,
- measuring scale (0.01g accuracy).

Method

Potassium iodide was mixed with distilled water in the proportion of 16.6g/litre. The catalyst, ammonium hepthomolydate, was then added with a concentration of 0.1g/litre. The solution was mixed thoroughly, exhibited an endothermic reaction and resulted in a solution called "The Weissler solution". The Weissler [12] solution was then poured directly into the cavitation vessel and ultrasound was generated for a predetermined time of five minutes.

The five-minute exposure was found to be sufficient as a significant light absorption at 352nm could be achieved.

After exposure a 1ml sample of the liquid was compared to a blanking sample taken before cavitation exposure. The light absorbance at 352nm was measured using a spectrophotometer and the result was the difference between the sample and the blank. Repeatability of the test was performed by the completion of five consecutive tests.

Result

The graph shown in Figure 4-5 shows the result of five consecutive chemical dosimetry tests. The expected result was achieved showing a near linear relationship between the electrical power and the Weissler result.

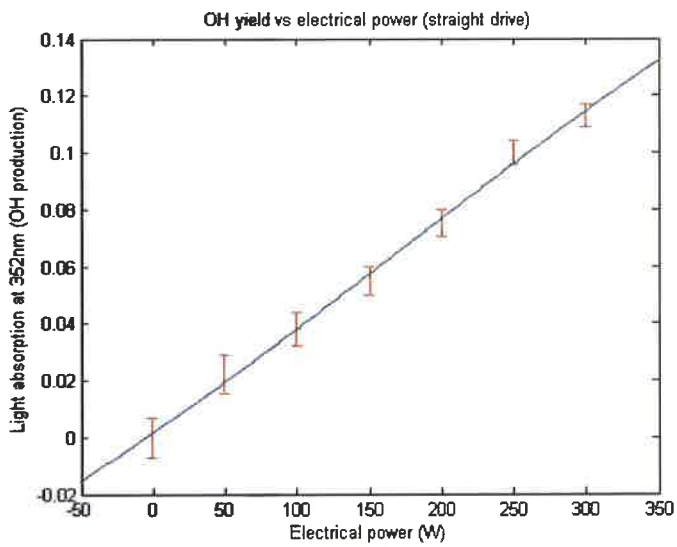

Figure 4-5: The chemical dosimetry results of the straight drive system. As expected, a near linear relationship between OH yield and electrical power was achieved

4.5.3 Tinfoil test

Aim

This test was used to crudely illustrate both cavitation location and the amount of cavitation activity inside the vessel by means of the visible destruction of the foil. The results were used to ascertain whether or not standing waves were present and if all the transducers in the array were functioning properly.

Apparatus

- The test bath, discussed in Chapter 3;
- Crest Audio Amplifier (CA6);
- function generator (Escort EFG-3210);
- tinfoil with thickness of $10\mu m$ and,
- 4l of distilled water.

Method

During this test a sheet of aluminium foil was placed inside the cavitation medium 10mm from the bottom of the bath. The electrical power being dissipated in the system was measured over the 1.5 minute exposure time using the National Instruments data acquisition card.

Result

The tinfoil in Figure 4-6 shows five definite holes representing the positions of five of the six transducers in the array. One transducer showed minimal impact on the foil, disclosing it was either functioning in a mechanical mode not transferring acoustic energy into the liquid, or being driven off its resonant frequency.

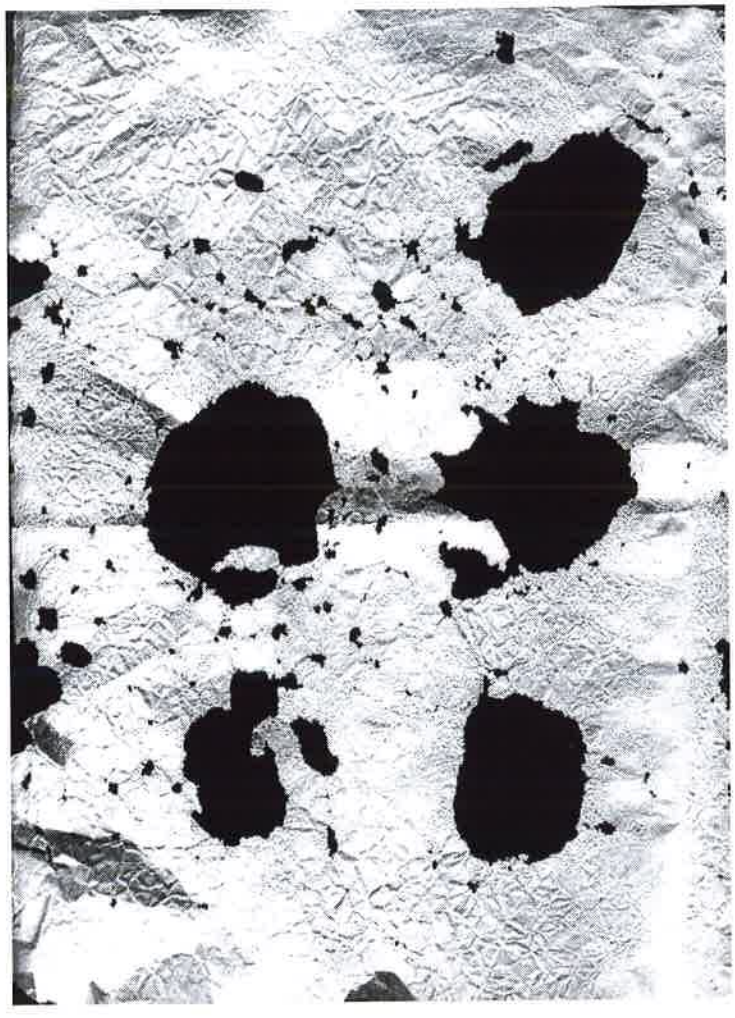

Figure 4-6: The straight drive tinfoil test result shows one of the six transducers was not fully functional

This result clearly showed straight driving techniques were unsuited in applications requiring high powered PZT arrays because of the changing electrical characteristics of the PZT array.

Chapter 5

Phase Locking versus Admittance Locking

5.1 Overview of Locking Systems

Piezoelectric transducers used in high power applications are either sandwich or horn concentrators [7]. These transducers have high quality factors, implying the usable bandwidth is narrow. Locking systems are used to maintain specific operation conditions as the characteristics of a load change. In order to maintain optimal operation in the narrow bandwidth, adjustments in the frequency domain can be continually made. The systems studied in this chapter track either a specified phase angle or the admittance peak of the load.

Figure 5-1 shows the admittance and phase of the load as well as the phase locking bandwidth and the point of lock used in admittance locking. Another method of phase locking is self-oscillation. To establish a self-oscillating system, unity gain and zero phase difference between voltage and current is required. Once these conditions are met, zero degree phase angle is tracked as the load changes. Self-oscillating driving systems are not evaluated in this thesis as the optimal phase angle for PZT transducers is not zero degrees [7].

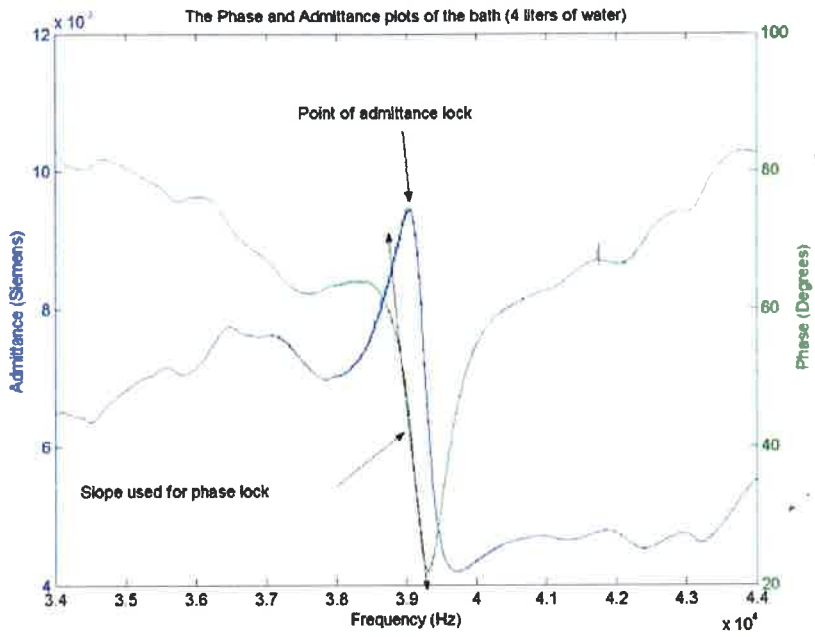

Figure 5-1: This graph shows the admittance and the phase of the bath with 4l of distilled water added. Phase locking requires a monotonic slope, indicated on the graph, on which to function. The peak of the admittance graph (indicated) is where admittance locking occurs

Many high power electronic applications driving complex impedance loads (such as PZT ultrasonic transducers) in resonance utilise PLL (phase locked loop) systems. In many cases, zero phase difference between the current and voltage ensures maximum active power to the load [19]. Self oscillating and PLL techniques are ideally suited to these applications as zero phase is achieved and tracked.

The Tonpilz PZT transducer's resonance point usually occurs when the voltage and current are not in, but are slightly out of phase [7]. PLL systems can be made to lock at a user defined phase angle away from the region of 0°. Phase locking techniques have been implemented successfully in many PZT systems in which single transducers are used.

Davies *et al [7]* recommend the changing dynamics in a PZT transducer can be controlled by an automatic control system that tracks the point of maximum admittance. Maximum power transfer from the transducer to the medium occurs at maximum admittance. Admittance locking continually tracks the maximum input admittance of the transducer in order to follow the maximum point of absolute electrical power [7].

Phase locking and admittance locking will be discussed and evaluated in this chapter. A comparison between these locking techniques and straight driving will be made.

5.2 Phase Locked Loops

5.2.1 Overview

Continuous wave phase locking systems are regarded as common elements in electronic design and are extensively used to drive both high and low power ultrasonic devices [6]. Phase locked loops are used to control an oscillator which maintains a constant phase angle relative to a reference signal [25].

When a PLL system is considered, the output frequency tracks the input frequency by means of a phase feedback mechanism using the phase difference between the input and output signals. The difference in phase is represented by a DC voltage that is used to control a voltage-controlled oscillator.

Upon lock, the controlling DC voltage from the phase detector maintains the output frequency of the VCO to exactly equal the average input frequency [6].

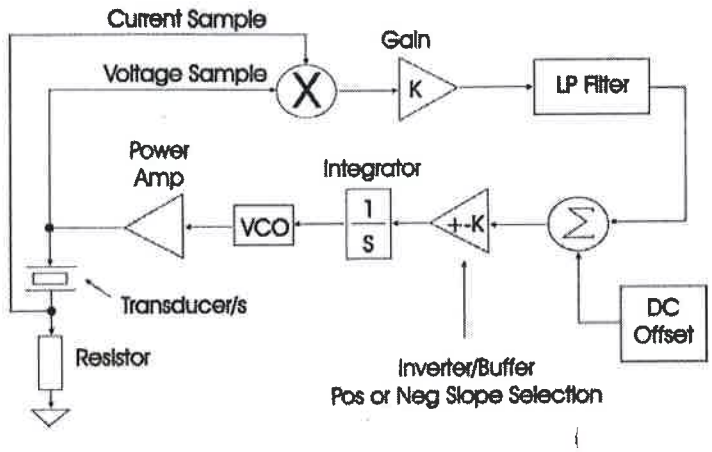

Figure 5-2: A block diagram showing the main components of a phase locking system. Note the DC offset used to lock the system onto a point other than that of zero degrees phase

In order to manually lock a PLL at a frequency off that of 0° phase (where, at resonance, the phase of the voltage and current of PZT transducers is not 0°) a DC offset (see Figure 5-2) is added to the phase detectors DC output. This forces the system to lock at a predetermined phase angle away from 0°, generally required at the PZT transducers resonant point. A block diagram of a phase locked loop is seen in Figure 5-2.

Simple operation and vast use in the power electronics field make PLL systems a choice for use in resonant ultrasonic arrangements. The fact the phase at resonance is not 0° requires the system locks to a user-determined phase angle rather than 0°. The problem with a preset phase angle is the characteristics of the load change [24] meaning the resonance point might drift causing the system to lock off resonance and be driven in an inefficient electromechanical manner [24].

The inverse piezoelectric effect causes high powered piezoelectric transducers to act as receivers, receiving reflected waves from the medium.

The high pressures created during transient cavitation cause much noise to be converted into electrical energy which causes "noise" to be superimposed on the monotonic phase slope. PLL systems are monotonic and, therefore, require a smooth resonant curve on-which to operate correctly. Slight variations in the resonant system can drive the PLL away from the desired resonant point. Received mechanical signals are sometimes so strong and irregular that the equivalent impedance characteristics of the loaded transducer become variable, losing any controllable form [21].

5.3 Evaluation of Phase Locking

Primary evaluation of phase locking was used to assess cavitation activity being created in the bath. This was to be compared to the admittance driving technique. The suspicion that all the transducers were not dissipating equal amounts of electrical energy would be evident, in the tinfoil test, as the cavitation density around each transducer would not be equal. This was evident by varying amounts of local tinfoil decay around the transducers. The test was also used to evaluate whether phase locking could be locked off resonance resulting in an ineffective driving method.

5.3.1 Tinfoil

Aim

This test was used to illustrate both cavitation location and the amount of cavitation activity inside the vessel when driven by the phase locking system. The results were used as evaluation tools to compare driving techniques. The test was also used to prove that phase locking, if set at the incorrect phase angle, was ineffective.

Apparatus

- The test bath (see Chapter 3);
- Crest Audio Amplifier (CA6);

- phase locking circuit (see *Appendix D*);
- function generator (Escort EFG-3210);
- tinfoil with a thickness of $10\mu m$ and,
- 4l of distilled water.

Method

During this test a sheet of aluminium foil was placed inside the cavitation medium 10mm from the bottom of the bath. The electrical power injected into the system was measured for 1.5 minute exposure.

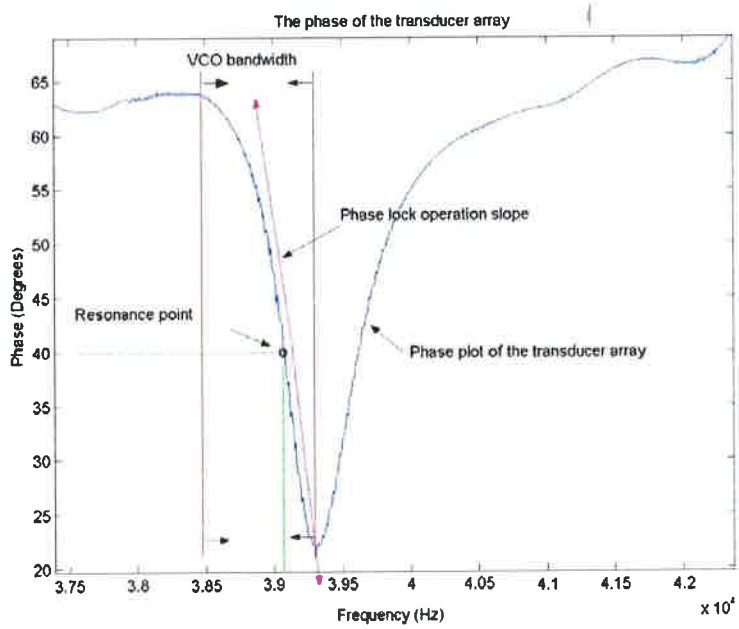

Figure 5-3: The monotonic slope on which the phase locked loop will operate is represented by the magenta arrow. The bandwidth, determined by the slope falls between the two red lines and the resonance point of the array has been marked on the plot

Figure 5-3 shows the region including and surrounding the frequency of the resonance of the transducer array. The bandwidth of the VCO was set to 800Hz, from 38.5kHz to 39.3kHz.

The resonance point of the array was measured to be at a phase of 40° which fell within the bandwidth and has been indicated by a o in Figure 5-3. The monotonic slope on-which the PLL was operated is represented by the magenta arrow.

Results

The test result shown in Figure 5-4 depicts a large amount of destruction resulting from a measured electrical power of 70W RMS. The phase angle was set at 40°. It can be seen that two transducers functioned indifferently, while four others functioned well. Circular patterns can be seen around the holes depicting the presence of standing waves, some of which are marked in red in Figure 5-4. Standing waves such as those responsible for the ring patterns are undesirable in most cavitation field applications as components in cleaning baths and chemicals being processed might be damaged [21].

In an attempt to illustrate the fundamental problem with phase locking systems, the bath was deliberately locked at a phase angle 10° away from the optimal phase angle. The phase was locked at 30° as opposed to the previous phase angle of 40°. The destruction of the foil (electrical power of 64W RMS measured over test cycle) is seen in Figure 5-5. Far less destruction occurred although electrical power was decreased by only 8.6%. The system was clearly not functioning optimally. Instead of being converted into usable mechanical energy, much of the electrical power was dissipated in the imaginary domain and unwanted mechanical modes of the transducers.

The results support the hypothesis that driving methods such as phase locking, which lock onto a combinational resonance point of a transducer array, are inefficient driving techniques for such loads. Also, the effectiveness of the technique depended directly on the user defined phase angle. In mass produced systems, each device would require manual tuning and even then, because of the dynamics of the PZT transducer [24], the system could, over time, become inherently inefficient.

Figure 5-4: The destruction of tinfoil after exposure for 1.5 minutes when the bath was driven by the phase locking system. The average electrical power measured over this test was 70W RMS. Note the large amount of destruction to the upper section of the foil and the four holes showing that four transducers were dissipating most of the electrical power. The relatively undamaged area in the lower portion shows two transducers were not dissipating enough electrical power to cause destruction of the tinfoil

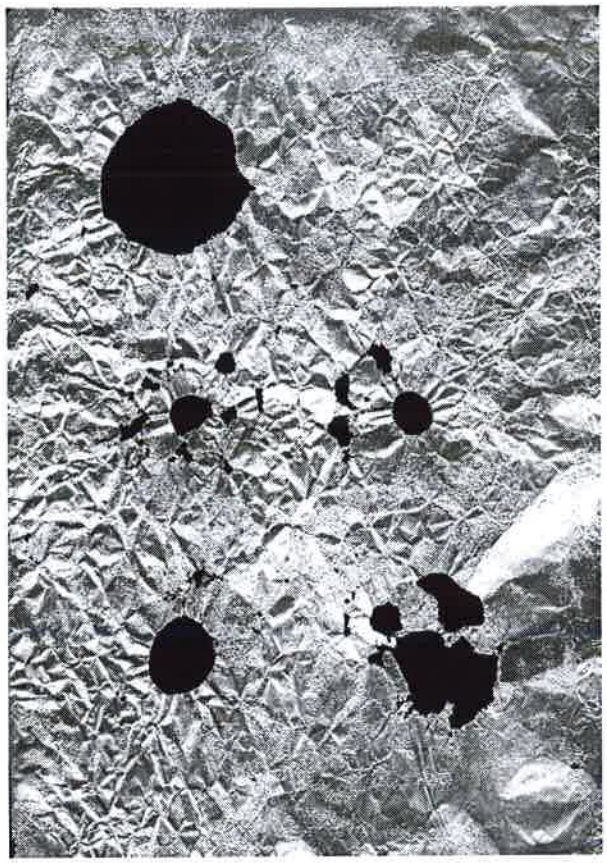

Figure 5-5: The result of the system being locked 30° from the optimal phase angle. Here an RMS power of 64W was measured over the test cycle. Note the large reduction in the destruction of the foil meaning that much electrical power was dissipated in the imaginary domain

5.4 Admittance Locking

5.4.1 Background

To overcome the need for a preset, user defined, resonance point, such as the user defined phase angle required for phase locking, a tracking technique nonreliant on the phase of the load needed to be assessed. When ultrasonic transducers are driven as voltage fed systems the power dissipated is proportional to the electrical current. Maximum electrical power delivery is achieved at resonance and, therefore, maximum current is required. Admittance is calculated by dividing the current by the voltage and the voltage is kept constant leaving the variable, current, proportional to the admittance which itself is proportional to the electrical power being dissipated. A current sample was the only sample required in this locking technique making it simple to implement. The current sample was used to effectively plot the admittance curve of the system, while the transducers were driven at high power. "Hill climbing" techniques can be used to continually track the highest admittance peak in a predetermined frequency band and maintain operation at this frequency [7].

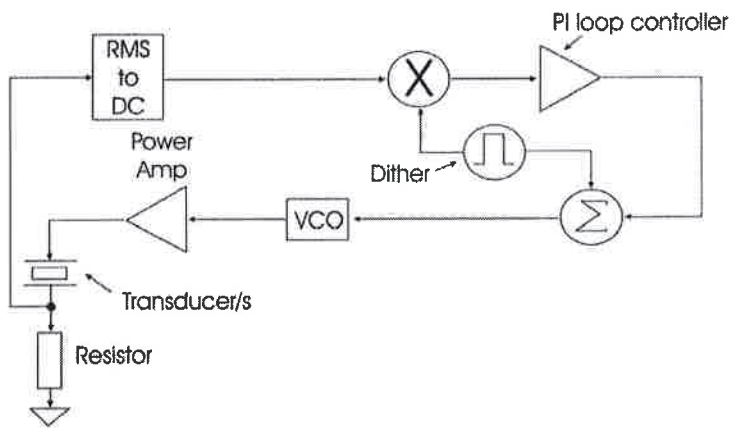

Figure 5-6: "Admittance locking" as proposed by Davies *et al* [7]

An RMS to DC converter is used to convert a current sample into a DC value to be used in the feedback loop.

A small dither with a 50% duty cycle is then added to the transducer drive frequency. The dither causes a small modulation on the transducer current due to the fact that the transducer shifts its operating frequency slightly. The magnitude of the transducer current detected by the RMS to DC converter includes a small signal because of the dither modulation. The dither oscillator is used to synchronously detect and demodulate this small signal. The output of the demodulator represents the slope of the admittance curve, $\frac{dY}{df}$ (Y = Admittance, f = Frequency). A PI controller moves the VCO set point to the local admittance maximum. This circuit establishes the direction in which to move the operating frequency. Admittance locking shifts the operation frequency to the point where the transducer current is maximum and $\frac{dY}{df} = 0$ and continually tracks this frequency.

This arrangement has the advantage that only the current needs to be sampled in the locking process. Furthermore, it is claimed the locking system will establish the optimum operating point for the case of any frequency dependent load [7].

5.4.2 Digital Admittance Locking

For the purpose of this study a digital admittance locking system was built using a PIC microcontroller (PIC16F877). The current was converted to a DC value by means of an RMS to DC converter. The DC value was sampled by the on-board 10-bit analogue to digital converter. The data was processed and a resultant 8-bit PWM signal with a carrier frequency of 15kHz produced. This value was filtered via a low pass filter resulting in a signal to control the VCO driving the transducer array.

The software developed to run the system performed the following routines and can be seen in *Appendix E*:

On startup the digital admittance locking system was made to perform a frequency sweep of the entire preset bandwidth. As the sweep commenced, the frequency at which the highest admittance was achieved was recorded. At the end of the sweep the drive frequency was set to the point of maximum current demand (the admittance peak) and tracking began.

Tracking the admittance peaks was performed using a process called "Hill climbing" [7] (see Figure 5-7).

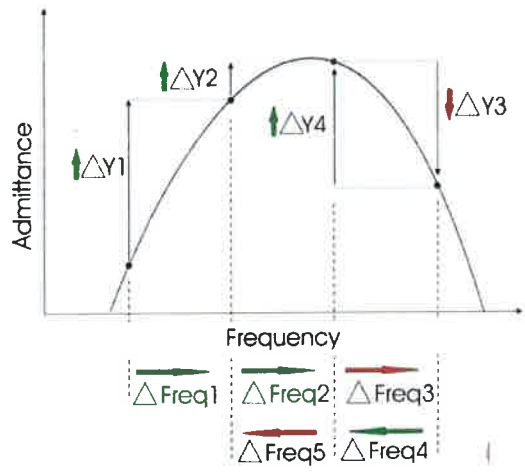

Figure 5-7: An illustration of the "Hill climbing" technique used in admittance locking. A 'dither' is used to assess whether the admittance decreases or increases as the frequency is changed

"Hill climbing" [7] is a technique used to track the highest peak of a frequency dependent, dynamic resonant system. The system is pre-programmed with a specific bandwidth. When initiated, a sweep of the bandwidth was used to identify the dynamic centre frequency of an ultrasonic load. The tracking shifted the drive frequency in set incremental step sizes (Δ frequency) and acquired a current sample at each point that was compared to the previous sample. If the current amplitude was less than the previous reading the system stepped down in frequency and remeasured the current. If the current read more than the previous step, an increase in frequency was required. This process continued until the admittance peak was found and even then continued in order to track the dynamic changes of the load. If Figure 5-7 is consulted one can see that for the first and second frequency steps (Δ freq1 & Δ freq2) the admittance increased (ΔY1 & ΔY2), therefore, the frequency was increased a third time (Δ freq3). The third step resulted in a decrease in the admittance (ΔY3) leading to a resultant decrease in the frequency (Δ freq4).

This caused an increase in the admittance (ΔY4) and another decrease in the frequency was made (Δ freq5). This step caused a decrease in the admittance and the system responded. Figure 5-7 shows large frequency steps or a low resolution. The step sizes used in the experiment were smaller resulting in a higher resolution and a closer lock to the maximum admittance peak was made possible.

5.5 Evaluation of Admittance Locking

Tinfoil was used to evaluate admittance locking in terms of cavitation produced and its distribution inside the vessel. The results were primarily used to compare admittance locking and phase locking. A chemical dosimetry test was also performed to measure which driving technique delivered more cavitation into the vessel when driven at specific electrical power levels.

5.5.1 Tinfoil

Aim

This test was used to illustrate both cavitation location and the amount of cavitation activity inside the vessel. The results were used as evaluation tools to compare straight driving, phase locking and admittance locking.

Apparatus

- The test bath (see Chapter 3);
- Crest Audio Amplifier (CA6);
- admittance locking circuit;
- function generator (Escort EFG-3210);
- tinfoil with thickness of 10μm and,
- 4l of distilled water.

Method

During this test a sheet of aluminium foil was placed inside the cavitation medium 10mm from the bottom of the bath. The electrical power dissipated over the array was measured for a duration of 1.5 minutes.

Results

Compared with phase locking, admittance locking created a large amount of destruction to the foil inside the vessel. This meant a large amount of cavitation activity had occurred. The activity, however, was centered around only three transducers of six showing an ineffectual distribution of cavitation to the bath and electrical power over the array. Standing waves were evident and represented by circular patterns, some of which have been marked in red in Figure 5-8.

The tinfoil result clearly showed admittance locking systems are unsuitable for applications where multiple PZT transducers are used, as equal decay at the transducer locations was not achieved.

5.6 Phase Locking vs Admittance Locking

5.6.1 Chemical Dosimetry

Aim

It is clear that phase locking and admittance locking systems deliver large amounts of acoustic energy into the vessel. A chemical dosimetry test can be performed to evaluate which driving system creates more transient cavitation. This evaluation will be performed on both techniques using the same experimental setup. The results from the tests will be plotted showing which of the two driving systems proved more effective. The result from the straight driving system will also be plotted to permit comparison between the three systems.

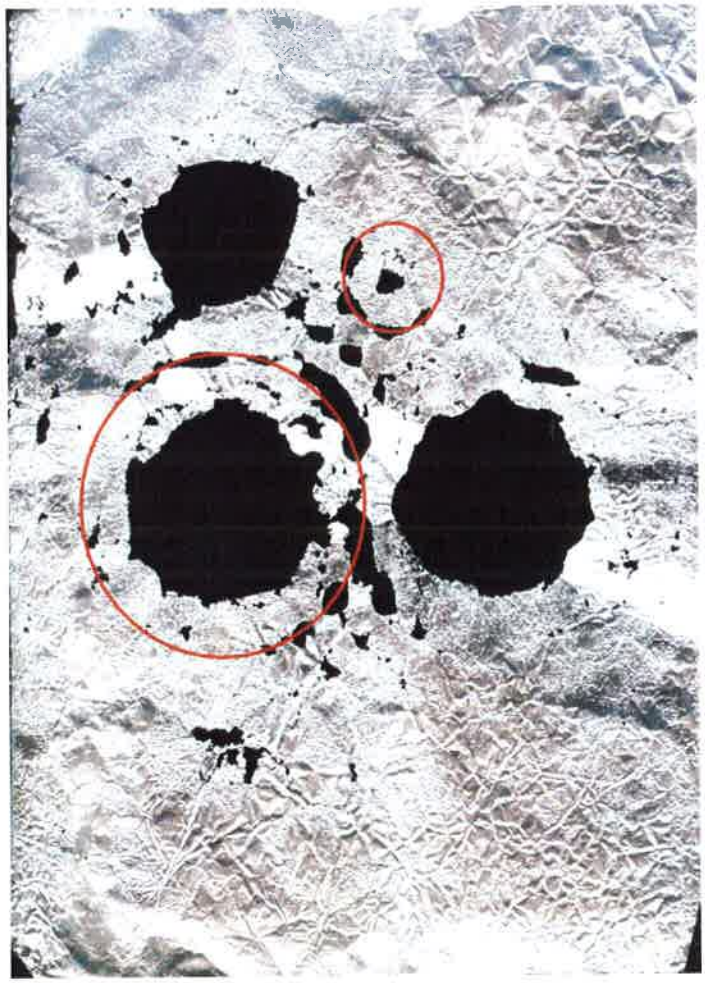

Figure 5-8: The result of the tinfoil test performed using digital admittance locking. Areas if intense cavitation activity as well as areas of minimal cavitation activity can be seen. The result shows that admittance locking does not optimally drive a PZT array at high power. Three transducers are barely operating while the other three are functioning well, illustrating an uneven spread of both electrical and acoustic energy

Apparatus

- The test bath, discussed in Chapter 3;
- Crest Audio Amplifier (CA6);
- phase locking and admittance locking system circuits;
- function generator (Escort EFG-3210);
- spectrophotometer capable of measuring wavelengths of 352nm (Jenway 6300);
- cuvettes for spectrophotometer (1000μl);
- 4l of distilled water;
- ammonium hepthomolydate, catalytic agent ($(NH_4)^6MO_7(O_2)^4 4H_2O$);
- potassium iodide (KI);
- 1ml Gilson pipette (P1000) and,
- measuring scale (0.01g accuracy).

Method

Potassium iodide was mixed into distilled water in a proportion of 16.6g/l. A catalyst, ammonium hepthomolydate, was then added at a concentration of 0.1g/l. The solution was mixed thoroughly and exhibited an endothermic reaction. The Weissler [12] solution was then poured directly into the cavitation vessel and cavitation produced for a predetermined time. Five minutes of ultrasonic exposure was used for the tests in this project. The five minute exposure was found to be sufficient in the production of iodine as a significant light absorption at 352nm could be achieved.

After exposure a 1ml sample of the liquid was compared to a blanking sample taken before cavitation exposure. The light absorbance at 352nm was measured and the difference between the sample and the blank became the result.

A linear increase in cavitation production with increased electrical power was expected.

The chemical dosimetry results were assessed and are graphically represented in Figure 3-4. The graph shows a linear relationship between electrical power and OH produced with a correlation coefficient of 0.982 proving a just quantification method.

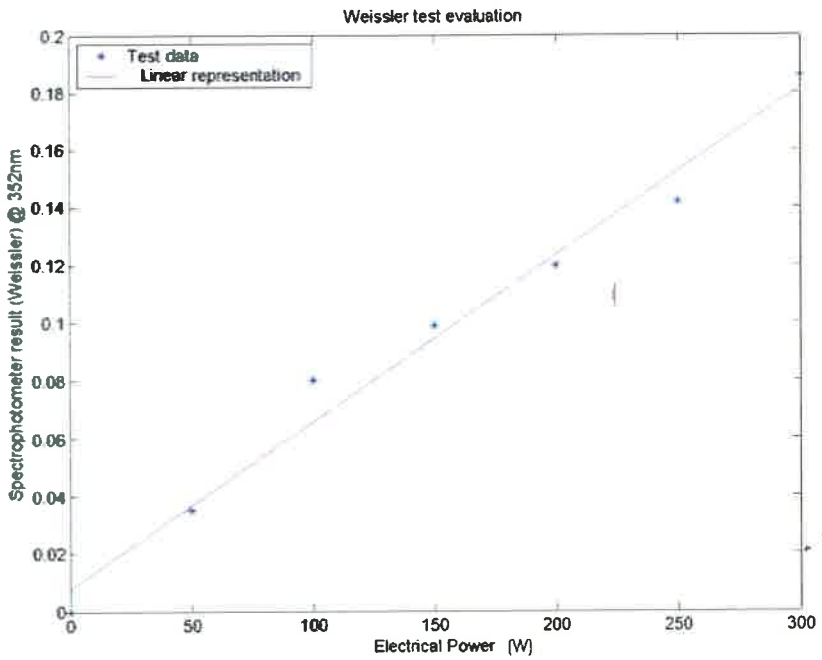

Figure 3-4: The varification of the Weissler Test. The bath was driven at 50W power increments from 0W to 300W RMS. A linear reponse was achieved confirming the Weissler Test's accuracy

Chapter 4

Straight Driving Techniques

4.1 Introduction

The resonant system of a PZT transducer is usually defined by a high quality factor and can be characterised by the graphs in Figure 4-1 [27].

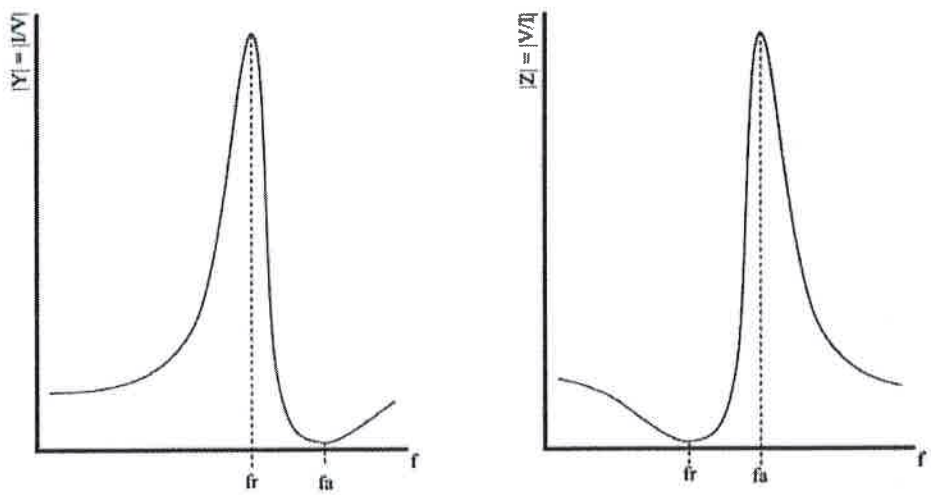

Figure 4-1: A visual description of the resonant characteristics of a typical PZT transducer. fr represents the series resonant frequency and fa represents the anti-resonant frequency;. fr can be seen as the series tuned mechanical resonant frequency

It was possible to determine the resonance point of the electro-mechanical series LCR (inductor/capacitor/resistor) system of the transducer model and drive it at that frequency. However, when PZT transducers driven at power were considered the resonance frequency shifted unpredictably [24] resulting in a pure straight driven system being inefficient both electrically and mechanically. Still, straight driving systems are used in industry [21] at a satisfactory level as the bandwidth of the load can be increased and the Q can be reduced by means of matching circuitry[4].

4.2 Inductor-Capacitor Resonant Circuits

When an LCR series circuit (or the electro-mechanical branch of the PZT transducer model) was driven at its resonance frequency, the current and voltage through the resistor were at maximum amplitude. The impedance of this system was then seen to be purely resistive and the phase angle between the current and voltage zero degrees. If the driving frequency was changed, the system would not act in its resonant mode, but become inefficient as reactive power was dissipated. The narrow bandwidth of most PZT transducers results in large changes in the phase and admittance of the load for small shifts in the frequency domain. The changes result in the system being inefficiently driven. As the mechanical loading of the transducer was increased the Q decreased and the bandwidth increased, making the system more compatible with straight driving techniques. High frequency transducers (above 100kHz) are more susceptible to straight driving techniques than low frequency transducers (20kHz to 100kHz) as the reduction in the Q and increased bandwidth is considerably more apparent in such transducers [4]. Coates *et al* [4] suggests using straight driving techniques in ultrasonic systems functioning above 100kHz, rather than systems functioning at lower frequencies.

4.3 Matching Networks

To simplify the electro-mechanical model of the PZT transducer, reactive components could be added to match the system at particular frequencies. Phillips [27] recommends electrically tuning PZT transducers in series or parallel topologies with a single inductor.

Figure 4-2 shows a series tuned circuit with an inductor added in series to a transducer. The mechanical capacitance (C) added to the static capacitance (C-static) and the new inductor (Ls, added inductor) are made to resonate at the anti-resonant frequency, fa. In this case, the anti-resonant frequency was used as at this frequency the impedance of the series tuned transducer was purely resistive [27]. This is the frequency at which the minimum admittance (Y) peak was found after fr (see Figure 4-1). The minimum admittance peak could be equated to the maximum impedance (Z) peak, because $Y = \frac{1}{Z}$

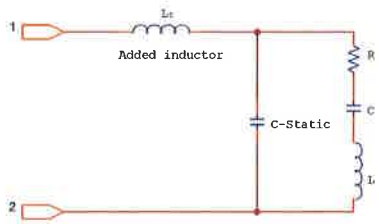

Figure 4-2: The series tuned transducer system showing the added series inductor (Ls). This inductor is calculated to resonate with the combined capacitance of C-static and C at the anti-resonant frequency of the system

The following equation (4.1) can be used to calculate the value of the required inductor for series tuning:

$$Ls = \frac{1}{(2\pi f_a)^2 C_{static}} \tag{4.1}$$

A parallel matched circuit is seen in Figure 4-3. This method matches the driving device to the load using an inductor added in parallel to the transducer. The added inductor, seen in figure 4-3, is tuned to the electrical 'static' capacitance (C_{static}) allowing the inverter to drive only the motional series tuned circuit (R, L and C).

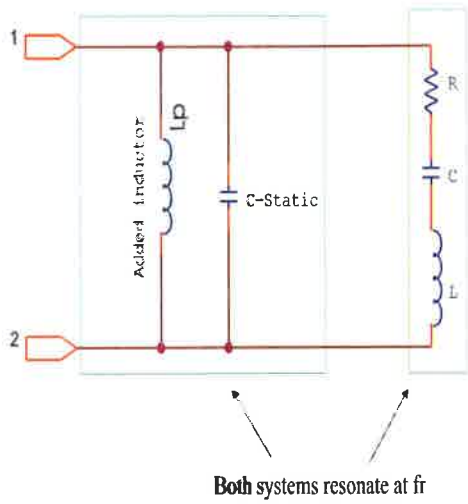

Figure 4-3: The parallel tuned PZT transducer showing the added inductor (Lp) and the two resonant systems. This method of tuning forces the driving power to be directed through the motional arm of the transducer ensuring the generation of acoustic power at the series resonant frequency (fr)

Equation 4.2, can be used to calculate the value of the inductor required for parallel tuning [27]:

$$Lp = \frac{1}{(2\pi f_r)^2 C_{static}} \tag{4.2}$$

This driving technique can be used only at the designed frequency, fr, [27] which by definition changes when the transducer is driven at power [24].

A third type of matching used is termed Q matching. This technique is mainly used when switching power amplifiers are utilised. The technique enables the user to change the Q of the PZT load and use it to filter the harmonics of the produced square wave. As Q matching is mainly considered for switching power amplifiers, a brief discussion was added as an appendix (see *Appendix C*), to this document.

4.3.1 Problems with Straight Driving

All matching systems rely on the addition of expensive reactive components and the common assumption is made that the fundamental resonance frequency of the system will always be identical. Unfortunately PZT transducers, cavitation and resultant energies make PZT systems nonconstant electrical loads. Matching can make the system appear more stable by increasing bandwidth but inevitably energy will be lost in the reactive form causing heat and an inefficient system as compensation is not made for the changes in the resonant frequency. For the tests in this project matching systems were not implemented as they are not suitable over the large bandwidths used in sweeping techniques. As sweeping systems were tested, additional external matching circuitry was not feasible.

4.4 Circuit Design and Analysis

The straight driving system was developed using a function generator and a power amplifier. The signal generator created a sinusoidal wave that was amplified and used to drive the transducer array directly. The frequency and amplitude of the drive signal could be changed by alteration of the function generator's output during testing procedures. No matching circuitry was used in tests conducted.

4.5 Test Procedures and Results

The straight driving technique was evaluated using acoustic scans, chemical dosimetry tests and the tinfoil test. The three tests were performed to create a benchmark to which the other driving techniques could be compared.

4.5.1 Acoustic Scan

Aim

The aim of this test was to evaluate the spread of acoustic energy inside the test rig by means of a graphical representation of the average pressure throughout a single level of the bath. This was used to determine the node and antinodal behaviour. The result could be evaluated by visual inspection and compared to scans of other driving techniques. This test was valid only at low power levels where cavitation did not occur, as the delicate hydrophone faced damage if exposed to a cavitation field.

Apparatus

- Needle hydrophone: An HP series high performance hydrophone measurement set from Precision Acoustic UK was used. A tip with a diameter of 0.5mm was used for the tests;

- the constructed XY plotter: Discussed in Chapter 3;
- a programme written in LABVIEW (7) and a National Instruments high speed data acquisition interface card (PCI-6221);
- the test bath, discussed in Chapter 3;
- Crest Audio Amplifier (CA6);
- function generator (Escort EFG-3210) and,
- 4l of distilled water.

Method

The XY plotter was positioned above the bath with the needle hydrophone tip set 50mm from the bottom of the bath. This level was chosen as it was about halfway between the liquid surface and the bottom. The bath was filled with 4l of distilled water. Labview was used as a tool to automate the scanning process. The user entered the length and width of the surface to scan as well as the step size between measurements. The step size used for the tests was set at 5mm. When the programme ran, the plotter moved to the required position, read a measurement from the hydrophone and saved its average acoustic pressure value to an array, along with the X and Y position of the tip. The movement of the probe followed a pattern of one length scan, followed by one width movement followed by a length scan in reverse. This was followed by another width scan until the entire surface was scanned at the required depth and readings saved (Labview programme, see *Appendix A*). The saved file was then manipulated in Matlab (see *Appendix B*) resulting in a three-dimensional surface plot of the power profile inside the vessel. The signal generator was used as a VCO to generate a sinusoidal wave which was amplified using the Crest Audio Amplifier to drive the transducer array directly.

Results

The acoustic field occurring during low power operation showed definite regions of high and low acoustic power levels, see Figure 4-4. Note specifically the two deep blue areas near the centre of the plot. These areas showed to be little affected by the acoustic field, whereas the regions in red were greatly affected.

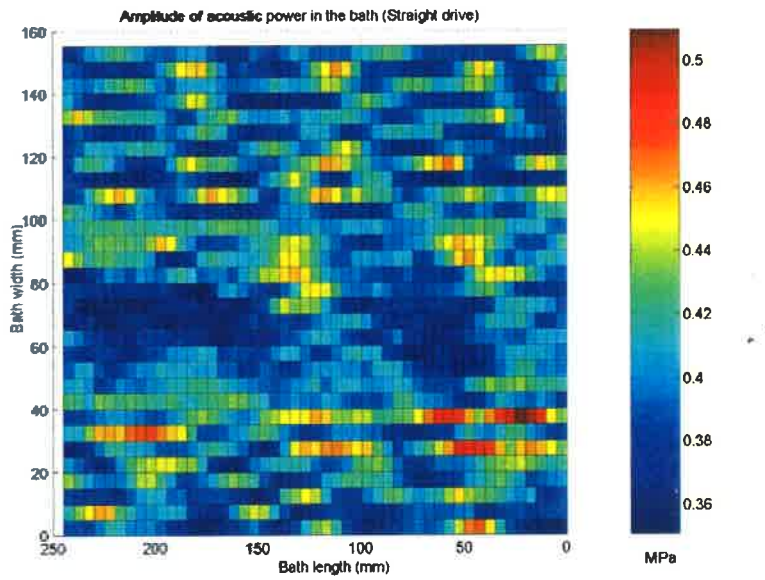

Figure 4-4: The result of the low powered acoustic scan. An uneven distribution of acoustic pressure can be seen indicating that straight driving is not the ideal driving method for high powered PZT arrays

Figure 4-4 shows that an even distribution of acoustic power was not achieved. This driving technique was therefore, not ideal for large application volumes where PZT transducer arrays are required.

4.5.2 Chemical Dosimetry

Aim

A chemical dosimetry test, sometimes referred to as the Weissler Test [12] can be performed to evaluate the amount of transient cavitation occurring inside a cavitation vessel. Later the result will be compared with the results from other driving techniques.

Apparatus

- The test bath, discussed in Chapter 3;
- Crest Audio Amplifier (CA6);
- function generator (Escort EFG-3210);
- spectrophotometer capable of measuring wavelengths of 352nm (Jenway 6300);
- cuvettes for spectrophotometer ($1000\mu l$);
- 4l of distilled water;
- ammonium hepthomolydate, catalytic agent ($((NH_4)^6MO_7(O_2)^44H_2O)$;
- potassium iodide (KI);
- 1ml Gilson pipette (P1000) and,
- measuring scale (0.01g accuracy).

Method

Potassium iodide was mixed with distilled water in the proportion of 16.6g/litre. The catalyst, ammonium hepthomolydate, was then added with a concentration of 0.1g/litre. The solution was mixed thoroughly, exhibited an endothermic reaction and resulted in a solution called "The Weissler solution". The Weissler [12] solution was then poured directly into the cavitation vessel and ultrasound was generated for a predetermined time of five minutes.

The five-minute exposure was found to be sufficient as a significant light absorption at 352nm could be achieved.

After exposure a 1ml sample of the liquid was compared to a blanking sample taken before cavitation exposure. The light absorbance at 352nm was measured using a spectrophotometer and the result was the difference between the sample and the blank. Repeatability of the test was performed by the completion of five consecutive tests.

Result

The graph shown in Figure 4-5 shows the result of five consecutive chemical dosimetry tests. The expected result was achieved showing a near linear relationship between the electrical power and the Weissler result.

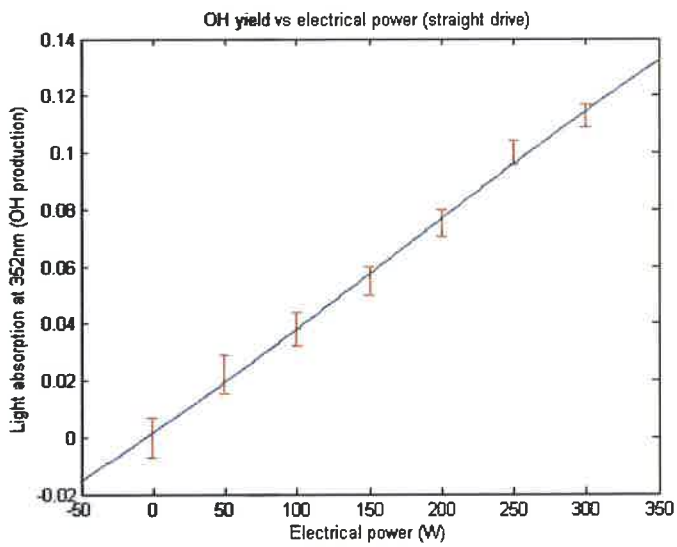

Figure 4-5: The chemical dosimetry results of the straight drive system. As expected, a near linear relationship between OH yield and electrical power was achieved

4.5.3 Tinfoil test

Aim

This test was used to crudely illustrate both cavitation location and the amount of cavitation activity inside the vessel by means of the visible destruction of the foil. The results were used to ascertain whether or not standing waves were present and if all the transducers in the array were functioning properly.

Apparatus

- The test bath, discussed in Chapter 3;
- Crest Audio Amplifier (CA6);
- function generator (Escort EFG-3210);
- tinfoil with thickness of $10\mu m$ and,
- 4l of distilled water.

Method

During this test a sheet of aluminium foil was placed inside the cavitation medium 10mm from the bottom of the bath. The electrical power being dissipated in the system was measured over the 1.5 minute exposure time using the National Instruments data acquisition card.

Result

The tinfoil in Figure 4-6 shows five definite holes representing the positions of five of the six transducers in the array. One transducer showed minimal impact on the foil, disclosing it was either functioning in a mechanical mode not transferring acoustic energy into the liquid, or being driven off its resonant frequency.

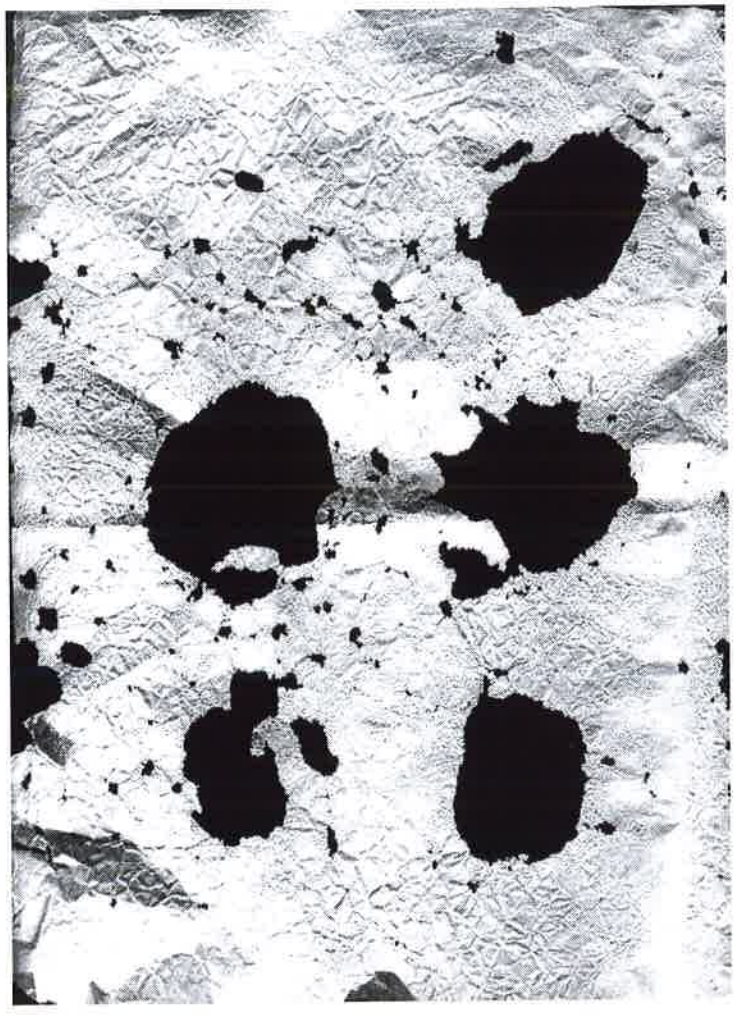

Figure 4-6: The straight drive tinfoil test result shows one of the six transducers was not fully functional

This result clearly showed straight driving techniques were unsuited in applications requiring high powered PZT arrays because of the changing electrical characteristics of the PZT array.

Chapter 5

Phase Locking versus Admittance Locking

5.1 Overview of Locking Systems

Piezoelectric transducers used in high power applications are either sandwich or horn concentrators [7]. These transducers have high quality factors, implying the usable bandwidth is narrow. Locking systems are used to maintain specific operation conditions as the characteristics of a load change. In order to maintain optimal operation in the narrow bandwidth, adjustments in the frequency domain can be continually made. The systems studied in this chapter track either a specified phase angle or the admittance peak of the load.

Figure 5-1 shows the admittance and phase of the load as well as the phase locking bandwidth and the point of lock used in admittance locking. Another method of phase locking is self-oscillation. To establish a self-oscillating system, unity gain and zero phase difference between voltage and current is required. Once these conditions are met, zero degree phase angle is tracked as the load changes. Self-oscillating driving systems are not evaluated in this thesis as the optimal phase angle for PZT transducers is not zero degrees [7].

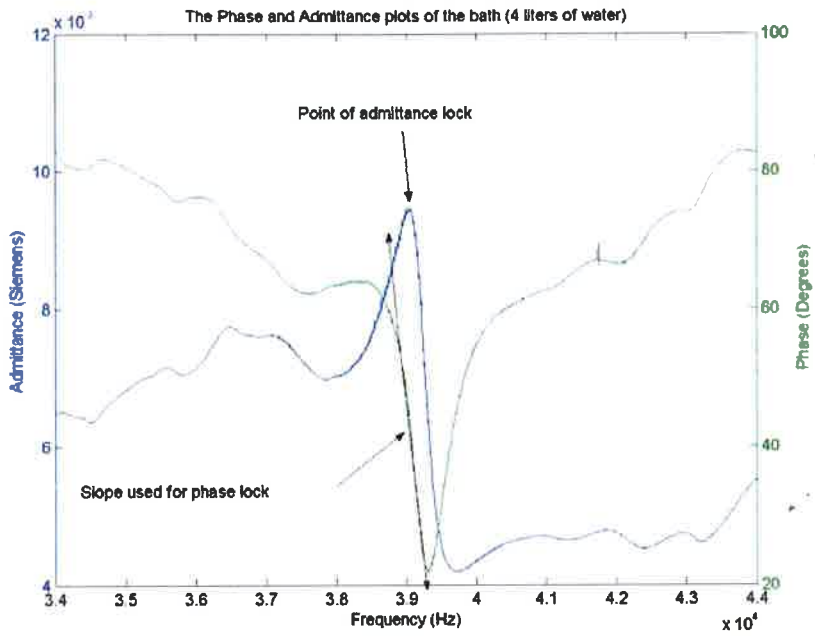

Figure 5-1: This graph shows the admittance and the phase of the bath with 4l of distilled water added. Phase locking requires a monotonic slope, indicated on the graph, on which to function. The peak of the admittance graph (indicated) is where admittance locking occurs

Many high power electronic applications driving complex impedance loads (such as PZT ultrasonic transducers) in resonance utilise PLL (phase locked loop) systems. In many cases, zero phase difference between the current and voltage ensures maximum active power to the load [19]. Self oscillating and PLL techniques are ideally suited to these applications as zero phase is achieved and tracked.

The Tonpilz PZT transducer's resonance point usually occurs when the voltage and current are not in, but are slightly out of phase [7]. PLL systems can be made to lock at a user defined phase angle away from the region of 0°. Phase locking techniques have been implemented successfully in many PZT systems in which single transducers are used.

Davies *et al [7]* recommend the changing dynamics in a PZT transducer can be controlled by an automatic control system that tracks the point of maximum admittance. Maximum power transfer from the transducer to the medium occurs at maximum admittance. Admittance locking continually tracks the maximum input admittance of the transducer in order to follow the maximum point of absolute electrical power [7].

Phase locking and admittance locking will be discussed and evaluated in this chapter. A comparison between these locking techniques and straight driving will be made.

5.2 Phase Locked Loops

5.2.1 Overview

Continuous wave phase locking systems are regarded as common elements in electronic design and are extensively used to drive both high and low power ultrasonic devices [6]. Phase locked loops are used to control an oscillator which maintains a constant phase angle relative to a reference signal [25].

When a PLL system is considered, the output frequency tracks the input frequency by means of a phase feedback mechanism using the phase difference between the input and output signals. The difference in phase is represented by a DC voltage that is used to control a voltage-controlled oscillator.

Upon lock, the controlling DC voltage from the phase detector maintains the output frequency of the VCO to exactly equal the average input frequency [6].

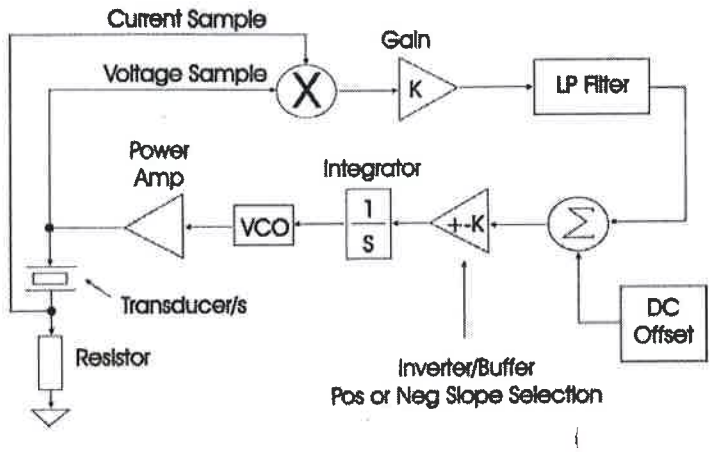

Figure 5-2: A block diagram showing the main components of a phase locking system. Note the DC offset used to lock the system onto a point other than that of zero degrees phase

In order to manually lock a PLL at a frequency off that of 0° phase (where, at resonance, the phase of the voltage and current of PZT transducers is not 0°) a DC offset (see Figure 5-2) is added to the phase detectors DC output. This forces the system to lock at a predetermined phase angle away from 0°, generally required at the PZT transducers resonant point. A block diagram of a phase locked loop is seen in Figure 5-2.

Simple operation and vast use in the power electronics field make PLL systems a choice for use in resonant ultrasonic arrangements. The fact the phase at resonance is not 0° requires the system locks to a user-determined phase angle rather than 0°. The problem with a preset phase angle is the characteristics of the load change [24] meaning the resonance point might drift causing the system to lock off resonance and be driven in an inefficient electromechanical manner [24].

The inverse piezoelectric effect causes high powered piezoelectric transducers to act as receivers, receiving reflected waves from the medium.

The high pressures created during transient cavitation cause much noise to be converted into electrical energy which causes "noise" to be superimposed on the monotonic phase slope. PLL systems are monotonic and, therefore, require a smooth resonant curve on-which to operate correctly. Slight variations in the resonant system can drive the PLL away from the desired resonant point. Received mechanical signals are sometimes so strong and irregular that the equivalent impedance characteristics of the loaded transducer become variable, losing any controllable form [21].

5.3 Evaluation of Phase Locking

Primary evaluation of phase locking was used to assess cavitation activity being created in the bath. This was to be compared to the admittance driving technique. The suspicion that all the transducers were not dissipating equal amounts of electrical energy would be evident, in the tinfoil test, as the cavitation density around each transducer would not be equal. This was evident by varying amounts of local tinfoil decay around the transducers. The test was also used to evaluate whether phase locking could be locked off resonance resulting in an ineffective driving method.

5.3.1 Tinfoil

Aim

This test was used to illustrate both cavitation location and the amount of cavitation activity inside the vessel when driven by the phase locking system. The results were used as evaluation tools to compare driving techniques. The test was also used to prove that phase locking, if set at the incorrect phase angle, was ineffective.

Apparatus

- The test bath (see Chapter 3);
- Crest Audio Amplifier (CA6);

- phase locking circuit (see *Appendix D*);
- function generator (Escort EFG-3210);
- tinfoil with a thickness of $10\mu m$ and,
- 4l of distilled water.

Method

During this test a sheet of aluminium foil was placed inside the cavitation medium 10mm from the bottom of the bath. The electrical power injected into the system was measured for 1.5 minute exposure.

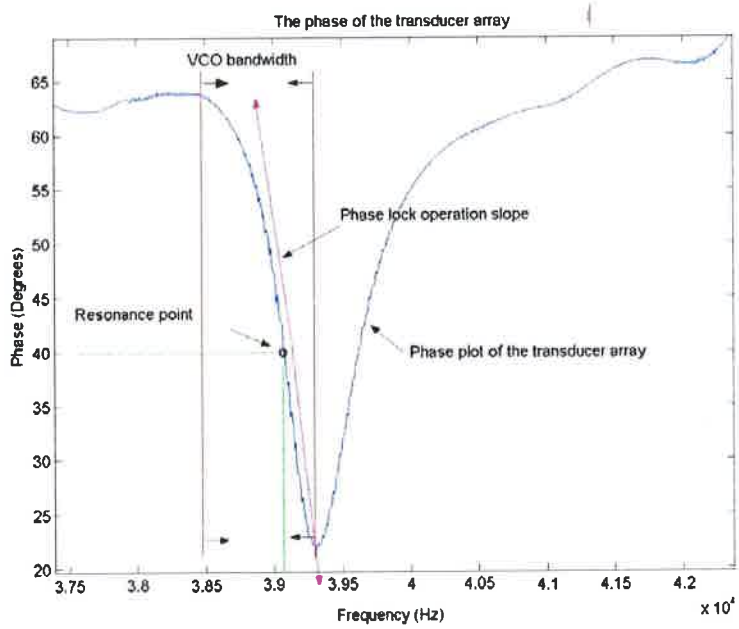

Figure 5-3: The monotonic slope on which the phase locked loop will operate is represented by the magenta arrow. The bandwidth, determined by the slope falls between the two red lines and the resonance point of the array has been marked on the plot

Figure 5-3 shows the region including and surrounding the frequency of the resonance of the transducer array. The bandwidth of the VCO was set to 800Hz, from 38.5kHz to 39.3kHz.

The resonance point of the array was measured to be at a phase of 40° which fell within the bandwidth and has been indicated by a o in Figure 5-3. The monotonic slope on-which the PLL was operated is represented by the magenta arrow.

Results

The test result shown in Figure 5-4 depicts a large amount of destruction resulting from a measured electrical power of 70W RMS. The phase angle was set at 40°. It can be seen that two transducers functioned indifferently, while four others functioned well. Circular patterns can be seen around the holes depicting the presence of standing waves, some of which are marked in red in Figure 5-4. Standing waves such as those responsible for the ring patterns are undesirable in most cavitation field applications as components in cleaning baths and chemicals being processed might be damaged [21].

In an attempt to illustrate the fundamental problem with phase locking systems, the bath was deliberately locked at a phase angle 10° away from the optimal phase angle. The phase was locked at 30° as opposed to the previous phase angle of 40°. The destruction of the foil (electrical power of 64W RMS measured over test cycle) is seen in Figure 5-5. Far less destruction occurred although electrical power was decreased by only 8.6%. The system was clearly not functioning optimally. Instead of being converted into usable mechanical energy, much of the electrical power was dissipated in the imaginary domain and unwanted mechanical modes of the transducers.

The results support the hypothesis that driving methods such as phase locking, which lock onto a combinational resonance point of a transducer array, are inefficient driving techniques for such loads. Also, the effectiveness of the technique depended directly on the user defined phase angle. In mass produced systems, each device would require manual tuning and even then, because of the dynamics of the PZT transducer [24], the system could, over time, become inherently inefficient.

Figure 5-4: The destruction of tinfoil after exposure for 1.5 minutes when the bath was driven by the phase locking system. The average electrical power measured over this test was 70W RMS. Note the large amount of destruction to the upper section of the foil and the four holes showing that four transducers were dissipating most of the electrical power. The relatively undamaged area in the lower portion shows two transducers were not dissipating enough electrical power to cause destruction of the tinfoil

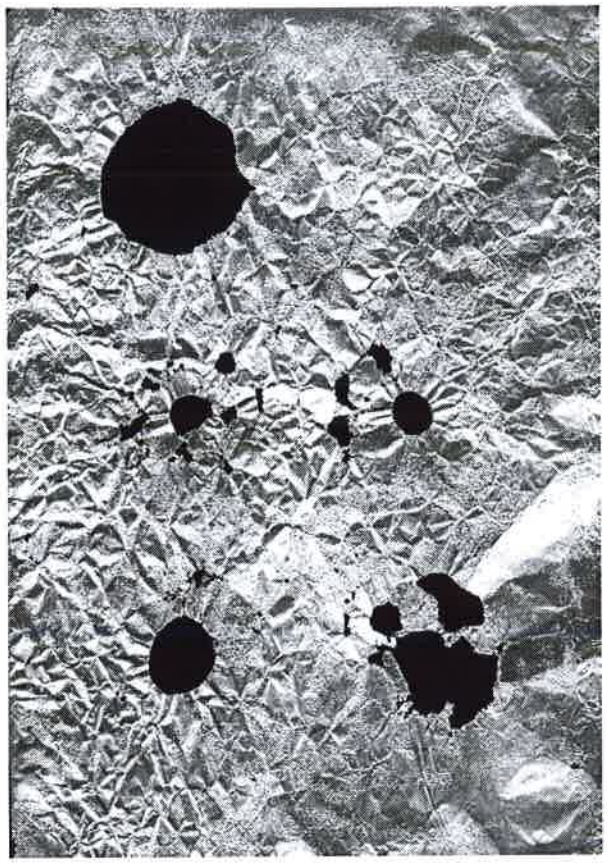

Figure 5-5: The result of the system being locked 30° from the optimal phase angle. Here an RMS power of 64W was measured over the test cycle. Note the large reduction in the destruction of the foil meaning that much electrical power was dissipated in the imaginary domain

5.4 Admittance Locking

5.4.1 Background

To overcome the need for a preset, user defined, resonance point, such as the user defined phase angle required for phase locking, a tracking technique nonreliant on the phase of the load needed to be assessed. When ultrasonic transducers are driven as voltage fed systems the power dissipated is proportional to the electrical current. Maximum electrical power delivery is achieved at resonance and, therefore, maximum current is required. Admittance is calculated by dividing the current by the voltage and the voltage is kept constant leaving the variable, current, proportional to the admittance which itself is proportional to the electrical power being dissipated. A current sample was the only sample required in this locking technique making it simple to implement. The current sample was used to effectively plot the admittance curve of the system, while the transducers were driven at high power. "Hill climbing" techniques can be used to continually track the highest admittance peak in a predetermined frequency band and maintain operation at this frequency [7].

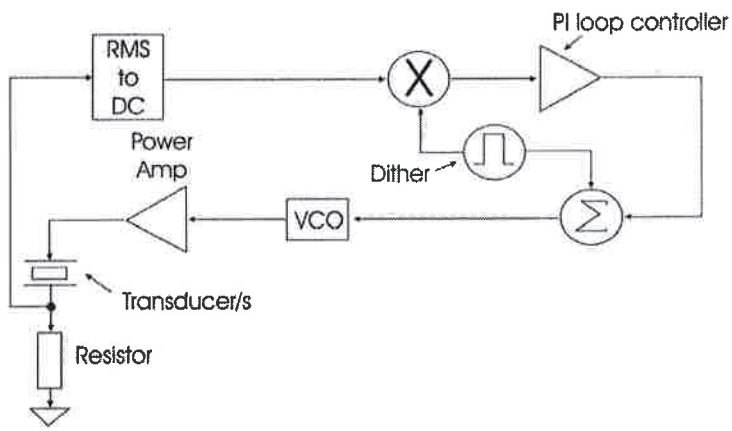

Figure 5-6: "Admittance locking" as proposed by Davies *et al* [7]

An RMS to DC converter is used to convert a current sample into a DC value to be used in the feedback loop.

A small dither with a 50% duty cycle is then added to the transducer drive frequency. The dither causes a small modulation on the transducer current due to the fact that the transducer shifts its operating frequency slightly. The magnitude of the transducer current detected by the RMS to DC converter includes a small signal because of the dither modulation. The dither oscillator is used to synchronously detect and demodulate this small signal. The output of the demodulator represents the slope of the admittance curve, $\frac{dY}{df}$ (Y = Admittance, f = Frequency). A PI controller moves the VCO set point to the local admittance maximum. This circuit establishes the direction in which to move the operating frequency. Admittance locking shifts the operation frequency to the point where the transducer current is maximum and $\frac{dY}{df} = 0$ and continually tracks this frequency.

This arrangement has the advantage that only the current needs to be sampled in the locking process. Furthermore, it is claimed the locking system will establish the optimum operating point for the case of any frequency dependent load [7].

5.4.2 Digital Admittance Locking

For the purpose of this study a digital admittance locking system was built using a PIC microcontroller (PIC16F877). The current was converted to a DC value by means of an RMS to DC converter. The DC value was sampled by the on-board 10-bit analogue to digital converter. The data was processed and a resultant 8-bit PWM signal with a carrier frequency of 15kHz produced. This value was filtered via a low pass filter resulting in a signal to control the VCO driving the transducer array.

The software developed to run the system performed the following routines and can be seen in *Appendix E*:

On startup the digital admittance locking system was made to perform a frequency sweep of the entire preset bandwidth. As the sweep commenced, the frequency at which the highest admittance was achieved was recorded. At the end of the sweep the drive frequency was set to the point of maximum current demand (the admittance peak) and tracking began.

Tracking the admittance peaks was performed using a process called "Hill climbing" [7] (see Figure 5-7).

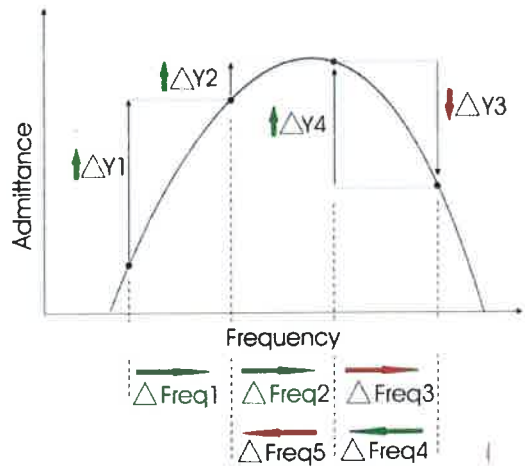

Figure 5-7: An illustration of the "Hill climbing" technique used in admittance locking. A 'dither' is used to assess whether the admittance decreases or increases as the frequency is changed

"Hill climbing" [7] is a technique used to track the highest peak of a frequency dependent, dynamic resonant system. The system is pre-programmed with a specific bandwidth. When initiated, a sweep of the bandwidth was used to identify the dynamic centre frequency of an ultrasonic load. The tracking shifted the drive frequency in set incremental step sizes (Δ frequency) and acquired a current sample at each point that was compared to the previous sample. If the current amplitude was less than the previous reading the system stepped down in frequency and remeasured the current. If the current read more than the previous step, an increase in frequency was required. This process continued until the admittance peak was found and even then continued in order to track the dynamic changes of the load. If Figure 5-7 is consulted one can see that for the first and second frequency steps (Δ freq1 & Δ freq2) the admittance increased (ΔY1 & ΔY2), therefore, the frequency was increased a third time (Δ freq3). The third step resulted in a decrease in the admittance (ΔY3) leading to a resultant decrease in the frequency (Δ freq4).

This caused an increase in the admittance (ΔY4) and another decrease in the frequency was made (Δ freq5). This step caused a decrease in the admittance and the system responded. Figure 5-7 shows large frequency steps or a low resolution. The step sizes used in the experiment were smaller resulting in a higher resolution and a closer lock to the maximum admittance peak was made possible.

5.5 Evaluation of Admittance Locking

Tinfoil was used to evaluate admittance locking in terms of cavitation produced and its distribution inside the vessel. The results were primarily used to compare admittance locking and phase locking. A chemical dosimetry test was also performed to measure which driving technique delivered more cavitation into the vessel when driven at specific electrical power levels.

5.5.1 Tinfoil

Aim

This test was used to illustrate both cavitation location and the amount of cavitation activity inside the vessel. The results were used as evaluation tools to compare straight driving, phase locking and admittance locking.

Apparatus

- The test bath (see Chapter 3);
- Crest Audio Amplifier (CA6);
- admittance locking circuit;
- function generator (Escort EFG-3210);
- tinfoil with thickness of 10μm and,
- 4l of distilled water.

Method

During this test a sheet of aluminium foil was placed inside the cavitation medium 10mm from the bottom of the bath. The electrical power dissipated over the array was measured for a duration of 1.5 minutes.

Results

Compared with phase locking, admittance locking created a large amount of destruction to the foil inside the vessel. This meant a large amount of cavitation activity had occurred. The activity, however, was centered around only three transducers of six showing an ineffectual distribution of cavitation to the bath and electrical power over the array. Standing waves were evident and represented by circular patterns, some of which have been marked in red in Figure 5-8.

The tinfoil result clearly showed admittance locking systems are unsuitable for applications where multiple PZT transducers are used, as equal decay at the transducer locations was not achieved.

5.6 Phase Locking vs Admittance Locking

5.6.1 Chemical Dosimetry

Aim

It is clear that phase locking and admittance locking systems deliver large amounts of acoustic energy into the vessel. A chemical dosimetry test can be performed to evaluate which driving system creates more transient cavitation. This evaluation will be performed on both techniques using the same experimental setup. The results from the tests will be plotted showing which of the two driving systems proved more effective. The result from the straight driving system will also be plotted to permit comparison between the three systems.

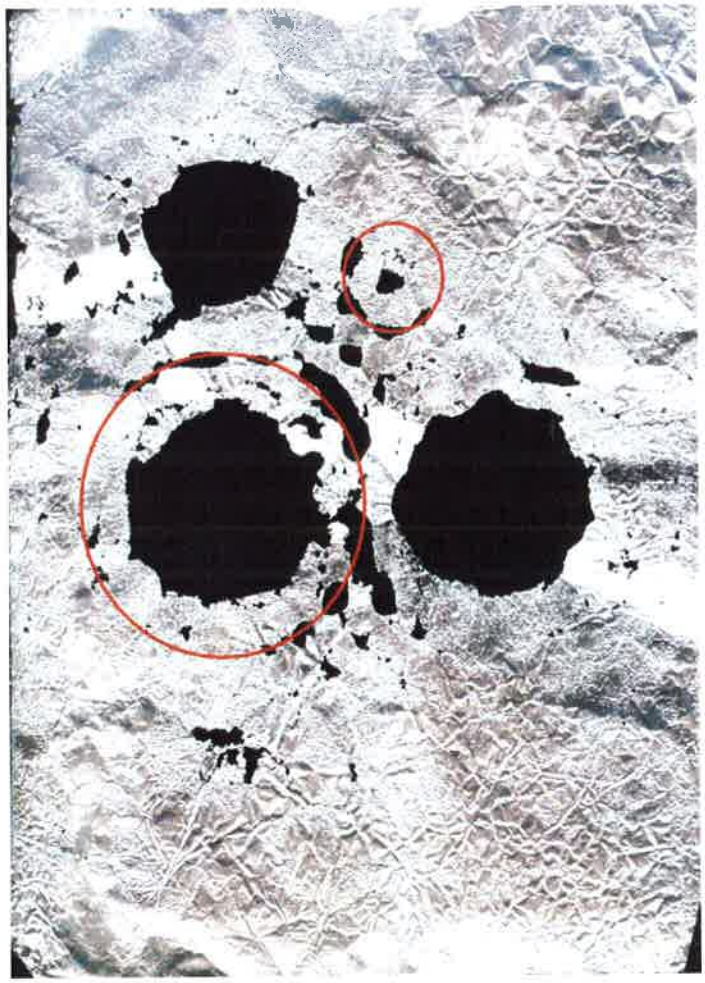

Figure 5-8: The result of the tinfoil test performed using digital admittance locking. Areas if intense cavitation activity as well as areas of minimal cavitation activity can be seen. The result shows that admittance locking does not optimally drive a PZT array at high power. Three transducers are barely operating while the other three are functioning well, illustrating an uneven spread of both electrical and acoustic energy

Apparatus

- The test bath, discussed in Chapter 3;
- Crest Audio Amplifier (CA6);
- phase locking and admittance locking system circuits;
- function generator (Escort EFG-3210);
- spectrophotometer capable of measuring wavelengths of 352nm (Jenway 6300);
- cuvettes for spectrophotometer (1000μl);
- 4l of distilled water;
- ammonium hepthomolydate, catalytic agent ($(NH_4)^6MO_7(O_2)^4 4H_2O$);
- potassium iodide (KI);
- 1ml Gilson pipette (P1000) and,
- measuring scale (0.01g accuracy).

Method

Potassium iodide was mixed into distilled water in a proportion of 16.6g/l. A catalyst, ammonium hepthomolydate, was then added at a concentration of 0.1g/l. The solution was mixed thoroughly and exhibited an endothermic reaction. The Weissler [12] solution was then poured directly into the cavitation vessel and cavitation produced for a predetermined time. Five minutes of ultrasonic exposure was used for the tests in this project. The five minute exposure was found to be sufficient in the production of iodine as a significant light absorption at 352nm could be achieved.

After exposure a 1ml sample of the liquid was compared to a blanking sample taken before cavitation exposure. The light absorbance at 352nm was measured and the difference between the sample and the blank became the result.

5.6.2 Results

One might expect the results of the admittance locking and phase locking systems to be similar as both locked onto, then tracked driving conditions as the load was driven (assuming the phase of the PLL was set to the resonance point of the load). Figure 5-9 shows the OH production at incremental electrical power levels. The results show phase locking yields more free radicals (OH) than admittance locking.

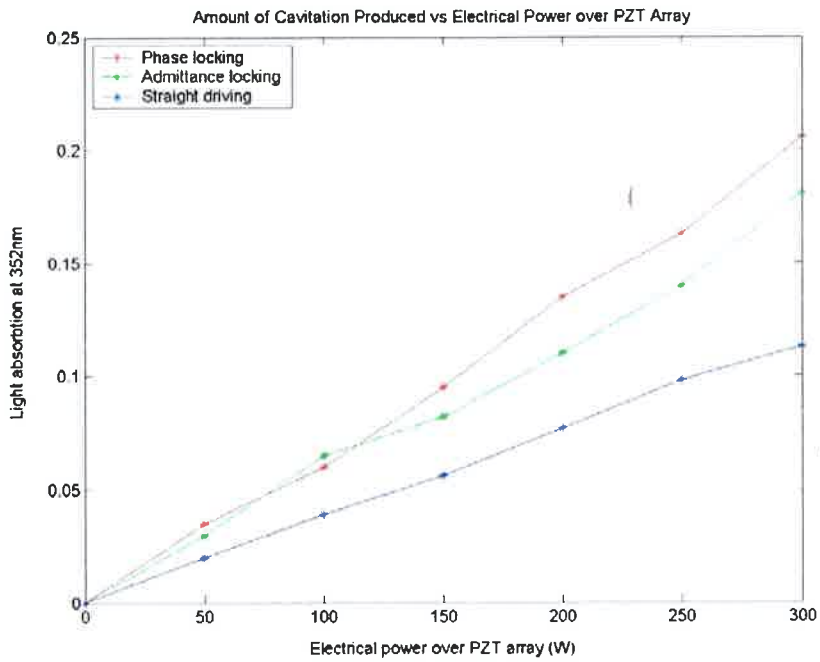

Figure 5-9: The graph shows the amount of cavitation occurring during each drive system test

A possible reason for the difference in performance was the sample time required for the analogue to digital conversion in the digital admittance locking system. The sample rate of the microcontroller (PIC16F877) was 80ms which meant the admittance locking system was too slow to accommodate the rapid changes in the load resulting from surface activity (ripples) in the vessel. The surface activity influenced the load to the extent that substantially less cavitation activity was achieved than expected.

It is assumed that if the admittance locking system response time was decreased, more cavitation activity would occur. Ideally the system would need to be fast enough to react to any changes occurring in the bath. This could have been accomplished if a faster analogue to digital device was used. The study did not require the optimisation of the admittance locking system and the circuit built was, therefore, deemed adequate as it tracked all the changes in the admittance profile except those caused by surface ripples (such changes occurring at a faster rate than 80ms).

If the blue plot in figure 5-9 is examined, one can see fewer OH (free radicals) were produced when the bath was driven by the straight drive system. The reduction in the OH produced results from the resonance of the system changing because of loading conditions (waves in the bath) and the bath being driven in an inefficient mode without feedback.

Chapter 6

Frequency Sweeping Systems

6.1 Overview and background

The fact that high power piezoelectric transducers change their fundamental characteristics when driven at power [24] swayed designers toward a type of driving system unreliant on one resonance point of the driven system [9]. This meant separate resonance points of the piezoelectric transducers, especially in multiple transducer arrays, could be excited individually, causing the system to distribute the electrical power between the transducers. The concept is to sweep the load through a frequency bandwidth including all resonance points of the separate devices forming the array. This is accomplished using repetitive frequency modulation (FM) - where a frequency bandwidth is swept from a lower limit to an upper limit, then back down to the lower limit. Blackstone-Ney [21] use frequency modulation techniques to drive ultrasonic baths used to clean delicate components, with minimal damage from the resultant violent cavitation process.

In their discussion "*Ideal Ultrasonic Parameters for Delicate Parts Cleaning*", Blackstone-Ney [21] describe the most effective parameters for sweeping systems to be a fast sweeping rate over as large a bandwidth as the transducers allow. They state the size of the cavitation bubble as indirectly proportional to the drive frequency and directly effecting cleaning properties in ultrasonic cleaning bath applications.

The following equation can be used to calculate the bubble radius [21]:

$$R_0 = \frac{1}{\omega}\sqrt{\frac{3kP_0}{\rho}} \tag{6.1}$$

Where:

k=polytropic index

P_0=Hydrostatic liquid pressure outside the bubble

ρ=medium density

ω=$2\pi f$

Blackstone-Ney recommend that in most aqueous solutions k=1.3, P_0=$10^6 \frac{dynes}{cm^2}$ and ρ=$1\frac{g}{cm^3}$ [21]. A large bubble size population leads to effective cleaning. The wide bandwidth required, however, reduces the electrical power dissipated as the transducers are not continually driven at their resonance frequencies [21]. It is a game of diminishing returns, for a large bubble size spectrum is required, but the bandwidth is limited by the mechanical resonance frequencies of the transducers.

6.2 Swept Frequency Modulation-defining variables

A swept frequency modulation system is defined by:

1. The system centre frequency (usually determined by the centre frequency of the transducer or the frequency in the centre of the separate transducer resonance frequencies)

2. Bandwidth

3. Sweep rate

As SFM systems are usually driven by a VCO, the controlling waveform takes the form of a triangle wave. Figure 6-1 shows the triangle wave and the adjustments made to change the sweep rate and bandwidth of the process. The centre frequency usually falls halfway between the upper and lower peaks of the wave. The defining variables will be discussed in later sections.

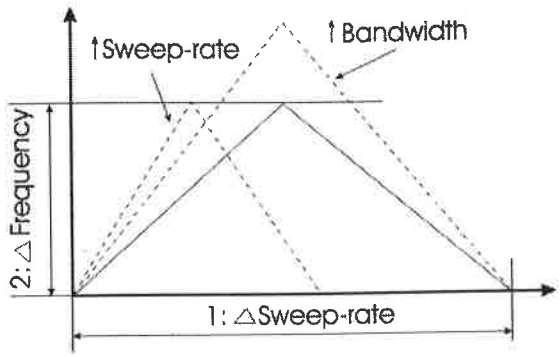

Figure 6-1: The two adjustable properties of the SFM driving system, the bandwidth and the rate of the sweep. The solid plot represents the original signal and the two dashed line plots represent the labeled changes in the sweeping signal

6.2.1 Defining the centre Frequency

Two measurements were used to ascertain the centre frequency of the test rig:

1. The electrical characteristics of the bath using the measured admittance plot.
2. The acoustic characteristics of the bath using an impulse response study.

The admittance of the test rig was measured using an impedance analyser (HP4192A). The impulse response was performed using a single square wave with a duration of $1\mu s$, pulsed onto the transducer array. The acoustic response of the rig was recorded using a needle hydrophone submerged in the liquid.

Figure 6-2 shows the FFT of the impulse response from the needle hydrophone depicting the test rig's frequency components as well as the measured admittance. The FFT shows a definite resonance around the 40kHz mark. The admittance plot shows a piezoelectric response with a series resonance just below 40kHz. Both results show many resonance modes occuring below 40kHz, but not many above, meaning the centre frequency should be shifted lower than the fundamental transducer resonance. The centre frequency, in this case, will be determined by the upper and lower frequency limits of the bandwidth and be placed in the centre of this range.

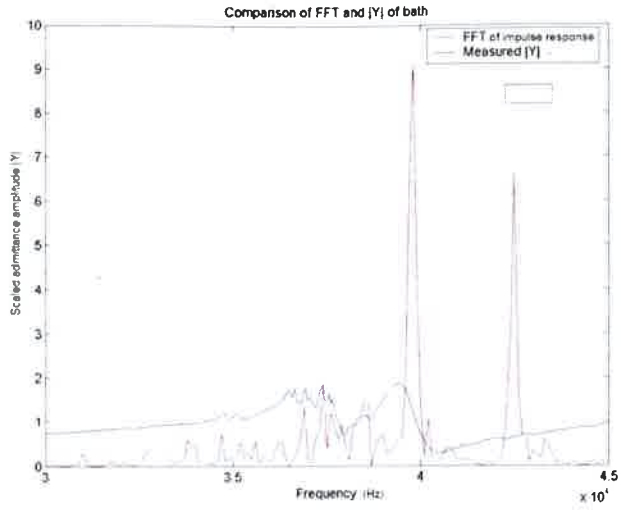

Figure 6-2: The FFT of the impulse response and the measured admittance are shown here. This plot was used to determine the center frequency and the bandwidth of the test rig

6.2.2 Defining the Bandwidth

The bandwidth of the sweeping system was calculated using the same measurements shown in Figure 6-2. The results established where series resonance modes of other transducers were superimposed. These appear as admittance peaks in the electrical evaluation and resonance frequencies in the FFT appearing adjacent to the centre frequency. The bandwidth was made to include the resonances of the separate transducers shown in both the mechanical impulse study and the electrical admittance plot; but not the adjacent areas where minimal frequency components occurred.

In this case the bandwidth could roughly incorporate the frequencies from 37kHz to 40kHz. This bandwidth may be a good starting point from which to design a sweeping system. The centre frequency was made 38.5kHz, the centre of the bandwidth frequency range.

6.2.3 Defining the Sweep Rate

It was previously mentioned that the sweep rate should be slow enough to give the transducers sufficient time to "ring up" to oscillation and "ring down" from resonance. The sweep rate needed to be slow enough so that the phase of the oscillator (transducers) had time to become equal to that of the driving frequency. Once the sweep cycle swept through the resonance point of the oscillator the difference in phase between the natural resonance frequency of the transducers and the driving frequency could cause oscillations. These were caused as the driving force, sometimes pushing with relative phase, helped to build up the oscillation amplitude, but sometimes pushing with opposing phase, resulting in diminishing oscillations [5]. The oscillations in the system can cause an unpredictable power profile over the sweep cycle.

To try to calculate the maximum sweep rate, the impulse response in the time domain was used to establish the "ring down" time and the maximum sweep rate of the SFM. Figure 6-3 shows the superposed resonances of all the transducers in the array. The highest Q (or most dominant oscillator) was used to calculate the sweep rate, as this would require the most time to "ring up and down" ensuring a slow enough sweep to accomodate all the array's transducers.

The acoustic impulse response can be seen in Figure 6-3. A characterising curve was drawn in red and can be defined by the following equation [5]:

$$y = P(1 + e^{-(\frac{1}{2})\Gamma t})^2 \tag{6.2}$$

Where:

y =Characteristic curve

P =Gain of the characterising curve

Γ =Time constant

t =Time

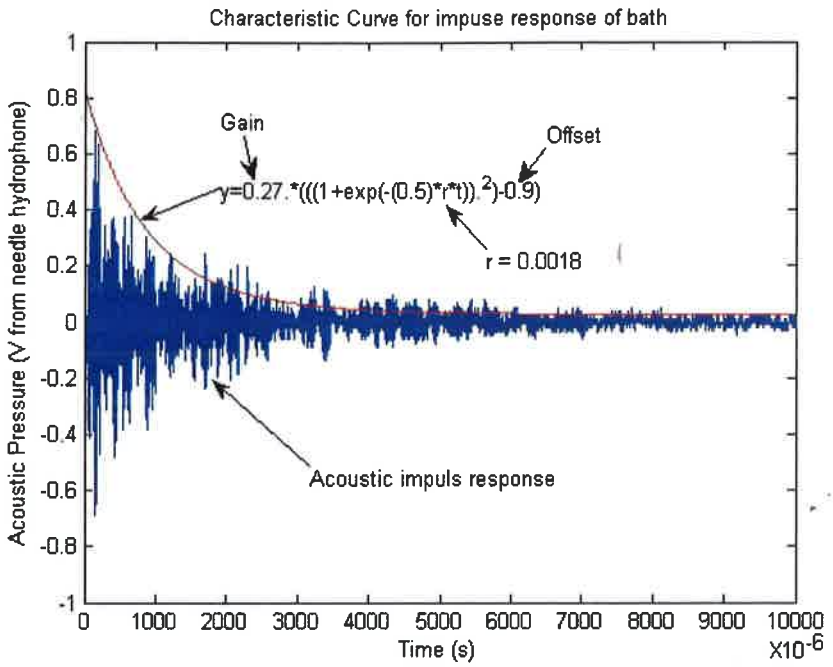

Figure 6-3: Characteristic curve of the impulse response of the bath (Red). The blue curve represents the measured acoustic pressure in the bath when an electrical impulse was applied to the transducer array. The equation models the damping and was used to calculate the 'ring down' time of the highest Q of the array

From equation 6.2 and the graph shown in Figure 6-3, the time constant, Γ, was calculated as 1.8ms. "Ring down" time is assumed to be equal to "ring up" time making the total sweep cycle time twice 1.8ms equalling 3.6ms. This results in a maximum sweeping frequency for the test bath of about 277Hz.

6.3 The Swept Frequency Modulation System

Swept frequency modulation requires a triangular wave to drive a VCO that in turn drives a power amplifier. The main component of the system consists of a triangle wave generator with variable amplitude and frequency controls. A block diagram of the SFM can be seen in Figure 6-4.

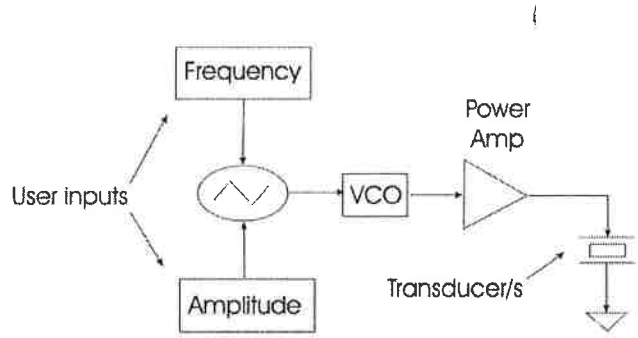

Figure 6-4: The Swept Frequency Modulation (SFM) system. A triangular wave is made variable by means of user inputs in the form of DC voltages. This wave drives a VCO which in turn creates a sinusoidal output proportional to the amplitude of the triangle. The sine wave is amplified by means of a power amplifier and drives the transducer array

6.3.1 Method

In order to create a simple and effective SFM system, two function generators with VCO inputs (Escort EFG-3210 Function Generator) were used. One was used to create a triangle wave (modulation signal) and another to create a sinusoidal wave (carrier signal) to control the frequency of the power amplifier driving the transducers. Figure 6-5 shows an oscilloscope trace of the working SFM system.

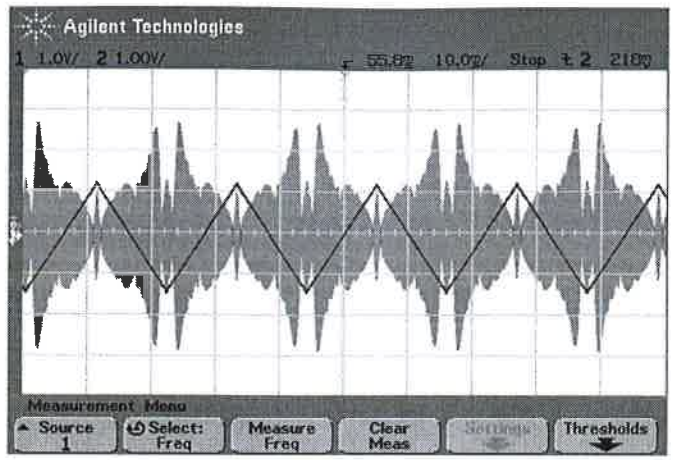

Figure 6-5: SFM frequency control signal and the current amplitude showing the power profile through the sweeping bandwidth

SFM was used to drive a single transducer into air with a 1Hz modulation signal. The resultant current and sweep signal is seen in Figure 6-6.

Result

The result achieved showed the current profile was asymmetrical around the resonance point of the device (band pass result). The shape of the first half of the scope trace was anticipated, but after the maximum current amplitude, resonant behaviour was observed. This was because the sweep rate was too fast to accomodate the high Q of the transducer being driven into air. A mathematical evaluation of the current response was calculated to varify the measurement.

6.3.2 Mathematical Verification of the Power Profile

In order to simulate the transducer, a model needed to established for the device being examined. The circuit diagram of a single transducer model coupled with air can be seen in Figure 6-7 in the form of a Butterworth Van Dyke (BVD) circuit, which was discussed in Chapter 2.

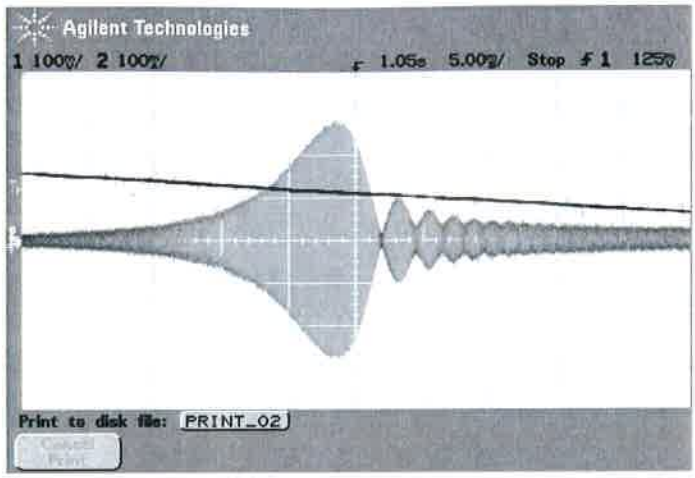

Figure 6-6: The current envelope acquired when sweeping a single transducer into air. Oscillations can be seen after the current peak meaning that the particular transducer was being swept through the bandwidth too fast

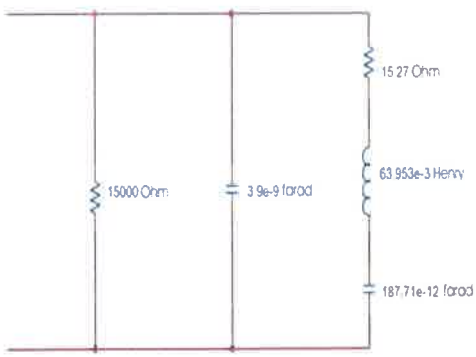

Figure 6-7: The component values used to simulate a single transducer being driven into air.

The following process was followed to calculate the model shown in Figure 6-7:

The points Y_{fm} (admittance at the series resonant system point), Y_{fn} (admittance at the parallel resonant point), f_n and f_m (frequencies of the parallel and series resonance points respectively) were read directly off the admittance plot of the respective transducer. An impedance analyser (HP 41925A) was used to measure the admittance of the transducer over a specified bandwidth:

The measured admittance plot showing the four points used in the BVD circuit calculations, can be seen in Figure 6-8:

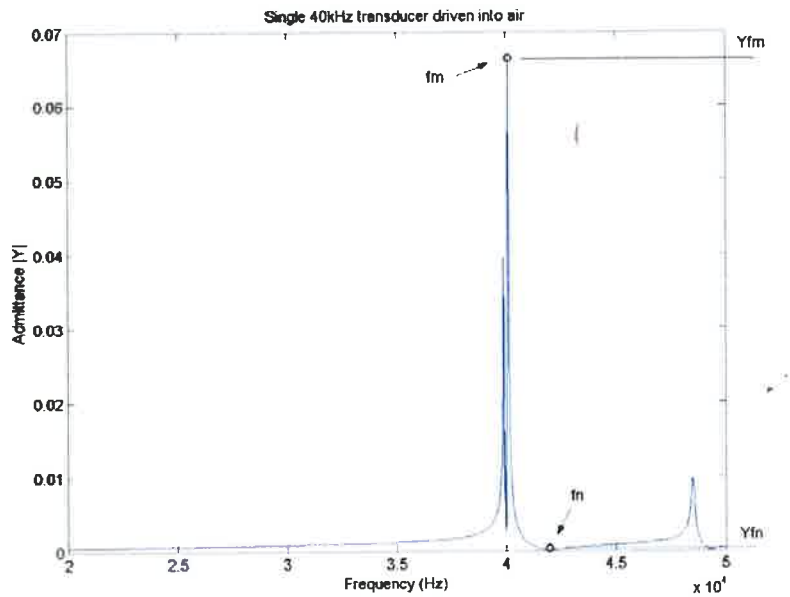

Figure 6-8: The figure shows the admittance plot of a single PZT transducer when driven into air at low power. The values used to build the transducer model as a BVD circuit have been marked

Reading from the graph:

$$f_m = 40.090kHz$$

$$f_n = 41.950kHz$$

$$Y_{fm} = 0.0668\ S$$

$$Y_{fn} = 1.144X10^{-10}S$$

After calculating and plotting using Matlab (see *appendix X*) the simulated transducer could be evaluated against the measured transducer by means of a visual analysis of the plotted graphs. The closer the graphs matched, the more accurate the model.

Calculating the BVD circuit components

Refer to Figure 2.2(3) for the circuit and Figure 6-8 for admittance and frequency values.

$$Q_m = \frac{(F_m)}{2(F_n - F_m)} \frac{|Y_{Fm}|}{|Y_{Fn}|} \tag{6.3}$$

$$K_{eff} = \sqrt{1 - \frac{F_m^2}{F_n^2}} \tag{6.4}$$

$$R1 = \frac{1}{|Y_{fm}| - |Y_{Fn}|} \tag{6.5}$$

$$L1 = \frac{Q_m R}{2\pi F_m} \tag{6.6}$$

$$C1 = \frac{1}{2\pi F_m Q_m R} \tag{6.7}$$

$$C_0 = C(\frac{1}{K_{eff}^2} - 1) \tag{6.8}$$

The current envelope of the BVD circuit was used to compare the model to the real world transducer load. The voltage of the driving system was kept constant making the current proportional to the admittance which was proportional to the electrical power.

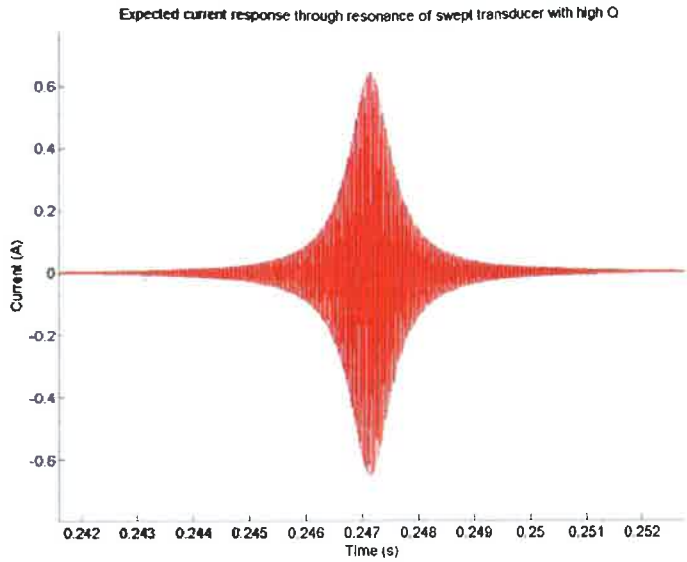

Figure 6-9: The expected current amplitude as the driving frequency is swept through the transducer's resonant point. Note the symmetry around the resonant frequency (point of maximum current amplitude)

Figure 6-9 is the result of the Matlab simulation and shows a typical band pass result of the current through a transducer. As the driving frequency was swept, the transducer current increased to a maximum point and then decreased in a symmetrical manner around the resonance frequency. The programme used to calculate this figure is included in *Appendix H.*

A correlation between the mathematical evaluation and the measured value could not be made, meaning that either the mathematical model was incorrect or an error had occurred during the measurement of the transducer current. To establish which of the two results was correct, a third assessment was required. Simulink was used to simulate the current through the transducer model.

6.3.3 Simulink Model

In order to further justify the result a third method of evaluation was explored. This took the form of a simulation using Matlab's Simulink. The model can be seen in Figure 6-10.

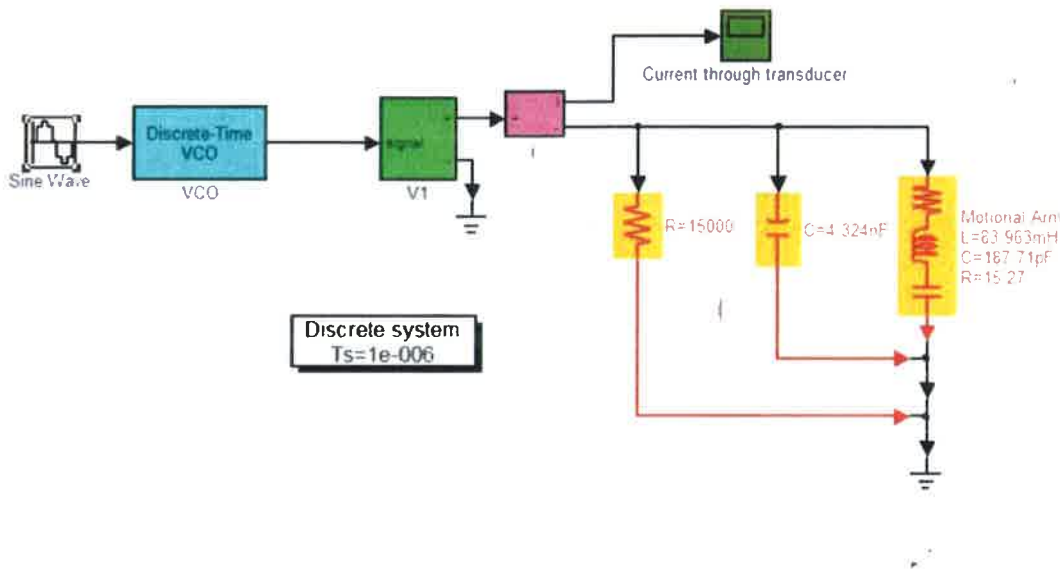

Figure 6-10: The Simulink model used to simulate SFM. The BVD equivalent transducer circuit can be seen on the right and the modulation signal on the left

In this case Simulink was used to model SFM and the transducer was driven by a frequency modulated signal with a sinusoidal modulation frequency of 1Hz.

The result of the Simulink model analysis, Figure 6-11, shows the simulation and the measurement graphs are similar, meaning an error was made in the initial mathematical calculation of the system (Figure 6-9). A second mathematical analysis was required so a realistic representation could be made.

6.3.4 Mathematical Model Reworked

Transient conditions of the system were not considered in the first calculation and were required for an accurate mathematical model. A differential equation for the transducer being driven into air was derived and solved:

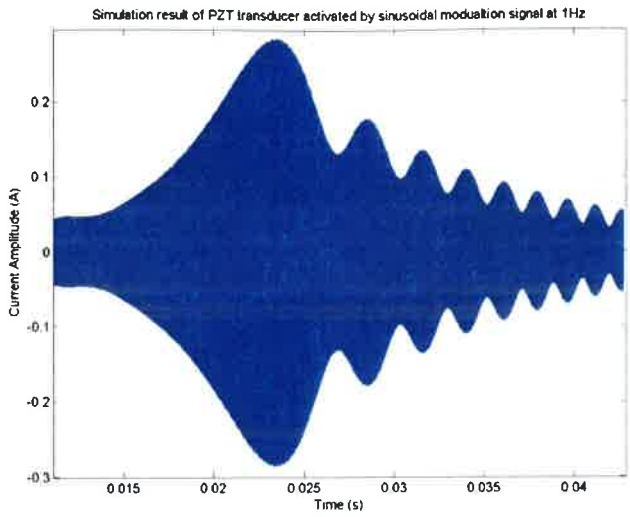

Figure 6-11: The Simulink model result showing concurrence between the Simulink simulation and the measured result of the system

Firstly the modulation signal was simplified by converting it from a triangle wave to a sinusoidal wave. The triangle wave was approximated with a sinusoidal wave:

Triangular sweep signal defined by,

$$F(t) = \frac{2}{\pi} \arctan[\sin(\omega t - \phi)] \tag{6.9}$$

Was replace with a sinusoidal sweep signal defined by:

$$F(t) = \sin(\omega t + \phi) \tag{6.10}$$

Where:

$\phi = Phase$

This was carried out to convert the sine of a sine function (triangle wave) to a pure sine wave simplifying the calculations. The Simulink model evaluated the difference between the current envelope when swept by both waves.

In Figure 6-12, minimal difference in the power profile between the triangular and sinusoidal modulation signals are seen.

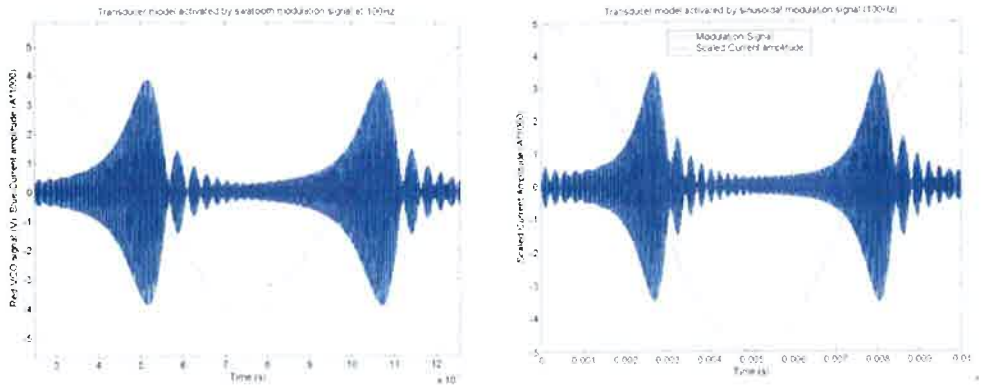

Figure 6-12: Difference between modulating with a sine and triangle wave. For simplicity in the calculations a sine wave was used as apposed to a triangle wave

The slope ($\frac{dv}{dt}$) of the sine wave at the resonance point is slightly steeper than that of the triangular signal, meaning a faster sweep rate was incurred. This is not an issue in the application, as only similar signals are compared.

The resonant point is positioned at the most linear section of the sinusoid, 90° and 270°, in order to closest simulate the triangular signal.

A sinusoidal current i(t) driving a series RLC circuit may be represented as follows:

$$Ri + L\frac{di}{dt} + \frac{1}{C}\int (i)dt = V_{\max}\sin(\omega t + \phi) \tag{6.11}$$

Where:

R=Resistance in the motional arm of the transducer

L=Inductance in the motional arm of the transducer

C=Capacitance in the motional arm of the transducer

V_{max}=Amplitude of the driving signal

This equation is solved in *Appendix I.*

However, because the system is not being driven by a sine wave, but rather a sine wave modulated by another sine wave, the formula becomes:

$$Ri + L\frac{di}{dt} + \frac{1}{C}\int (i)dt = V_{max}\sin(\omega_c t + [m_f sin(\omega_i t)]) \tag{6.12}$$

Where:

ω_c=$2\pi f_c$(f_c =frequency of carrier signal)

ω_i=$2\pi f_i$(f_i =frequency of modulation signal)

and,

$$mf = \frac{\delta}{f_i} \tag{6.13}$$

Where:

δ =Frequency deviation off the centre frequency

f_i =Frequency of the modulation signal

Because of the complexity of this equation the evaluation was made numerically rather than analytically[18]. The Matlab programme used to calculate the current envelope can be seen in *Appendix J.* The result of the mathematical evaluation can be seen in Figure 6-13.

Figure 6-13 shows a similar pattern to that of the measured transducer current envelope, Figure 6-6, and the Simulink model, Figure 6-11. The results back the discussion in section 6.2.3 and are the result of phase variations causing oscillatory patterns in the sweep cycle.

The current oscillations shown in Figures 6-6, 6-11 and 6-13 directly infuence a frequency sweeping driving system. It was found that the resonant behaviour is affected by the Q of the load and the sweep rate. The Q of the test transducer was calculated to be about 2000, as it was not mechanically damped when driven into air.

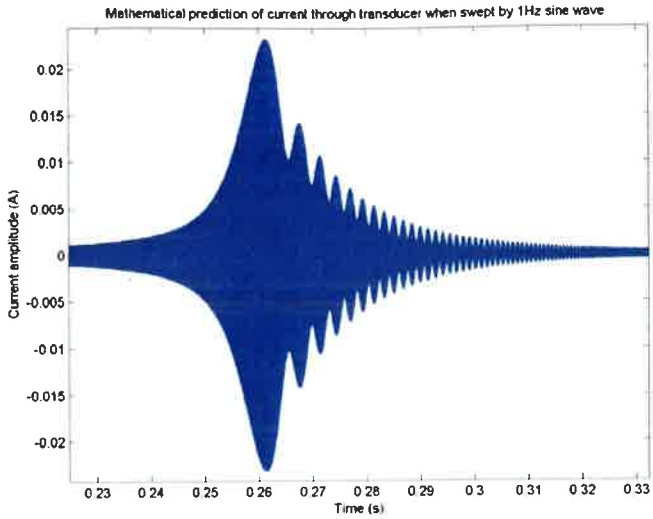

Figure 6-13: The result of the mathematical solution using transient states can be seen here. The result shows similar oscillations to the measured system and the simulink model proving correct results

Calculating the maximum sweep rate of the single transducer driven into air resulted in a maximum rate if 10Hz:

$$Q = \frac{f}{\Delta f} \tag{6.14}$$

where $Q = 2000$

$\Delta f = Bandwidth$

$f = centre\ frequency\ of\ transducer$

Result:

$$\Delta f = \frac{40000}{2000} = 20Hz$$

and,

$$\frac{\Delta f}{2} = \frac{1}{\Gamma} \tag{6.15}$$

so

$$\Gamma = 10ms$$

Ideally, in a frequency sweeping system a symetrical current envelope is required, similar to that displayed in Figure 6-9, ensuring the transducer is being driven through its resonance point and is dissipating maximum power through the sweep. High sweep rates result in a more asymetrical current envelope around the resonance point of the transducer.

As the Q of the transducer is characterised by its physical construction and mechanical loading, it cannot be changed, leaving compensations in the sweep rate to determine the symmetry of the current envelope around the resonance point.

If one looks at the stages of the resonant behaviour, as the modulation frequency is increased one can clearly see the response degrades as the sweep frequency increases: Figure 6-14, shows the degradation of the power profile as the sweep frequency increases from 10Hz to 200Hz when the sweep bandwidth and centre frequencies are kept constant. The reduction in electrical power occurs as the transducers do not have sufficient time to ring up to resonance as the sweeprate increases. The results show a near symetrical current envelope achieved at a 10Hz sweep rate.

In conclusion, the sweeping frequency must be calculated as a function of the Q and the bandwidth of the PZT load, so that the change in frequency over the change in time is not too high.

6.3.5 The Bath Model

A model of the bath was required for simulations of the test rig. BVD models of each transducer were calculated and connected in a parallel configuration with Simulink. The transadmittance circles of the transducers on the test bath and their corresponding models are included in *Appendix G.* The Matlab code used to calculate these circles are seen in *Appendix F.*

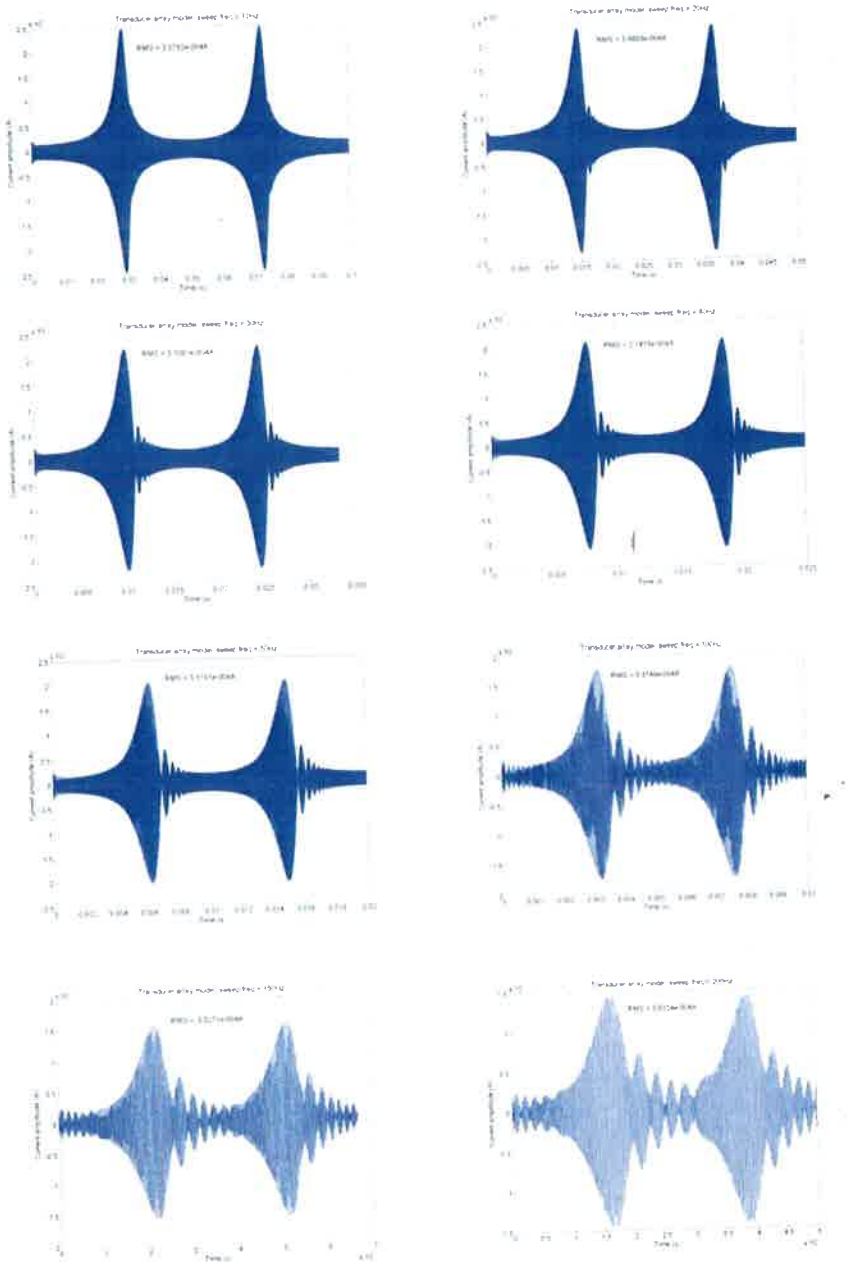

Figure 6-14: The stages of the current degredation as the sweep rate is increased from 10Hz to 200Hz; the bandwidth was kept constant

The process followed to acquire equivalent BVD circuits was the same as explained in Chapter 6.3.1. for the single transducer being driven into air and was performed on each of the six transducers as well as the entire bath array. The bath was filled with 4l of distilled water during this analysis.

6.4 Empirical Analysis of Swept Frequency Modulation

Two tests were performed to evaluate the SFM driving system, the Weissler Test (chemical dosimetry) and the tinfoil test.

6.4.1 Chemical dosimetry (Weissler Test)

Aim

The aim of this experiment was to ascertain whether SFM would yield less cavitation inside the vessel than the driving techniques discussed thus far.

Apparatus

- The test bath, discussed in Chapter 3;
- Crest Audio Amplifier (CA6);
- two function generators (Escort EFG-3210);
- spectrophotometer capable of measuring wavelengths of 352nm (Jenway 6300);
- cuvettes for spectrophotometer;
- 4l of distilled water;
- ammonium hepthomolydate, catalytic agent ($((NH_4)^6MO_7(O_2)^4 4H_2O$);
- potassium iodide (KI);
- 1ml Gilson pipette (P1000) and,
- measuring scale (0.01g accuracy).

Method

Potassium iodide was mixed with distilled water in a proportion of 16.6g/l. A catalyst ammonium hepthomolydate, was added at a concentration of 0.1g/l. After thorough mixing this solution exhibited an endothermic reaction. The solution was then poured directly into the cavitation vessel and cavitation was produced for a predetermined time. Five minutes of cavitation exposure was used for the tests in this project.

The five minute exposure was found to be sufficient in the production of iodine and a significant light absorption at 352nm could be achieved. The sweep frequency used was 100Hz and bandwidth 1kHz. The centre frequency was 38kHz.

After ultrasonic exposure, a 1ml sample of the liquid was compared to a blanking sample taken before cavitation exposure. The light absorbance at 352nm was measured and the difference between the samples became the result. Labview was used to measure the average electrical power dissipated over one sweep cycle of the test. The OH production and the electrical power were used to assess the driving technique.

Results

It was found that SFM caused an absorption at 352nm, of 0.021 when 87W of electrical power was dissipated.

Conclusion

If this result is compared to the admittance locking system (0.066 at 87W), a large drop in OH production is evident. This was expected and is because the transducers were not continually driven at their lowest impedance.

6.4.2 Tinfoil Test

Aim

This test was used to establish whether or not there was a more even spread of acoustic power inside the bath and across the transducers forming the array than in other driving techniques.

Apparatus

- The test bath, discussed in Chapter 3;
- Crest Audio Amplifier (CA6);
- two function generators (Escort EFG-3210);
- tinfoil with a thickness of $10\mu m$ and,
- 4l of distilled water.

Method

A sheet of aluminium foil was placed inside the cavitation medium 10mm from the bottom of the bath. The electrical power being injected into the system was measured over a single full cycle of the modulation signal. The exposure time was set to 1.5 minutes. The sweep frequency used was 100Hz and bandwidth 1kHz. The centre frequency was made to be 38kHz.

Result

The result showed all transducers caused enough cavitation to create total local destruction of the foil where the six transducers were positioned. Six holes were clearly visible, verifying that a better distribution of acoustic energy than other driving systems was achieved. The tinfoil can be seen in Figure 6-15.

A comparison may be made between this result and the results of the straight driving systems which shows achievement of a better distribution of electrical energy over the transducer array. This test showed the other driving systems were not fully activating the entire transducer array as six holes were not created in the foil tests (see tests in Chapters 4 and 5).

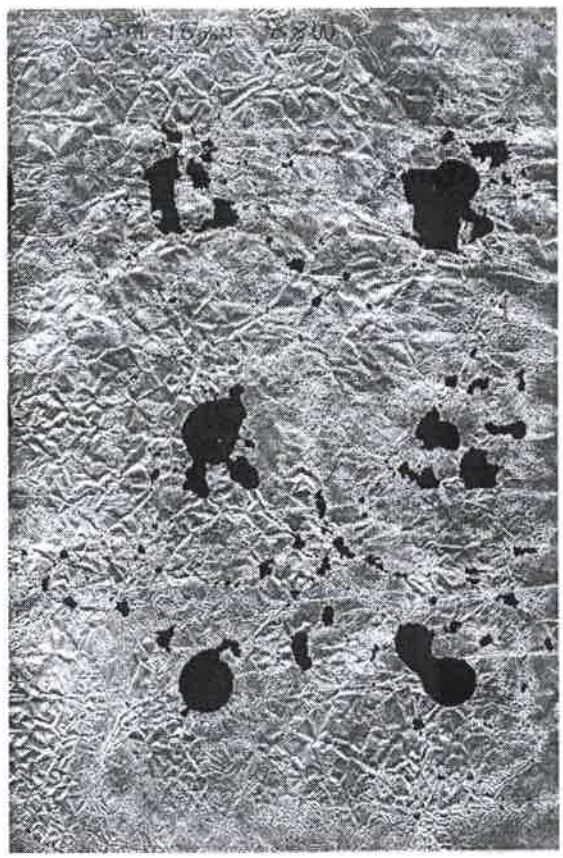

Figure 6-15: The result of the tinfoil test after 1.5 minutes of exposure. The SFM system was used in this test. The bandwidth was set to 1kHz and the sweep rate to 100Hz

Chapter 7

Swept Frequency Dwelling

7.1 Introduction

When compared to straight driving and locking systems, swept frequency modulation proved to be effective in creating a more even spread of acoustic power inside the cavitation vessel (powered by a multiple transducer array) as well as better electrical power distribution across the transdcuer array. Unfortunately, it suffered a fallback in that less electrical power was dissipated and, therefore, less cavitation generated. This was because the system was being driven in regions where the impedance was high, as opposed to the resonance points where impedance was low.

In an effort to improve the amount of electrical power delivered to a PZT array and maintain the favourable characteristics of a more even acoustic distribution, a novel driving technique was conceived. This technique was designed to utilise the power profile of the load as a feedback mechanism in real time as the system was swept. In this way the system was made to dwell at the resonance points of the array, then swiftly sweep through the points where resonances did not exist. The objective was that the system would deliver more electrical power to the transducer array than SFM and retain the beneficial qualities of a sweeping frequency system effectively bridging the gap between locking and SFM systems.

As this driving method combined a sweeping and dwelling process, it will be named "Swept Frequency Dwelling (SFD)".

7.2 The Concept of Swept Frequency Dwelling

SFD lingers on the resonance points of each transducer. This caused individual transducers to become excited and operate at their resonant frequencies, before the system moved on to the next resonance point. It was thought if the sweep rate was made fast enough the transducers would begin oscillating, then, ringing down but not fully, the sweep returns to excite the same transducer in the next sweep cycle. In this way the transducers would be excited for the entire duration of the sweep. Unfortunately the transducers and the bath as a resonant system required "enough" time to "ring up" to their maximum mechanical oscillation. It was assumed the "ring up" time was equal to the "ring down" time. This assumption led to a maximum usable sweep rate dependant on the rate of oscillation damping. Fundamentally SFD allowed a faster modulation frequency than SFM because the system "pauses" at the resonance points leaving more time for the major resonances to be fully excited. Also, the non-resonance points are not dwelt upon allowing less "wasted" time at these regions which in turn increased the amount of electrical power delivered to the array. "Wasted" time was time where minimal electrical energy is delivered to the system.

Figure 7-1 shows a block diagram of the proposed system and the components involved.

The resistor (bottom left of figure 7.1) was used as the current feedback mechanism. A device of low resistivity and high current handling capabilities was affordable and resulted in an accurate representation of the current of the system without any phase shifts or alterations of signal. The bath was driven as a voltage fed arrangement, so the current would be proportional to the electrical power being applied. The current feedback was converted to a DC voltage representing the current's amplitude. A peak detector was used for this portion of the system. The DC wave was multiplied with a square wave creating a square wave with an amplitude inversely proportional to the amplitude of the current.

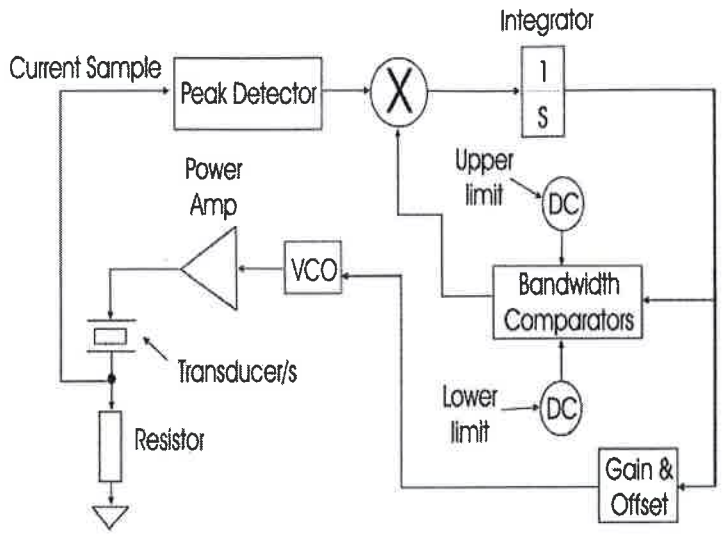

Figure 7-1: The SFD system showing the proposed components and their layout. The circles marked DC are user defined variable DC values used to determine the bandwidth of the sweep

The square wave with changing amplitude was fed into an integrator which created a triangular wave with a changing slope ($\frac{dv}{dt}$) proportional to the amplitude of the square wave. This wave was used as a VCO input and an output frequency proportional to the amplitude of the triangular wave was generated to drive the load.

Figure 7-2 shows a sketched prediction of the VCO input signal and the current amplitude with respect to time. Note how $\frac{dv}{dt}$ of the VCO input is reduced as the current amplitude peaks.

The VCO signal could be manipulated by means of gain and offset to achieve the required bandwidth and centre frequency of the particular array used. The output of the VCO was amplified using a power amplifier which in turn drove the transducer array.

It was assumed at this stage in the design that a comparator dependant system would be required to stabilise the integrator because of possible drift. The proposed comparators are used to define the limits of the square wave used in the multiplication section by means of preset high and low DC values. This part of the system will be discussed later in section 7.4.4.

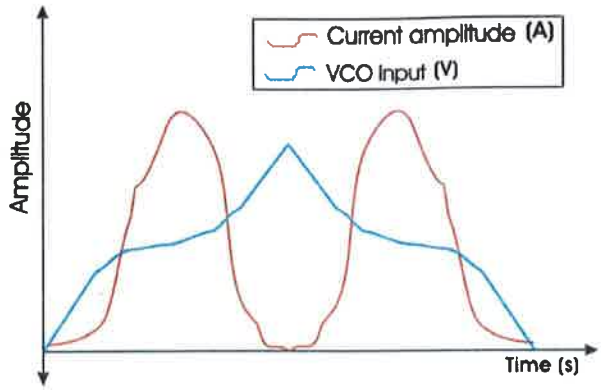

Figure 7-2: The graphs show a prediction sketch of how the sweep rate decreases as the current amplitude increases

7.3 Developing a Model for SFD

In an attempt to verify the planned circuit, a theoretical account was developed to simulate the system using a Matlab Simulink model.

In the model, Figure 7-3, the six transducer equivalent circuits and the current sensing resistor can be seen on the right hand side. The blue blocks represent mathematical calculations, the red blocks user changeable variables and scalers and the violet blocks, transitions from the mathematical domain into the electrical domain. The orange blocks are predetermined constants.

The model follows the same layout as the initial block diagram (Figure 7-1), but better describes the bandwidth comparator section. An RMS to DC converter was used instead of a peak detector. The model was found to be highly effective in the assessment of the concept of SFD.

7.3.1 Results

The simulation was used to evaluate the change in the shape of the current profile as the feedback was increased in percentage steps. Figure 7-4, shows how both the VCO signal (red) and the current profile (blue) change as the feedback is increased from 0% to 100%.

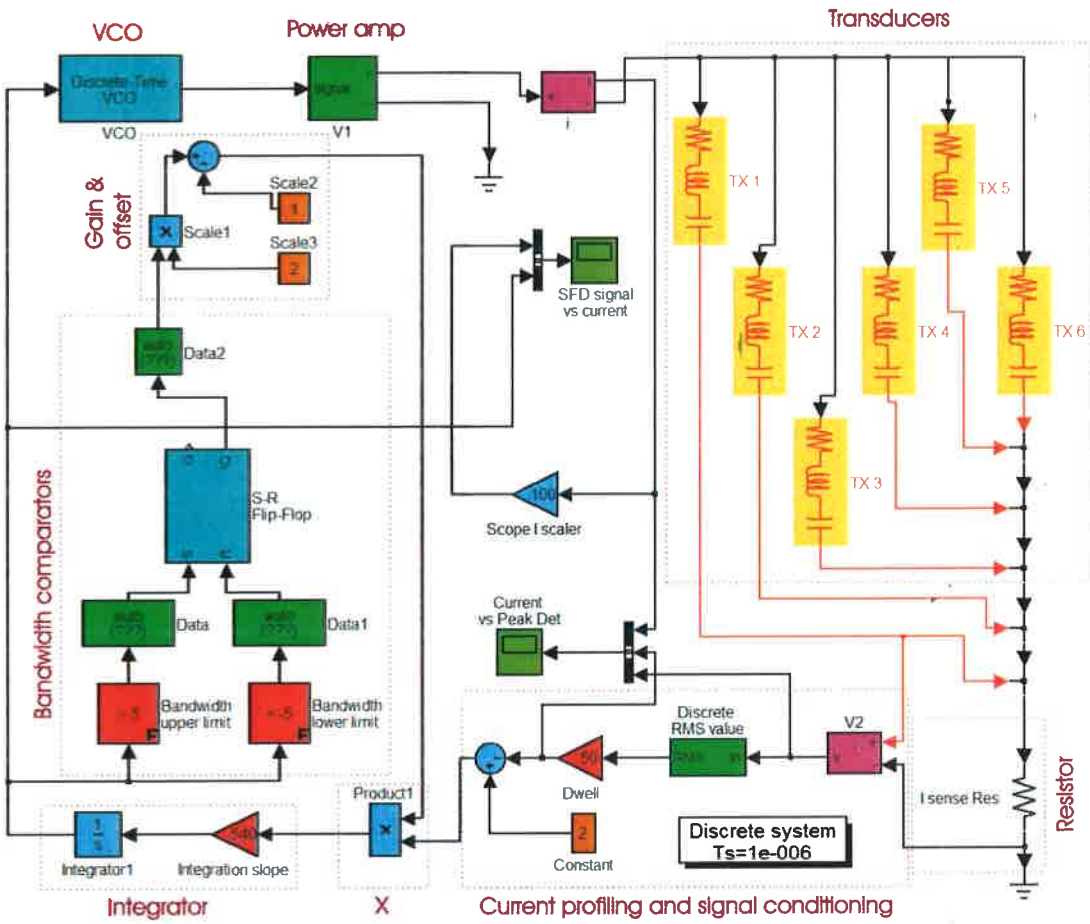

Figure 7-3: The model built to varify the fundamentals of the SFD system. The magenta text and grouped blocks represent the sections depicted in Figure 7.1

If the feedback increases to more than 100% the system locks on the point of maximum admittance during the sweep cycle. Note how the change in voltage over the change in time (slope) of the VCO signal was reduced and the width of the current peaks widened as the feedback increased. Effectively the system changed from a SFM system (0% feedback) to an admittance locking system (>100% feedback) as it locked on the points of maximum admittance when the feedback was too high. In other words, when the $\frac{dv}{dt}$ of the sweep system becomes smaller than 0 (or negative) on an upward sweep the system locks as the drive frequency begins to reduce. Therefore, the current feedback reduces and $\frac{dv}{dt}$ increases causing an increase in current feedback resulting in a decrease in $\frac{dv}{dt}$ resulting in a continuous loop and locked drive frequency.

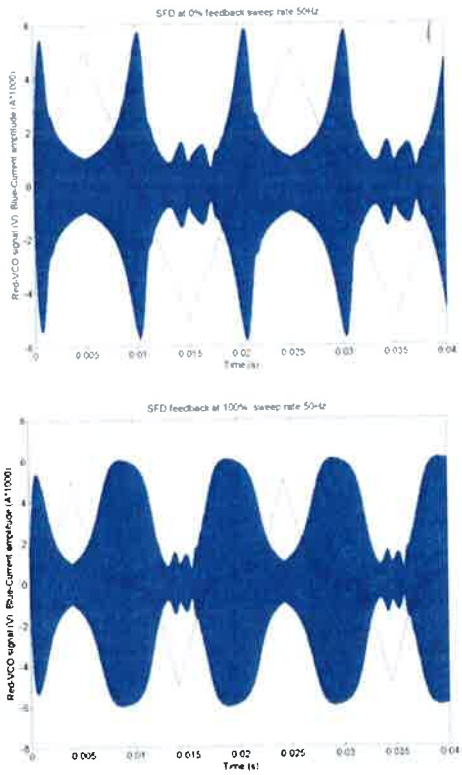

Figure 7-4: The graphs show the changes to the current profile as the feedback is increased. The feedback of the top graph is set at 0% (SFM) and the feedback of the bottom graph is 100% (maximum SFD dwell time)

The change in frequency over the change in time ($\frac{df}{dt}$) is decreased where larger currents amplitudes are required at the points of resonance of the PZT array. This causes a dwell at these particular frequencies in the sweep cycle. The dwell time is proportional to the current amplitude and the sweeprate is indirectly proportional to the amplitude of the current. Therefore, points where higher power is required have preference and more excitation time is applied.

The Simulink model was used to illustrate the effects of changes in the electrical power delivered to the system when the feedback and sweep rate were changed. The average power delivered to the array was assumed to be equal to the average power delivered over one full sweep cycle. The model was used to evaluate the effects of swept frequency dwelling by means of the effects of changes in feedback and sweep rate on the electrical power delivery to the load.

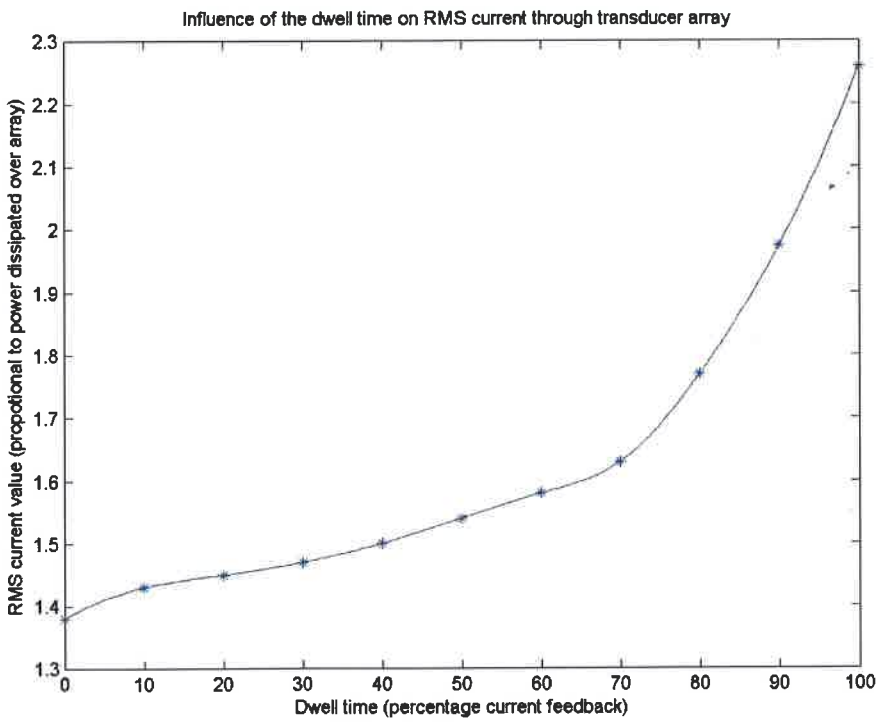

Figure 7-5: The change in power delivered as the feedback is increased. Note how the dwell time increases, possibly because of a reduction in the oscillation phenomenon

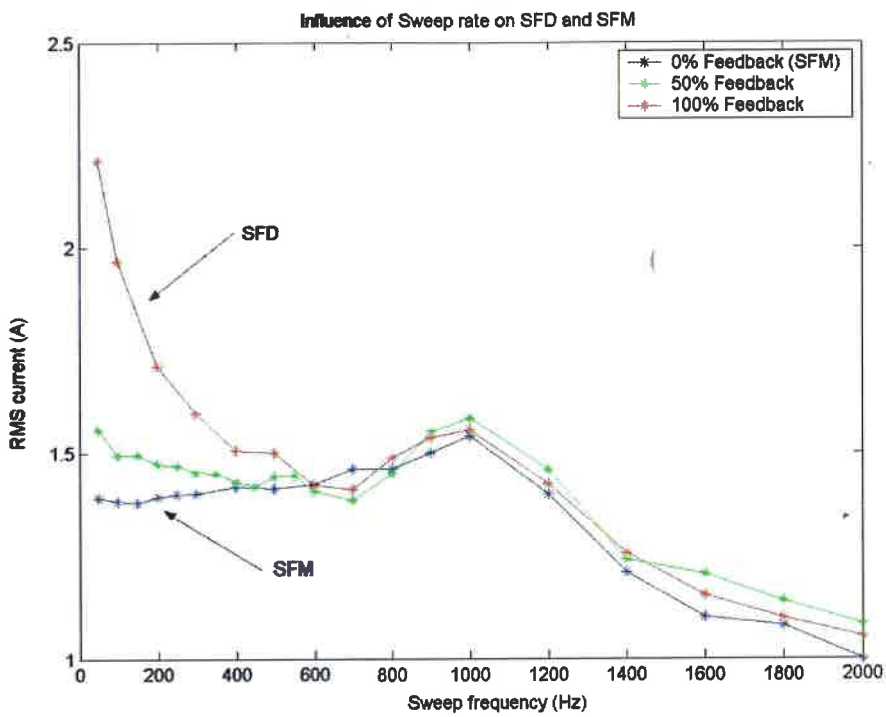

Figure 7-6: The influence that the sweep rate has on the electrical power delivered to the system. The graph shows the transition from SFM to SFD. The advantage of SFD occurs at sweep rates below 500Hz

7.3.2 Discussion

Influence of Feedback Amplitude on SFD

As feedback was increased the dwell time increased causing more power to be delivered to the load. Figure, 7-5 clearly shows the increase in electrical power as the feedback was increased. More electrical power was delivered as the drive system dwelt at the frequencies where resonances occurred and more electrical power was required. The sweep rate in the areas where no resonances occurred became quick enough to "skip through" the regions and return to excite the main resonance points before the "ring down" time expired.

Sweep Rate

The results in Figure 7-6 show a decrease in the delivered electrical power as the sweep rate increases. A possible reason is the transducers and the bath as a resonant system do not have sufficient time to "ring up" to their maximum oscillation amplitude, causing less power to be delivered. SFD seems most effective when its modulation signal frequency is less than 500Hz. This is justified if Figures 7-6 and 7-5 are perused. At higher modulation frequencies SFD and SFM exhibit similar power delivery characteristics.

Swept Frequency Dwelling Characterised

The graph in Figure 7-7, is a combination of results from the sweep rate tests and feedback analysis tests. The X and Y axes represent both variables, while the Z axis represents the electrical power dissipated over the transducer array.

The highest portion of the graph depicts the regions where most electrical power is being dissipated. This area occurs in the backmost corner of the plot where the sweep rate is low and the feedback amplitude high. This is where swept frequency dwelling is most effective in creating cavitation in the vessel.

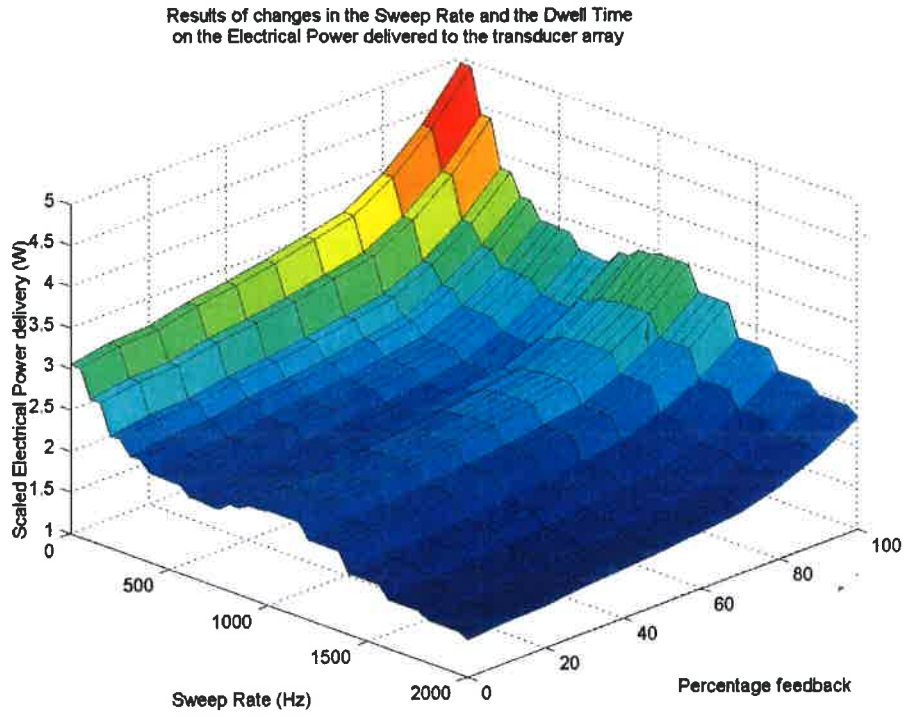

Figure 7-7: The power delivered to the array when both the sweep rate and the amount of feedback introduced to the SFD circuit are altered. Initial tests, gathered from the Simulink model, show that SFD is most advantageous when set at more than 70% feedback and at a sweep rate less than 500Hz. From this graph the best operating region occurs above 80% feedback (max feedback as risk of locking due to possible load changes could occur at higher levels) and a sweep rate in the region of 100Hz

7.4 Circuit design of Swept Frequency Dwelling

The format of the discussion in this section explains the circuits developed to perform the functions of the blocks in the block diagram, Figure 7-1. The subsections focus on separate portions of the circuit, showing relevant diagrams and waveforms. The whole system is briefly discussed and the circuit diagram shown in section 7.4.5.

7.4.1 Current Profile Detection

SFD utilises a current sample acquired from a current sensing resistor placed in series with the transducer array. The array was driven as a voltage fed load, making the current sample proportional to electrical power being delivered. A peak detector was used to acquire a DC representation of the envelope of the current sample.

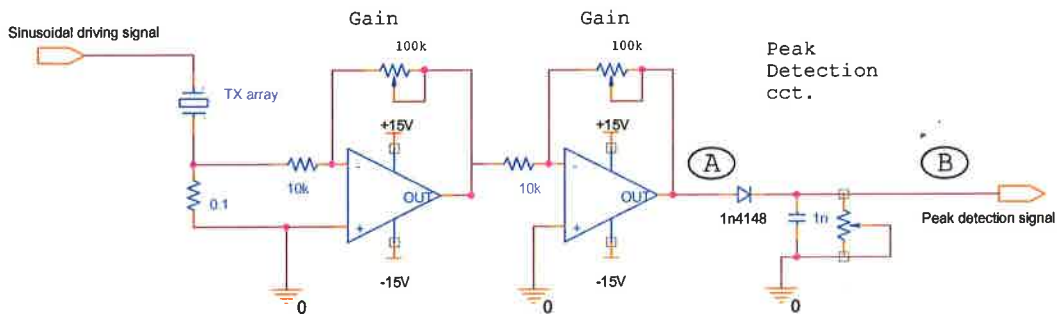

Figure 7-8: This portion of the circuit converts the current feedback sample into a dynamic DC value that has an amplitude proportional to the amplitude of the current profile

Figure 7-8, shows the sinusoidal transducer driving signal that powers the transducer array and the series current sensing resistor on the left hand side. The signal sample from the resistor was amplified by means of two inverting operational amplifiers. The amplified signal was then peak detected using a BAW768 signal diode charging a low pass RC filter with a time constant adjustable by means of a variable resistor. The measured result of the current and DC voltage are shown in Figure 7-9.

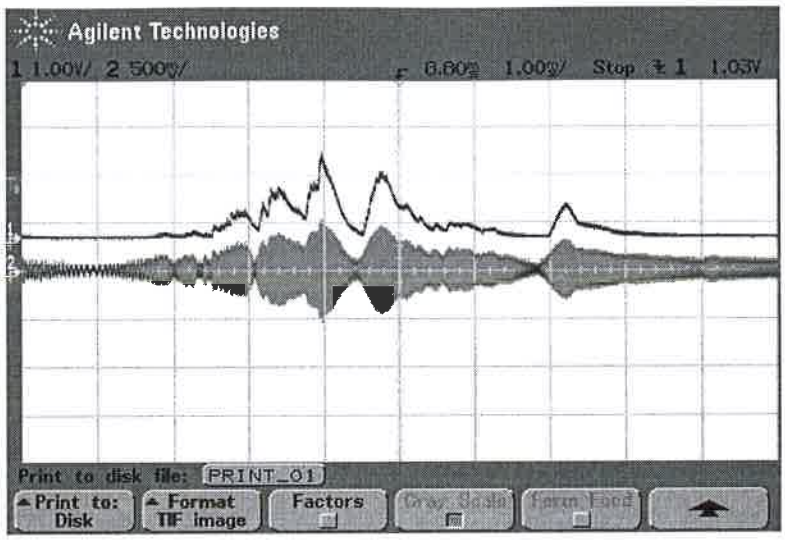

Figure 7-9: The scope trace shows the current through the transducer array, channel 2, and the peak detector signal, channel 1, following the current profile. The waves coincide with the points A and B from the circuit diagram respectively, A is shown as channel 2 and B channel 1

Figure 7-9 shows the current and the generated DC voltage tracking the current's envelope. A simple method of acquiring the envelope of the current was the implementation of a peak detector circuit. An RMS to DC converter could have been used and would have sufficed, but would have been a more expensive and complicated solution.

7.4.2 Generating an Amplitude Modulated Square Wave

Figure 7-10 shows the portion of the circuit discussed in this section. For the purpose of this study the waveform generated by this circuit will be referred to as "*a dynamic amplitude square wave.*"

The dynamic amplitude square wave required integration to generate a triangular wave to be used to drive the VCO. The signal shown in Figure 7-9 was summed to a negative DC value. The new wave was then multiplied by a square wave using an *AD633JN* analogue multiplier. Because the device attenuates the output by a factor of 10 an inverting amplifier was used to restore the signal to its original amplitude.

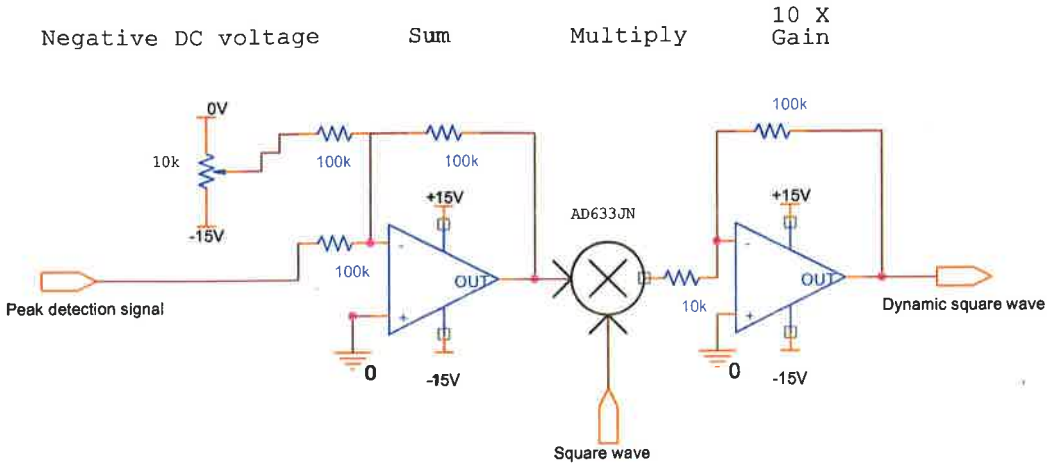

Figure 7-10: The peak detected signal is conditioned and multiplied with a square wave resulting in a dynamic square wave

The dynamic amplitude square wave can be seen in Figure 7-11.

The negative DC value used in this section of the system determined the percentage feedback introduced to the circuit. If it was set to -xV then a +xV amplitude in the peak detected signal resulted in 100% feedback and +0V amplitude in 0% feedback. If the feedback amplitude was to increase to more than +xV, greater than 100%, SFD would lock onto an admittance peak - an Admittance Locking system [7].

7.4.3 Integration and signal conditioning

This part of the circuit consisted of an integrator with two signal conditioning operational amplifiers for gain and offset control. The dynamic square wave was integrated resulting in a triangle wave with a slope ($\frac{dv}{dt}$) proportional to the amplitude of the dynamic square wave. In this way a triangular wave was produced with a steep slope at points where minimal current was being drawn and a gradual slope where high currents were required.

One of two signals produced was used to generate the square wave required for the multiplication shown earlier in Figure 7-10 and another was applied directly to the VCO.

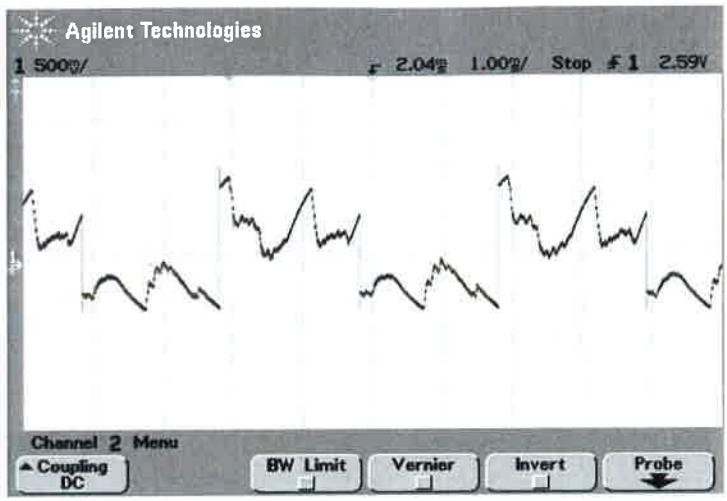

Figure 7-11: The dynamic square wave

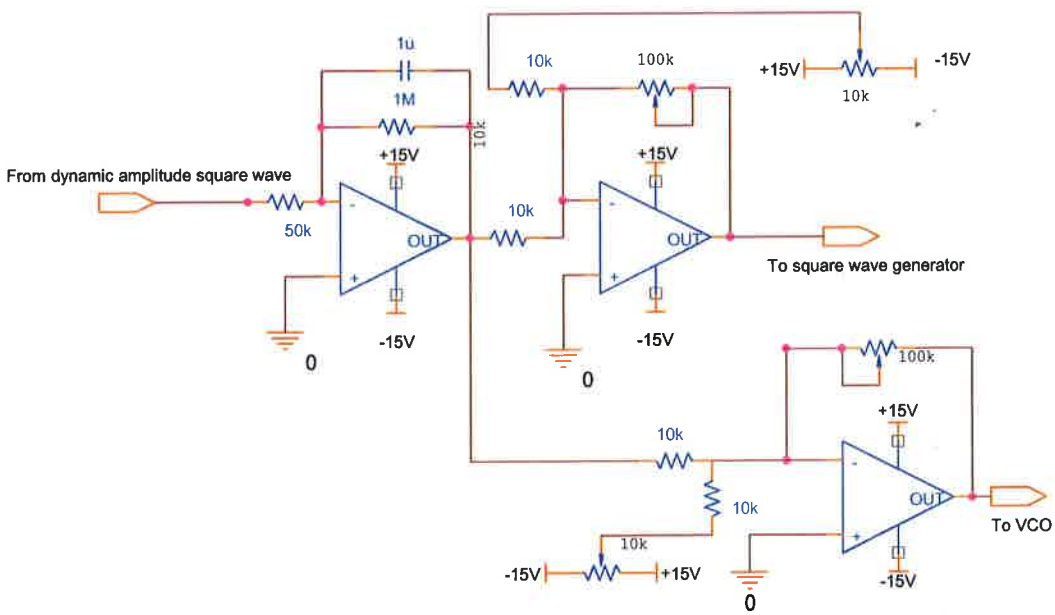

Figure 7-12: The circuit shows three components of the SFD circuit, the integrator used to create the triangular wave and two signal conditioning sections with adjustable gain and offset. The conditioned signals are used in the VCO and bandwidth determination circuits respectively

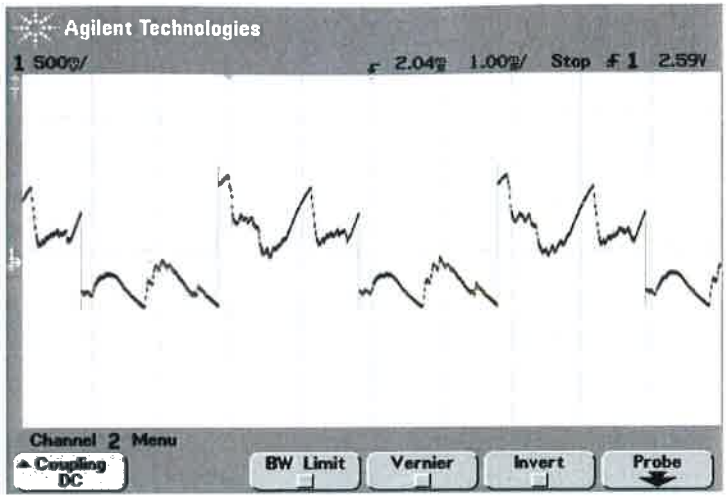

Figure 7-11: The dynamic square wave

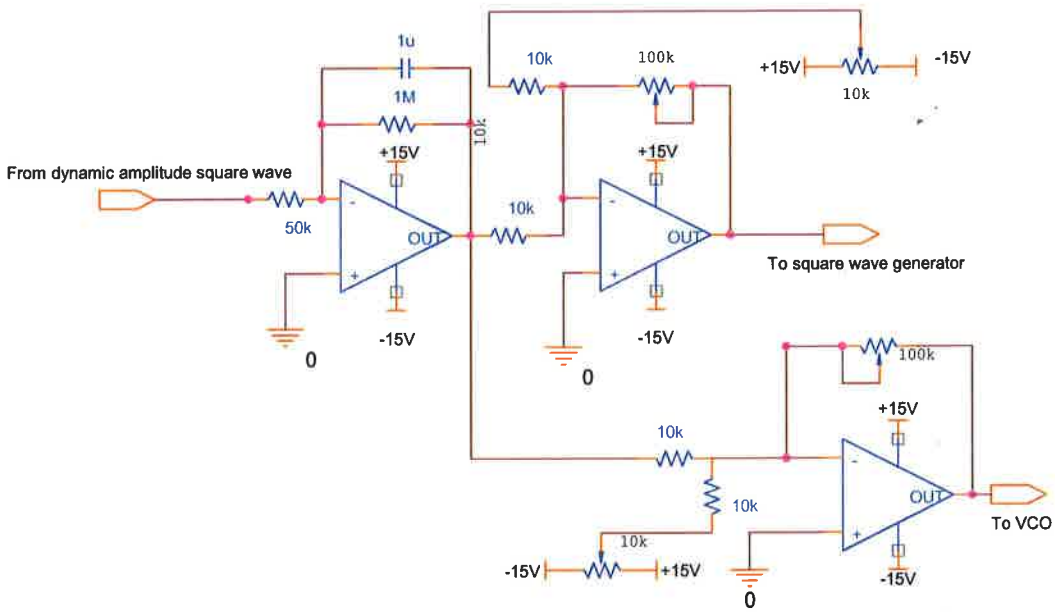

Figure 7-12: The circuit shows three components of the SFD circuit, the integrator used to create the triangular wave and two signal conditioning sections with adjustable gain and offset. The conditioned signals are used in the VCO and bandwidth determination circuits respectively

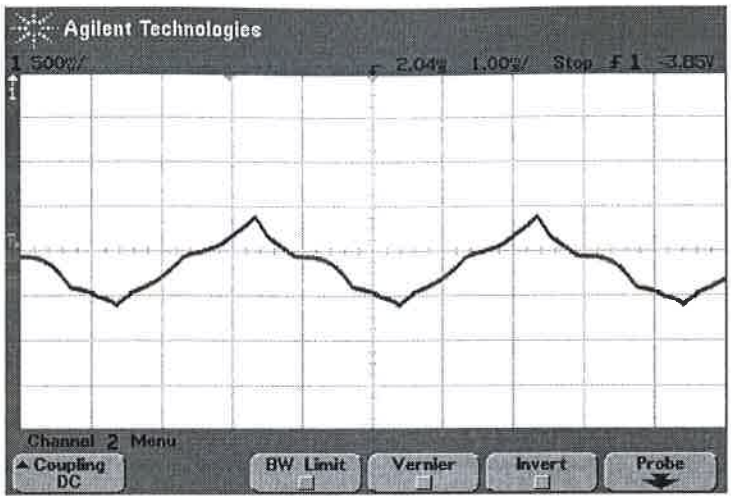

Figure 7-13: The driving signal of the VCO showing the dynamic sweep rate

The signal resulting from the integration section is shown in Figure 7-13. Note the changes in the slope of the waveform. The sweep rate of the system could be changed by altering the amplitude of the dynamic square wave applied to the integrator.

7.4.4 Bandwidth Control Circuit

During initial setup of the SFD system, a bandwidth was required. The choice depended on the load being driven and needed to include all the resonances of the separate transducers in an array (see section 6.2.2). The bandwidth control circuit was used to set the required bandwidth by determining the peak to peak value of the triangular wave driving the VCO. In order to create the triangular wave the result of the peak detected wave was multiplied with a square wave and the result integrated; the square wave used in the multiplication stems from the circuit in Figure 7.14.

The conditioned triangular wave was applied to two comparators with user-adjustable trigger levels. These were used to determine the peak to peak amplitude of the triangle wave (the bandwidth of the sweep). When a predetermined level was met, the respective comparator changed state which either set or reset an RS latch, resulting in a square wave.

The output of the latch was then level shifted and multiplied with the peak detected waveform.

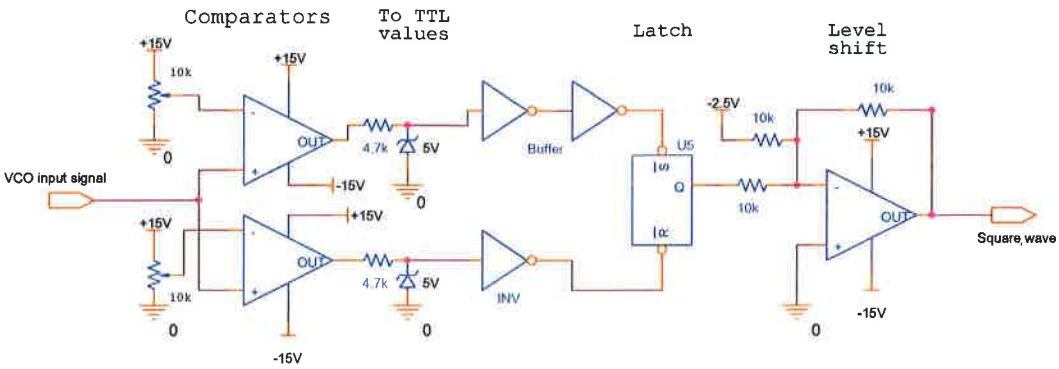

Figure 7-14: The circuit used to determine the bandwidth and produce a square wave to be multiplied with the peak detected value

The circuit shown in Figure 7-14 shows the high and low comparators, the zener diode arrangements used to signal condition the comparator outputs to TTL values, the buffering devices, the latch and the level shifting summer. This section of the circuit was developed as large shifts in the integrator output were experienced from drift. The shifts caused fluctuations in the bandwidth, resulting in an unstable system.

7.4.5 Overview of the Swept Frequency Dwelling circuit

Figure 7-15 shows the entire SFD system. All operational amplifiers used were type LF356N devices. The potentiometers were added to make a flexible system for testing and experimentation, but were replaced with resistors in a permanent application environment. The integrator was chosen to have a slow time constant, not to impose on the fast bandwidth detection loop.

The VCO signal, as well as the current amplitude, can be seen in Figure 7-16.

Note the changes in the slope of the VCO signal and the dwell around the areas where maximum current is being drawn.

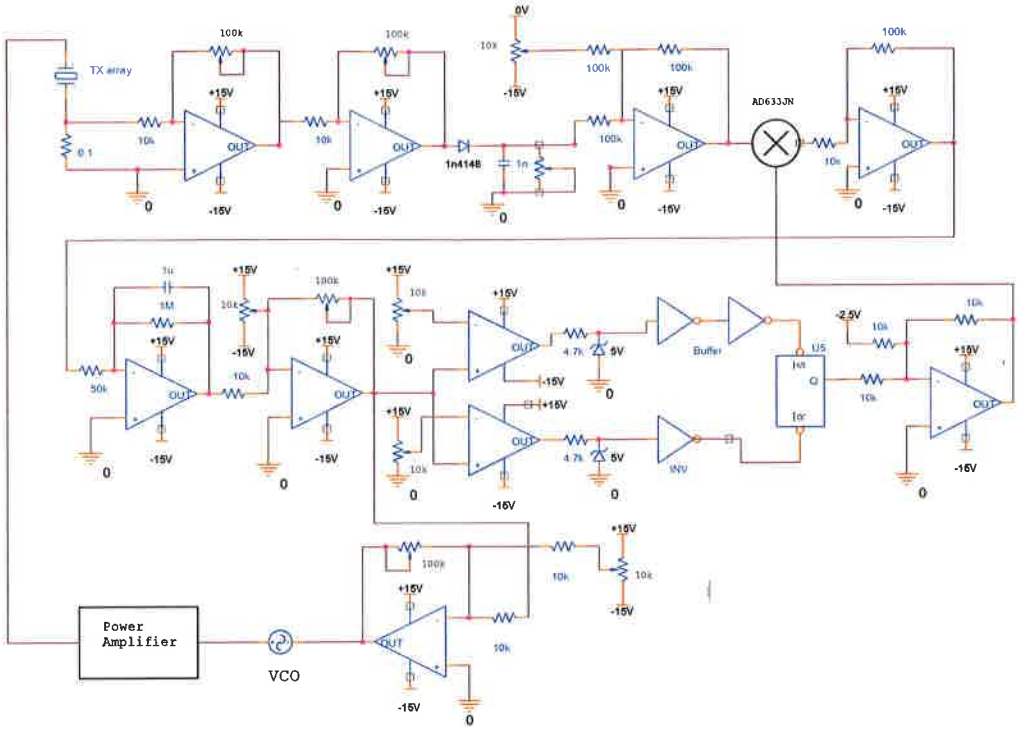

Figure 7-15: The entire SFD circuit showing all the components discussed

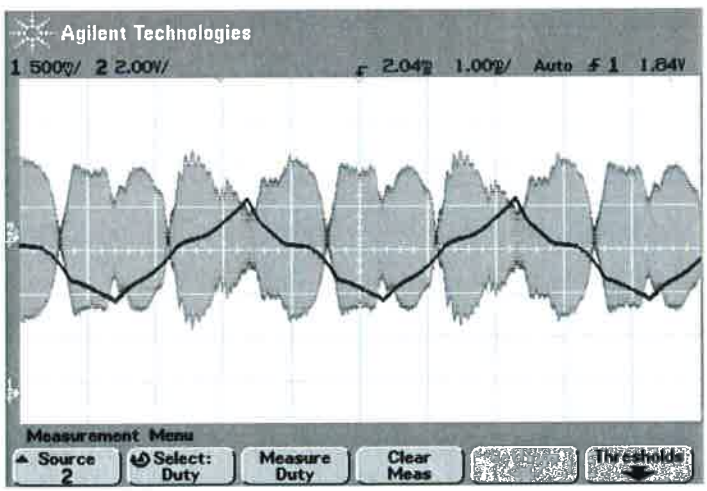

Figure 7-16: Scope trace of Swept Frequency Dwelling showing the current profile (channel 2) and the VCO control signal (channel 1). Note the decrease in sweep rate as the current amplitude increases and vice versa

7.5 Experimental analysis of SFD

Three tests were conducted in order to evaluate SFD numerically and compare it against other driving techniques. These methods were:

1. Acoustic pressure distribution: This test was used to graphically map the acoustic pressure profile inside the bath at low power to compare the acoustic distribution of SFD and other driving techniques;

2. chemical dosimetry: A method used to assess the amount of free radicals produced during transient cavitation to establish the amount of cavitation activity occurring in the vessel and,

3. tinfoil decay test: Also a method used to represent the amount of cavitation occurring and to depict the physical layout of the cavitation activity in the bath.

7.5.1 Acoustic pressure distribution test

Aim

Swept frequency type drive systems used in multiple transducer arrays were implemented to eliminate local areas of intense cavitation activity or "hot spots" created at the antinodes in the liquid [21]. These areas can damage delicate equipment in cavitation baths or affect chemical processes [21]. The aim of this test was to evaluate the spread of acoustic energy inside the test rig by means of graphical representation and inspection. The result could easily be evaluated visually and compared to scans of other driving techniques. This test is valid only at low power levels where cavitation does not occur, because of the delicate construction of the hydrophone used to measure the power.

Apparatus

- A needle hydrophone: An HP series high performance hydrophone measurement set from Precision Acoustic UK was used. The device was equipped with different tips. A tip with a diameter of 0.5mm was used for the tests;

- an XY plotter: The plotter was constructed using two stepper motors controlling the X and Y axes. The Z axis could be moved manually by sliding an aluminium tube inside a cylinder. The hydrophone assembly was fixed inside the moving aluminium tube. The stepper motors were geared in such a way that 1 step caused a movement of the device by 0.25mm. This accuracy was sufficient for the tests to be performed;

- a program written in Labview and a National Instruments high speed acquisition interface card (PCI-6221) were used to signal the stepper motor driving circuit and controlled the two stepper motors. The programme also read in the analogue values from the needle hydrophone and calculated an average value proportional to the acoustic pressure;

- the test bath, discussed in Chapter 3;

- Crest Audio Amplifier (CA6);

- the SFD circuit;

- function generator (Escort EFG-3210) and,

- 4l of distilled water.

Method

The XY plotter was positioned above the bath with a needle hydrophone tip set 50mm from its bottom. This level was randomly chosen and used in all the tests. The bath was filled with 4l of distilled water. Labview was used as a tool to automate the scanning process. The user entered the length and width of the surface to scan as well as the step size between measurements. The step size used for the tests was set at 5mm. When run, the programme moved the plotter to the required position, read a measurement from the hydrophone and saved its average acoustic pressure value to an array, along with the X and Y position of the tip.

The movement of the probe followed a pattern of one length scan followed by one width movement followed by a length scan in reverse, followed by another width scan until the entire surface was scanned at the required depth and the readings saved. The saved file was then manipulated in Matlab resulting in a three-dimensional surface plot of the power profile inside the vessel. The Matlab programme is included in *Appendix B*. The signal generator was used as a VCO to generate a sinusoidal wave which was amplified using the Crest Audio Amplifier to drive the transducer array directly. The bandwidth of the SFD circuit was set to 1kHz, the sweep rate 100Hz and the feedback 80%.

Results

The graph, Figure 7-17 shows the acoustic pressure profile of the bath driven by the SFD system. One can see a random spread of colours rather than clumps of grouped colours of similar shades, demonstrating a non uniform distribution of acoustic pressure across the bath. This was the desired result, showing the average power at each point in the acoustic field is more even than the straight driving and locking techniques tested. The power distribution graphs of SFM and SFD were similar, showing like acoustic pressure distribution.

Conclusion

Figure 7-18 shows the hydrophone scan of the bath being driven by the straight driving technique. This graph clearly shows localised areas of high and low acoustic pressure resulting from standing waves forming under the admittance locking drive system. If Figures 7-17 and 7-18 are compared the advantageous effects of SFD become apparent, as a more even distribution of acoustic pressure is evident.

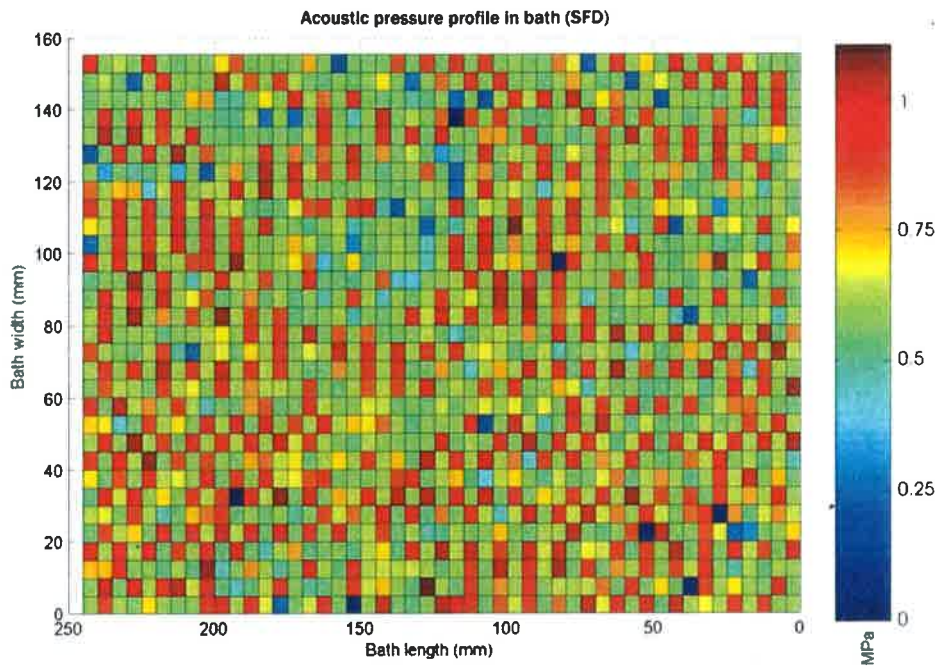

Figure 7-17: This scan shows the elimination of local areas of high and low acoustic pressure when frequency sweeping driving techniques are used. This particular graph is the result of the SFD driving system with a probe depth of 50mm from the bottom of the bath. SFD was driven at 80% feedback and a sweeprate of 100Hz

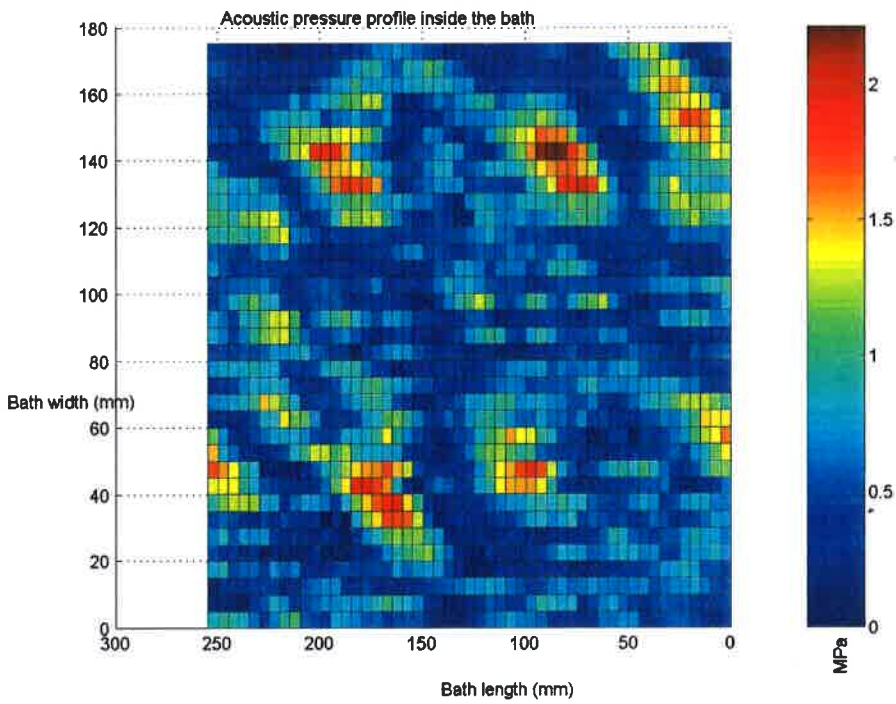

Figure 7-18: The result of the scan performed on the bath at low power levels. The areas of high and low acoustic pressure are evident in the scan and can be recognised as clumps of colour of similar tones. This scan has been added as a comparitive mechanism to highlight the improvements of SFD

7.5.2 Chemical dosimetry (Weissler Test)

Aim

The Weissler Test was used to numerically represent the amount of transient cavitation occurring in the bath when driven by different driving systems. The results were used to compare the driving systems.

Apparatus

- The test bath, discussed in Chapter 3;
- Crest Audio Amplifier (CA6);
- the SFD circuit;
- function generator (Escort EFG-3210);
- spectrophotometer capable of measuring wavelengths of 352nm (Jenway 6300);
- cuvettes for spectrophotometer;
- 4l of distilled water;
- ammonium hepthomolydate, catalytic agent ($((NH_4)^6MO_7(O_2)^44H_2O$);
- potassium iodide (KI);
- $1000\mu l$ Gilson Pipette (P1000) and,
- measuring scale (0.01g accuracy).

Method

Potassium iodide was mixed into distilled water in a proportion of 16.6g/l. A catalyst, ammonium hepthomolydate, was then added at a concentration of 0.1g/l. The solution was mixed thoroughly and exhibited an endothermic reaction.

The Weissler solution was then poured directly into the cavitation vessel and cavitation was produced for a predetermined time. Five minutes of ultrasonic exposure was used for the tests in this project.

The five minute exposure was found to be sufficient in the production of iodine and a significant light absorption at 352nm could be achieved.

After exposure a $1000\mu l$ sample of the liquid was compared to a blanking sample taken before cavitation exposure. The light absorbance at 352nm was measured and the difference between the samples was the result.

7.5.3 Results

Impact of sweep rate on SFD

The Weissler reaction was used to assess the change in the yield of cavitation produced as the sweep or modulation frequency was changed. In this test the sweep frequency was increased in 200Hz increments from 20Hz to 2020Hz. All other parameters were kept constant.

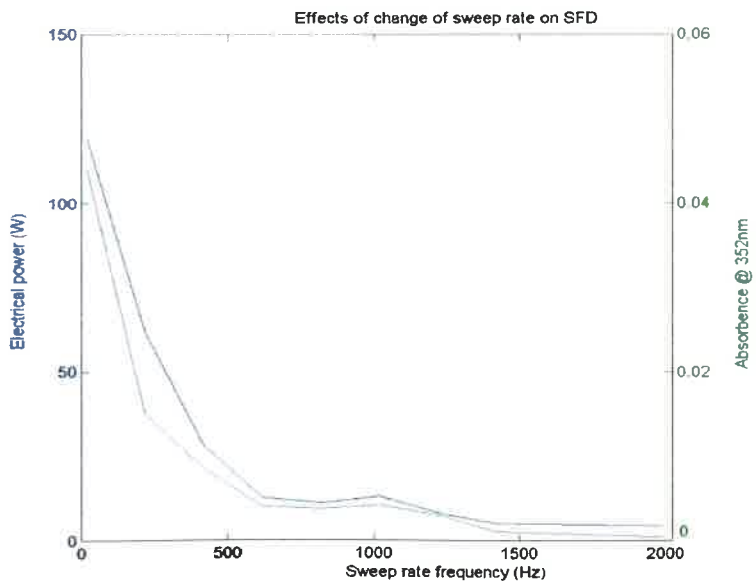

Figure 7-19: Effects of the change in cavitation and electrical power produced when the sweeprate is changed in the SFM system

Figure 7-19 shows a rapid drop in OH production for frequencies below 500Hz. It is assumed that the OH yield would increase to a finite value reaching a maximum point when the sweep rate was 0Hz and the system locked onto the maximum point of admittance. Here SFD became admittance locking. This graph, Figure 7-19, is similar to the simulation performed in Section 7.2.1 and supports the fact SFD is most effective at sweeping frequencies below 500Hz.

Impact of SFD feedback on OH production

The Weissler Test was also used to evaluate the changes in free radicals when the feedback of the SFD system was altered. Effectively changing SFM (no feedback, therefore, no dwelling) to admittance locking (SFD with saturated feedback, therefore, infinite dwelling). When the feedback for SFD was increased beyond its maximum amplitude the dwelling time became infinitely long. This caused the system to lock rather than dwell at the points of high admittance.

The feedback took the form of a current sample and the voltage was kept constant, therefore, an admittance locking system was achieved. When tested, the feedback for SFD was not made to exceed the maximum feedback value (defined as 100% feedback).

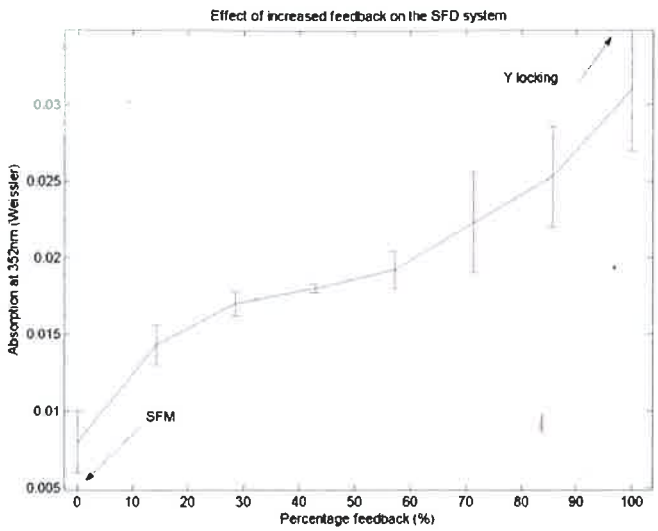

Figure 7-20: OH produced vs amount of feedback. Here SFM at 0% feedback becomes SFD as the feedback is increased. If the feedback increases past 100% the system becomes an admittance locking system

Once again the result is similar to the simulation results, that were shown in Figure 7-5 in Section 7.3.2.

7.5.4 Tinfoil test

This test identified the mechanical behaviour of cavitation located within the vessel. When the cavitation bubbles collapse, energy is released [12]. This energy takes the form of heat, pressure and sonochemical reactions inside the liquid volume. The destructive power of cavitation can be used to illustrate its distribution within a vessel. Tinfoil is ideal for the test as it is a soft metal that erodes fairly quickly because of its thickness ($10\mu m$). The result is regions of intense cavitation destroy the tinfoil, while areas of minimal cavitation cause the tinfoil to remain largely intact. This method of assessing mechanical behaviour is simple and visually effective.

A two-dimensional model of the cavitation profile was created and viewed showing slices of cavitation activity inside the vessel.

Aim

The test crudely illustrated both cavitation location and the amount of cavitation activity inside the vessel. The results were used as evaluation tools to compare driving techniques.

Apparatus

- The test bath, discussed in Chapter 3;
- Crest Audio Amplifier (CA6);
- the SFD circuit;
- one function generator (Escort EFG-3210);
- tinfoil (light weight) and,
- 4l of distilled water.

Method

During this test a sheet of aluminium foil was placed inside the cavitation medium 10mm from the bottom of the bath. The electrical power being injected into the system was measured over a single full cycle of the modulation signal. The exposure time was set at 1.5 minutes.

Results

The tinfoil shown below depicts the resultant decay after 90 seconds of exposure. The bath was driven by the SFD system at a measured electrical power of 48W RMS.

The positions of the transducers can clearly be seen indicating all transducers produced cavitation. This was not the case in the straight driving techniques, where it was found certain transducers did not function.

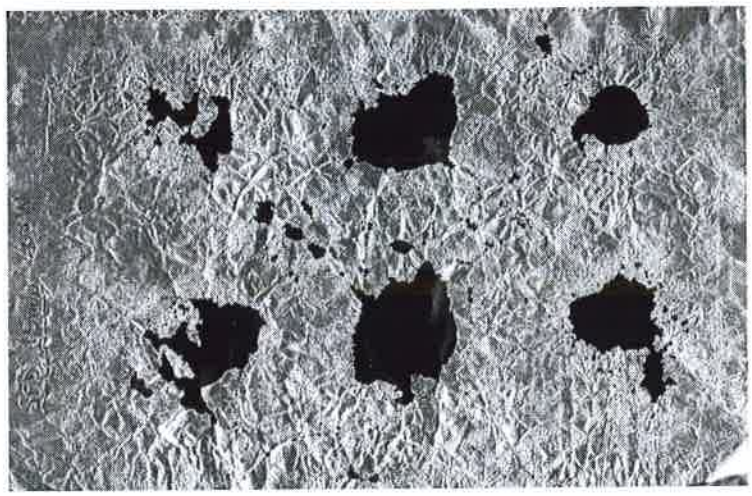

Figure 7-21: SFD: Result of cavitation exposure for 1.5 minutes at 48W RMS. The system was driven at 80% feedback and a sweeprate of 100Hz. Note the locations of the six transducers and the distribution of the holes formed by them showing that all six transducers are functioning

7.5.5 Discussions

Swept Frequency Dwelling versus Swept Frequency Modulation

The Weissler Test was used to measure the difference in cavitation yield between SFM and SFD in relation to the electrical power being dissipated over the array. In order to measure the electrical power dissipated, Labview was used to sample the electrical voltage, current and VCO signals simultaneously, at a rate of one million samples per second.

The aim of the experimentation was to evaluate if SFD would deliver more acoustic power, in the form of cavitation, to the vessel than SFM.

The test was performed on a 4l sample of liquid with a cavitation exposure time of five minutes. The result was confirmed by repeating the test four times in quick succession. The sinusoidal wave applied to the power amplifier was kept constant for all tests with respect to its centre frequency and amplitude. The bandwidth and sweep rate of SFM and SFD were also kept constant.

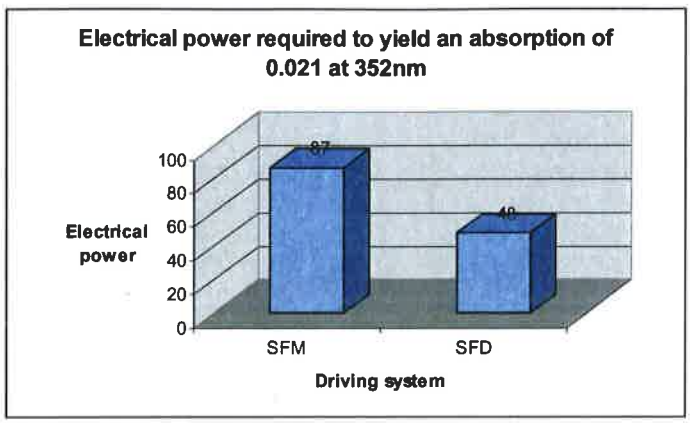

Figure 7-22: This graph shows the amount of electrical energy required to yield the same amount of cavitation. SFD proved mode efficient than SFM, requiring only 48W, where as SFD demanded 88W to yield an equal amount of cavitation

The results in Figure 7-22 indicate SFD produced almost twice the amount of cavitation as SFM when powered by the same amount of electrical energy. This finding was supported by the tinfoil results of SFM and SFD. Figure 7-23 shows the result of the SFM foil test driven at an average power of 88W for 90 seconds. If compared to the SFD foil, Figure 7-21, which was exposed for the same amount of time, but at an average power of 48W, more destruction of the foil was apparent.

Results show SFD produced about 50% more cavitation than SFM at equal sweep rates and bandwidths. This result, however, cannot be supported by the simulations, as those were purely electrical and did not support acoustic behaviour inside the vessel.

The acoustic scans depicted a more even spacial distribution of acoustic energy to that of straight driving and locking techniques at low power (no cavitation) showing SFD better suited to PZT array applications.

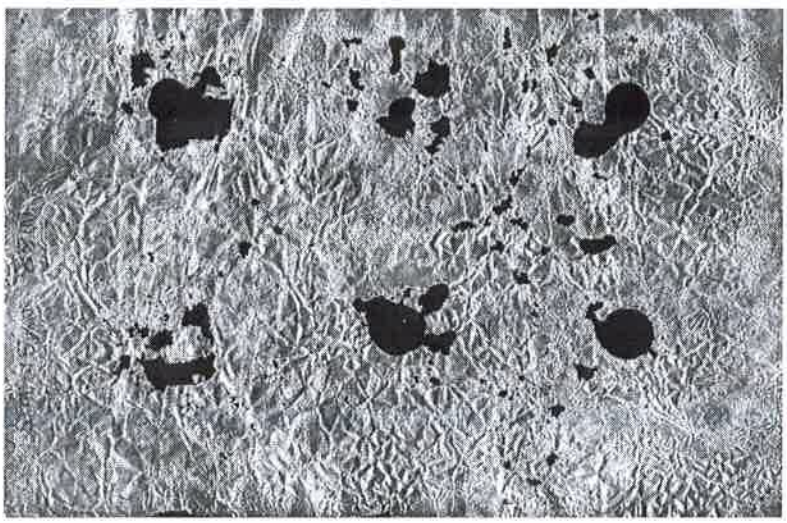

Figure 7-23: SFM: Result of cavitation exposure for 90 seconds at 88W RMS

Chapter 8

Conclusions

When high power PZT arrays are used, manufacturers strive to achieve two goals:

1. Maximum electroacoustic power dissipation over the transducer array, resulting in maximum produced cavitation in the liquid. Ideally, each transducer in the array should operate at its resonance frequency, ensuring maximum electrical power dissipation, mechanical movement and, therefore, cavitation in the vessel and,

2. an even acoustic field distribution within the cavitation medium (resulting in a field not characterised by local nodes and antinodes) ensures parts in the cleaning bath remain undamaged. Chemicals being treated in sonochemical reactors could also be ruined by local areas of intense cavitation.

The required testing of different driving techniques led to the successful construction of a test rig used to simulate an industrial high powered cavitation bath, powered by an array of six tonpilz transducers connected in parallel.

8.1 Single frequency drive systems

The first method tested was the straight driving technique, where the array was continually driven at its resonance frequency.

The low power testing using a hydrophone disclosed the distribution of acoustic power inside the liquid was uneven and showed local areas of high and low acoustic pressure, as would be expected with local standing waves. During high power testing with cavitation, the bath was found to operate in an inefficient manner as surface waves (caused by streaming) and loading conditions in the bath led to major changes in the resonance frequency of the system.

A tinfoil test indicated five transducers out of six caused significant damage, while one transducer did not operate. The reason for the inconsistency in the tinfoil damage in the region of each transducer was found to be a result of the transducers in the array having different series resonant frequencies.

The sum of the admittance plots of the separate transducers formed a net series resonance frequency uncommon to any individual transducer resonance frequency. This caused the devices to be driven in an inefficient electromechanical manner. The inconsistent damage to the tinfoil indicated that straight driving techniques are unsuitable for multiple PZT array applications.

In an effort to improve cavitation yields produced by the straight driving technique, two methods, phase and admittance locking were tested.

These methods utilised feedback as a means of tracking the shifting net resonance frequency of the load. Phase locking utilised the phase angle between the voltage and current as a feedback mechanism. In monitoring both the phase and shifting the frequency it was possible to track a particular phase angle corresponding to a particular resonant mode. This technique would be ideal had the resonance frequency of the transducer array occurred at a particular, unchanging phase angle.

In the case of PZT transducers, however, the phase angle at resonance changed as it was load dependant and generally did not occur at 0°. The particular phase angle required was, therefore, determined by the user which meant set-up errors were possible. The phase was deliberately off the corresponding resonance phase angle, resulting in a substantial reduction in cavitation activity within the vessel. Phase locking systems are monotonic, restricting them to narrow operating bandwidths because of the Q and the phase characteristics of the array.

The nature of PZT transducers caused the resonance phase angle to change with acoustic load resulting in a possibility for the system to lock off its resonance frequency.

When the resonance phase angle was set up correctly, results in the region of 50% improved over those of the straight driving technique were achieved. This was seen when the chemical dosimetry tests results of the two techniques were compared. Phase locking yielded the region of double the amount of cavitation than straight driving at equal electrical power levels.

Tinfoil tests showed large amounts of deterioration present, but two of the six transducers did not function. Although considerably more cavitation activity was achieved than straight drive, phase locking techniques exibited fundamental flaws in driving PZT arrays.

To overcome the narrow bandwidth problems associated with high quality factor transducers and the requirement of a user defined resonance phase angle, Davies *et al* [7] utilised power as a feedback mechanism to lock onto the series resonance peak of the bath and named the technique admittance locking.

At startup, this technique was made to scan the entire bandwidth of the load in order to locate the admittance peak. This elliminated the possibility of the system locking at a local minima. Once located, admittance locking continually tracked the admittance peak.

This automated procedure eliminated the need for any user input. Admittance locking was not monotonic resulting in considerably wider operating bandwidths (unlike that of phase locking).

Tests with admittance locking yielded much the same results as phase locking, when the phase angle was correctly set, but proved a better locking system as errors in user defined inputs were eliminated and wider operation bandwidths achieved.

Admittance locking can, therefore, be viewed as the best single frequency drive system and well suited to single transducer loads, but an inappropriate locking system for PZT arrays, as the electrical power was not evenly distributed across the transducer array.

8.2 Swept frequency drive systems

The tinfoil tests showed the driving techniques tested thus far developed an uneven electroacoustic distribution across the transducers in the array. This was because the net series resonance frequency of the array did not necessarily coincide with any of the single resonance frequencies of the transducers. To include all resonance frequencies into the driving procedure and, therefore, create a more even distribution of electrical power across the array, frequency sweeping was examined. Frequency sweeping, or swept frequency modulation (SFM), swept through a predetermined frequency bandwidth in a repetitive manner. As the frequency bandwidth was swept, individual resonances of the transducers were excited causing a more even distribution of electroacoustic power across the transducer array.

This was indicated in the tinfoil test result as mechanical destruction could be seen at each of the six transducer locations. A problem with this technique was a reduction in cavitation created in the vessel in comparison with that of straight driving techniques (chemical dosimetry test results). The amount of electrical power being dissipated in each sweep cycle was determined by the Q of each transducer. It was found that the maximum sweep rate was determined by the Q of the transducers in the array as unwanted resonant behaviour occurred at sweep rates that were too high.

The novel driving technique, named "swept frequency dwelling" (SFD), was conceived with the aim of maintaining an even acoustic distribution across the array created by SFM, while increasing the amount of cavitation produced in the vessel.

SFD is a simple, low cost analogue solution which can be implemented on any PZT load. It eliminates the need for costly additional components and more complex systems. SFD can be seen as a hybrid system containing elements of both SFM and admittance locking. The concept is an SFM system made to dwell on the points of high admittance as a frequency bandwidth is swept. In this way individual transducers have time to "ring up" during their activation period and continue ringing as the bandwidth is swept and while other transducer resonances are being excited.

Less time in the sweep cycle is then spent as minimal electrical power is dissipated, causing a significant increase in the cavitation produced over a cycle.

In comparison with SFM, chemical dosimetry test results showed half the electrical power dissipated yielded equal cavitation, indicating SFD was twice as efficient as SFM.

The tinfoil results for SFD echoed these findings, showing more destruction of the foil at about half the electrical power. The tinfoil also demonstrated all six transducers functioned. As the sweep rate was reduced at frequencies where admittance increased, a lingering at the resonance frequencies was achieved, resulting in more electrical power being dissipated during the sweep. The transducers had sufficient time to "ring up" to optimal mechanical oscillation resulting in better electroacoustic power transfer.

SFD could be set by the user to create optimal electrical power distribution across the transducers forming the array or maximum cavitation activity inside the vessel. The feedback could be changed from SFD (maximum electrical power delivery at 100% feedback) to SFM at 0% feedback to "inverse SFD" at negative feedback.

Inverse SFD dwelt on areas of low admittance rather than areas of high admittance, effectively skipping over the resonance points of the array. This caused a better electrical power distribution across the transducer array, but minimal cavitation activity. The graph in Figure 8-1 is a summary of the capabilities of SFD, showing the impacts of sweep rate and feedback on the distribution of electrical power across the array.

At frequencies higher than 500Hz SFD showed similar trends to SFM regardless of the feedback applied and the distribution of the electrical power was inversely proportional to the total power being dissipated. Figure 8-1 also shows that inverse SFD at low sweep rates resulted in an optimal spread of electrical power across the array and minimal electrical power dissipation. Maximum feedback at low sweep rates resulted in poor electrical power distribution, but maximised electrical power dissipation over the array.

Adjustable attributes make SFD a user friendly system aimed at driving high powered ultrasonic PZT arrays. The driving method can deliver high electrical power, even distribution of electrical power over the transducers forming the array or any variation thereof. This novel driving system is specifically suited to high powered piezoelectric tonpilz transducer arrays.

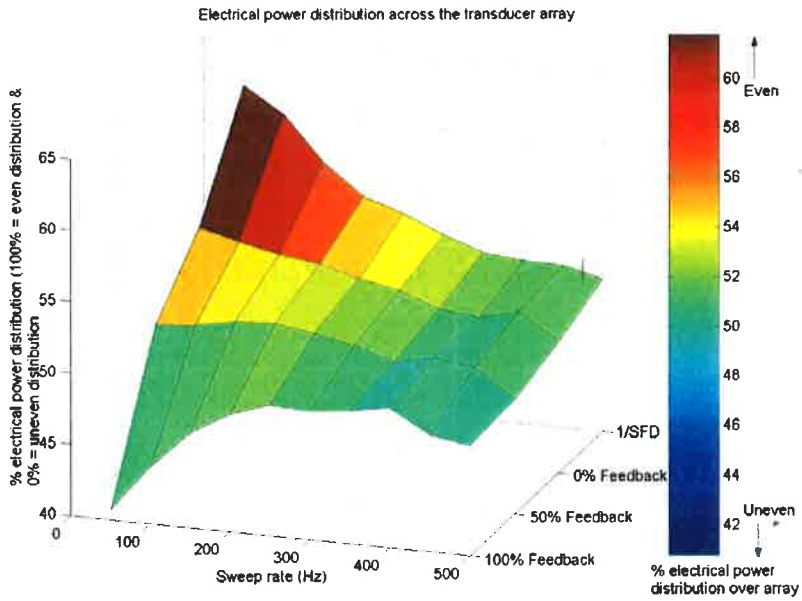

Figure 8-1: An illustration of the effects of feedback and sweeprate on the electrical power distribution over the transducer array. Even distribution occurs at minimum sweeprate when inverse SFD is applied. Minimum electrical power is dissipated across the array in this region of the graph. Maximum electrical power dissipation occurs when an uneven distribution of electrical power is achieved across the array when sweeprate is minimal and SFD feedback is maximum. The effects of SFD are most apparent in the bandwidth between 0 and 500Hz

8.3 Future work

There is room for further work on this project as different transducer types, including wide bandwidth modules, were not assessed. An experimental analysis of SFD on these types of transducers would verify if it would improve their performance in array applications.

The effects of SFD can be tested on cavitation vessels utilising minimal (two) transducers to large scale implementations, where large numbers of transducers, possibly exceeding tens of devices are used. There is no limit to the possibilities of the driving system and it will surely be found to be effective as long as the resonance frequencies of the transducers in the array fall within the bandwidth of the driving system.

SFD could be implemented with current and voltage feedback eliminating the need for constant voltage drive signals.

A digital SFD system could be undertaken eliminating analogue electronics.

References

[1] J. BELL. "Satellite Resonances in Ultrasonic Interferometry". Proc. Physical Society LXIII (1950).

[2] D. BERLINCOURT. "Piezoelectric Ceramics: Characteristics and Applications". Acoustical Society of America, 70(6), pp. 1586-1595 (1981).

[3] R. BEYER. "Nonlinear Acoustics". Brown University, Providence, Rhode Island (1974).

[4] R. COATES AND R. MATHAMS. "Design of Matching Networks for Acoustic Transducers". Ultrasonics, 26, pp. 59-64 (1988).

[5] F. CRAWFORD. "Waves, Berkeley Physics Course - Volume Three". McGraw-Hill Book Company, New York (1968).

[6] J. DAVIES. "Continuous Wave Mode Locking for the Determination of the Acoustic Nonlinear Parameter B/A". PhD thesis, University of Cape Town, South Africa. (Unpublished) (2001).

[7] J. DAVIES, T. DU BRUYN, B. MORTIMER, AND J. TAPSON. "High Power Resonant Tracking Amplifier Using Admittance Locking". Ultrasonics, 39, pp. 257-261 (2001).

[8] K. FIDDY, P. LORIMER, AND T. MASON. "Enhancement of Chemical Reactivity by Power Ultrasound: An Alternative Interpretation of the Hot Spot". Ultrasonics, 29, pp 338-343 (1991).

[9] F. FUCHS. Ultrasonic cleaning - fundamental theory and application (3 February 2006). http://www.blackstone-ney.com/04.tech$_papers.php$.

[10] A. GREEN. "Design of High Powered Ultrasonic Transducers". B.Sc. Thesis, University of Cape Town, South Africa. (Unpublished) (1999).

[11] A. HENGLEIN. "Sonochemistry: Historical Developments and Modern Aspects". Ultrasonics, 25, pp.6-16 (1987).

[12] T. KIMURA, T. SAKAMOTO, J. LEVEQUE, H. SOHMIYA, M. FUJITA, S. IKEDA, AND T. ANDO. "Standardization of Ultrasonic Power for Sonochemical Reaction". Ultrasonics Sonochemistry, 3, pp S157-S161 (1996).

[13] E. KINSLER, R. FREY, B. COPPENS, AND V. SANDERS. "Fundamentals of Acoustics, Third Edition". John Wiley and Sons (1982).

[14] T. MASON. "Use of Ultrasound in Chemical Synthesis". Ultrasonics, 4. pp. 245-253 (1986).

[15] T. MASON. "Industrial Sonochemistry: Potential and Practicality". Ultrasonics, 30(3), pp 193-196 (1992).

[16] T. MASON AND J. BERLAN. "Sonochemistry: From Research Laboratories to Industrial Plants". Ultrasonics, 30(4), pp. 203-212 (1992).

[17] W. MASON. "Electromechanical Transducer and Wave Filters, First Editon". D. Van Nostrand Company (1942).

[18] J. MATHEWS AND K. FINK. "Numerical Methods Using MATLAB, Third Edition". Prentice Hall (1999).

[19] R. MORKEL. "High Frequency Class-D Inverter for Ultrasonic Loads". B-Tech Thesis, Cape Technikon, South Africa, (Unpublished) (2002).

[20] A. MORRIS. "Principles of Measurement and Instrumentation, Second Edition". Prentice Hall, New York (1993).

[21] T. PIAZZA AND W. PUSKAS. Ideal ultrasonic parameters for delicate parts cleaning (20 May 2005). http://Blackstone-ney.com/04.tech_papers.php.

[22] L. RAYLEIGHLY. Phil. Trans. Roy. Soc, London, 175(1) (1884).

[23] T. SMITH. "Design of a High Powered Ultrasonic Cavitation Bath". B-Tech Thesis, Cape Technikon, South Africa, (Unpublished) (2004).

[24] D. STANFIELD. "Underwater Electroacoustic Transducers". Bath University Press and Institute Of Acoustics (1991).

[25] UNKNOWN. Federal standard: Telecommunications - glossary of telecommunication terms (1037C, 1996).

[26] UNKNOWN. "www.Piezo.Com". Piezo Systems, Inc. (12 April 2005).

[27] UNKNOWN. Phillips appication book: Piezoelectric ceramics, unknown author (2001).

[28] B. ZEQIRI, M. HODNETT, AND A. CARROLL. "Studies of a Novel Sensor for Assessing the Spatial Distribution of Cavitation Within Ultrasonic Cleaning Vessels". Ultrasonics, 44, pp. 73-82 (2006).

Appendix A

The Labview programme used to acquire acoustic scans

A.1 The primary block diagram

A.2 The block diagram of the function used to move the plotter

A.3 The block diagram of the function used to build the data array

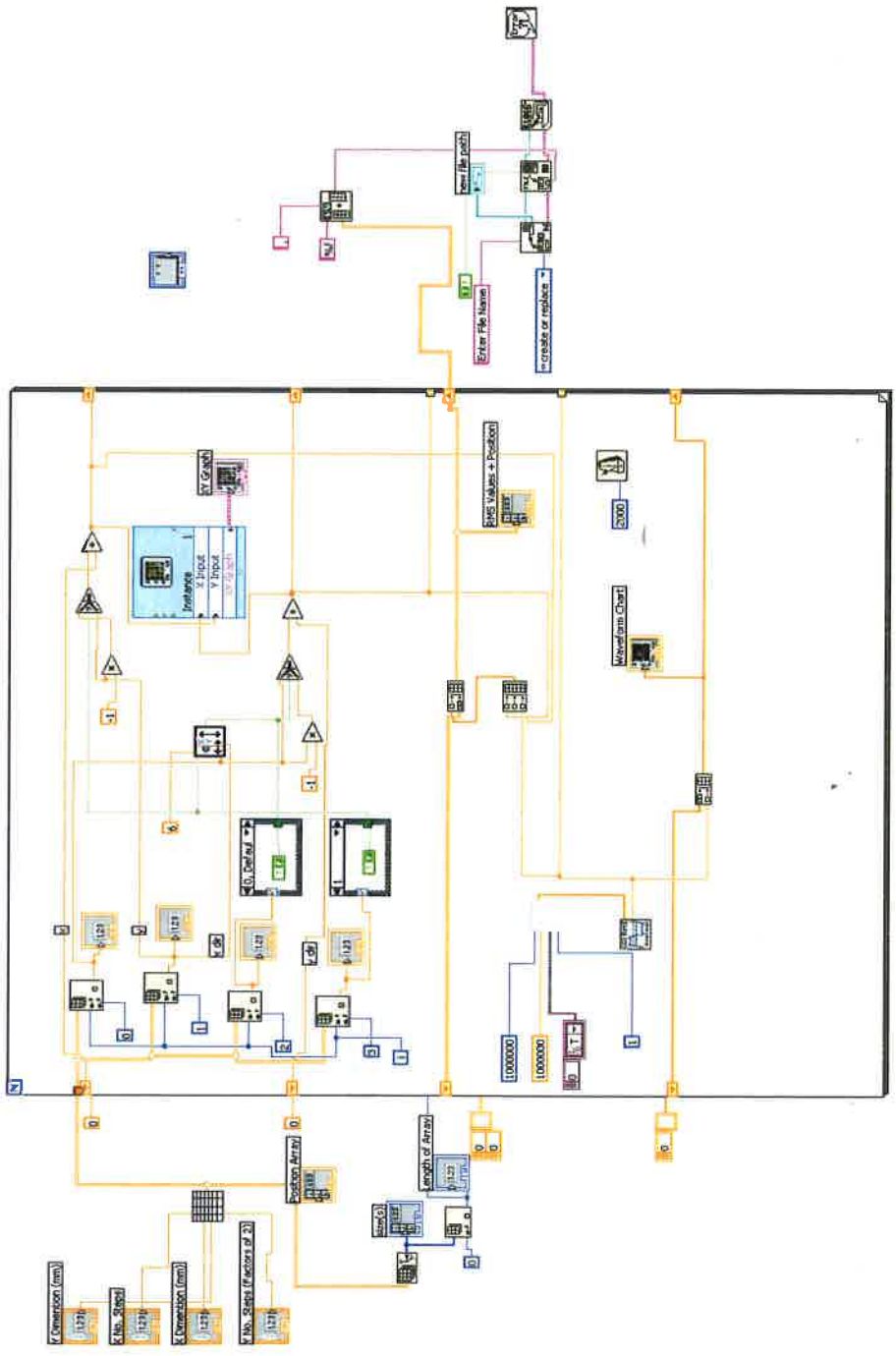
new file path
Enter File Name
create or replace
XY Graph
RMS Values + Position
2000
Waveform Chart
Instance
X Input
Y Input
Delay
1000000
1000000
Position Array
Length of Array
X Dimension (mm)
No. Steps
X Dimension (mm)
No. Steps (Factors of 2)

Figure A-1:

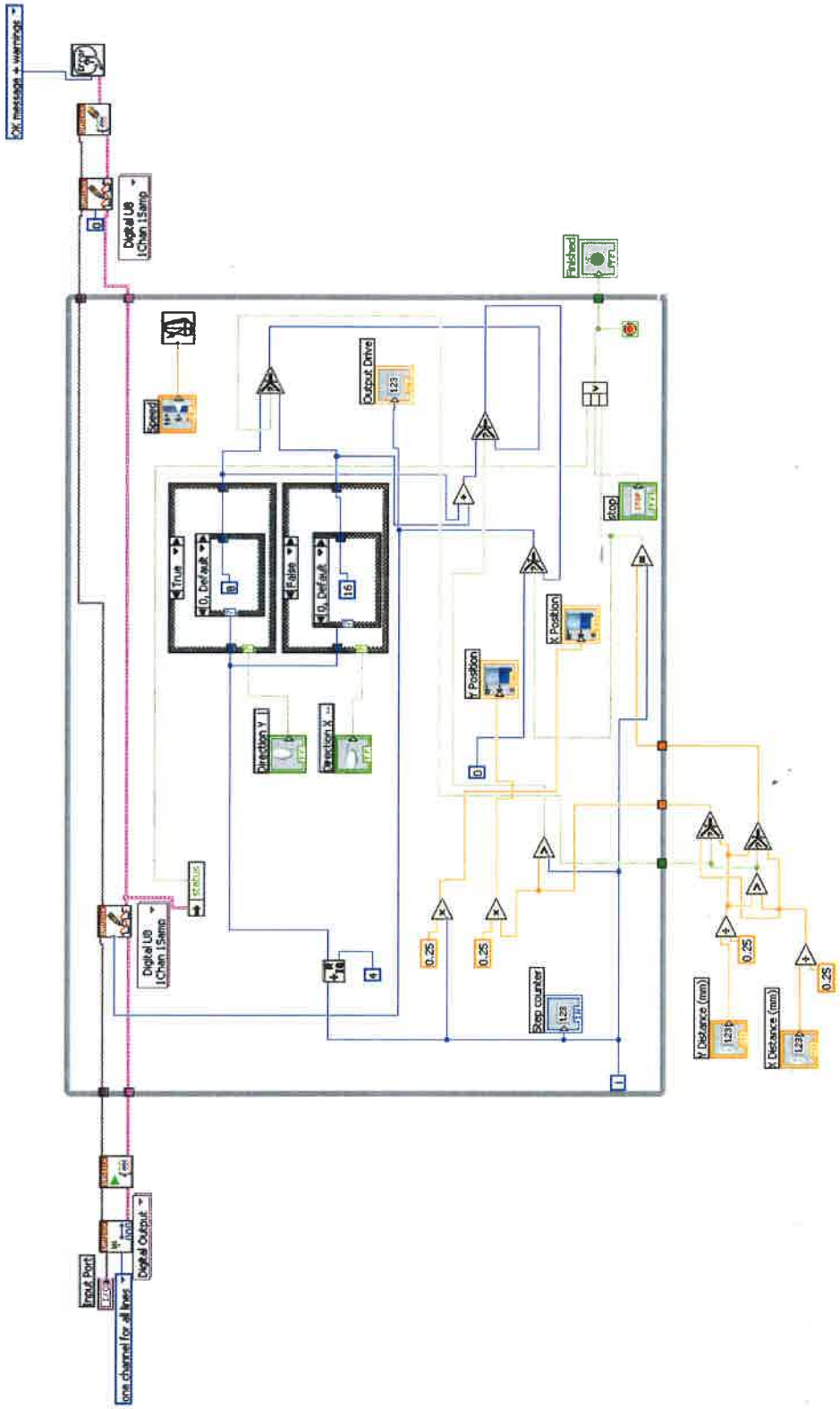
OK message + warnings
Digital I/O
1Chan 1Samp
Finished
Speed
Output Drive
True
0, Default
False
0, Default
16
Stop
X Position
Y Position
Direction Y
Direction X
Digital I/O
1Chan 1Samp
0.25
0.25
Stop counter
0.25
0.25
Y Distance (mm)
X Distance (mm)
Digital Output
Input Port
one channel for all lines

Figure A-2:

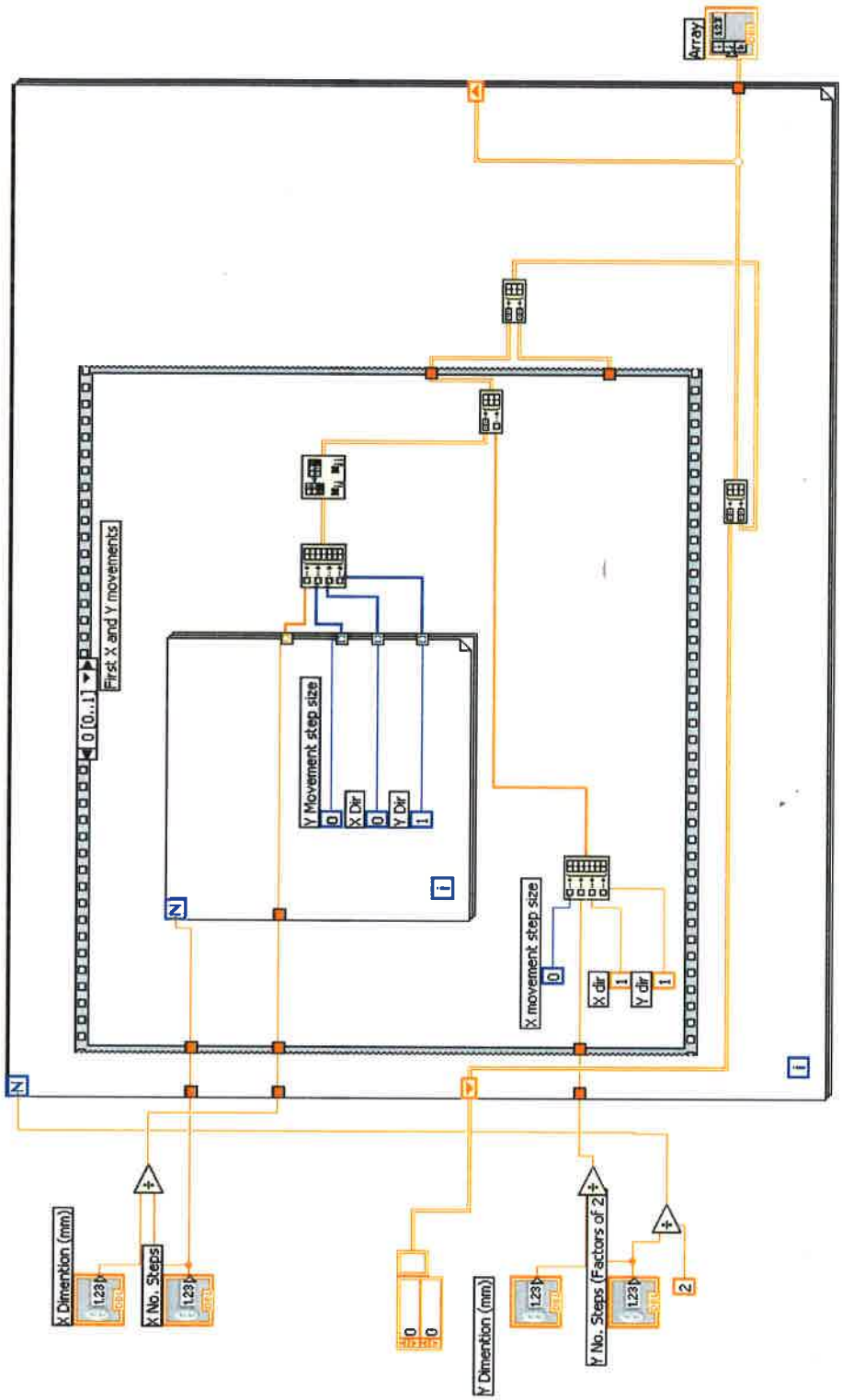
Array
First X and Y movements
Y Movement step size
X Dir
Y Dir
X movement step size
X dir
Y dir
X Dimention (mm)
X No. Steps
Y Dimention (mm)
Y No. Steps (Factors of 2)

Figure A-3:

Appendix B

Matlab programme written to draw a surface graph from the data measured during the acoustic power scan

```
%-------------------------------------------------
% Programme to build surface scan of Labview data file
%-------------------------------------------------
data = data';
%rotate array
a = data(:,1);
%extract data from array
b = data(:,2);
c = data(:,3);
ref = 0;
p = min(a)/a(3);
%length of new array
p = p + 1
```

Matlab programme written to draw a surface graph from the data measured during the acoustic power scan

```
%add on 1 for place 0 on scan grid
q = abs(a(3))
for r = (1:1:32);
    %change last to the number of Y steps + 1
     ref = ref + p;
     d(:,(r)) = c((ref-(p-1)):(ref));
end
d
c = 2;
b = size(d)/2;
for a = (1:1:b(:,2));
    %do loop length of array/2
     temp = d(:,c) ;
    %make temp the row (c)
     temp = invert(temp) ;
    %invert temp
     temp = temp';
     d(:,c) = temp;
    %put inverted row back into (d)
     c = c + 2;
end
[X,Y] = meshgrid(0:q:155,0:q:250);
%Y X grid must be (Xdim) same with Y in that order
figure(1)
surf(X,Y,d)
%draw graph
```

Appendix C

Q Matching

C.0.1 Q-matching

Q-matching can be viewed as a hybrid series-parallel resonant circuit. The combination allows the use of the attributes of both series and parallel circuits to manipulate the load to the requirements of the driving system, usually a class D switching amplifier. The Q of the load may be changed, making it compatible with D class amplifiers as harmonics can be filtered from the square wave input. The two capacitors, C1 and C2 (Figure C-1), result from a single series resonant capacitor split into two. The split capacitance is used as a voltage divider with which the voltage over the transducer array is controlled. This ensures ease of alteration of the voltage across the PZT or array by the proportional variation of the two capacitors.

When operating, the ultrasonic bath creates acoustic "noise" that is transformed via the transducers into electrical noise (inverse piezoelectric effect). This noise, if allowed back into the driving circuit, is capable of causing damage to other components of the arrangement. One of the main advantages of Q-matching when used in PZT ultrasonic applications is its filtering capability. High frequency noise is filtered out of the system before damaging other components (see Figure C-1).

Figure C-1 shows the path by which the acoustic noise can travel to earth via capacitor C2 filtering the generated high frequency noise from the system.

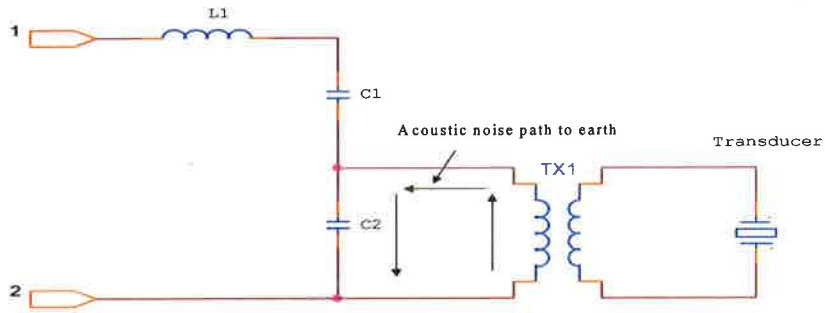

Figure C-1: The Q-matching circuit. L1 is in series with C1 which is in series with the parallel combination of C2 and the transducer array. The path of the generated noise in the Tonpilz array is also shown

The addition of the transformer to the system is mainly for isolation, but can also be used as a step-up device. When the transducers are driven, an RMS voltage in the 1KV region is required across their terminals.

The following section discusses the calculations involved in the Q matching system:

The Q factor of a circuit is a value applicable to a system at its resonant point. If we assume to be working with a simple series circuit that has been made to resonate, the following explanation applies. The resonant frequency (Fr) of a series tuned inductor (L), capacitor (C) and resistor (R) circuit can be calculated as follows:

$$F_r = \frac{1}{2\pi\sqrt{LC}} \tag{C.1}$$

At the specific resonance frequency of the circuit the current and voltage are in phase and, therefore, the total impedance (Z) of the circuit is equal to the physical resistance (R).

The Q factor of a circuit can be calculated using the following formula:

$$Q = \frac{2\pi f L}{R} \tag{C.2}$$

In order to explain the Q-matching circuit, it has been simplified into a series resonant circuit (Figure C-2).

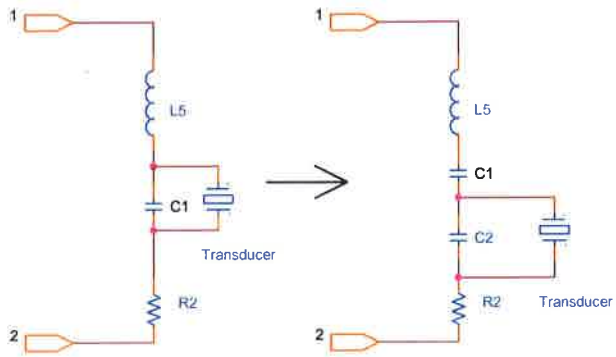

Figure C-2: The simplified series resonant circuit showing the transducer connected in parallel with the capacitor (left). The simple series circuit with split capacitor and the transducer across one of them (right)

If the quality factor of the circuit is altered, the voltage across the capacitor (C1 in fig C-2 left) can be adjusted to any value allowing the transducer to be driven at any specific voltage. However, in the Q-matching circuit the voltage can be further adjusted using a voltage dividing technique and the two capacitors (shown on the right hand side of Figure C-2). The transducer then placed in parallel with one of the resulting split capacitors (C2 right side), ensures a flexible system to design and, if required, to alter.

Appendix D

Phase locking circuit diagram

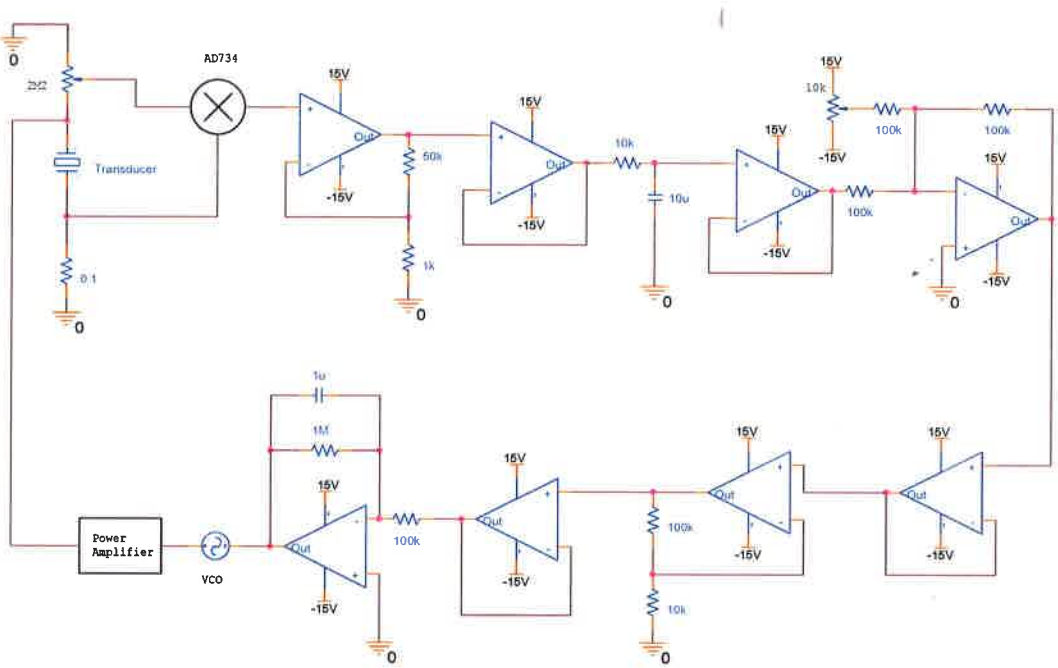

Figure D-1: The phase locking circuit used for the technique evaluations

Appendix E

Basic code for digital Admittance Locking

```
'*****************************************************************
   '* Name : Admittance locking.bas
   '* Author : T.M.J.Smith
   '* Notice : PIC 16F877 using boot loader
   '* Date : 6/10/03
   '* Version : 1.0
   '*****************************************************************
   DEFINE LOADER_USED 1
   DEFINE OSC 20
   DEFINE LCD_DREG PORTB
   DEFINE LCD_DBIT 0
   DEFINE LCD_RSREG PORTC
   DEFINE LCD_RSBIT 4
   DEFINE LCD_EREG PORTC
   DEFINE LCD_EBIT 5
   DEFINE LCD_LINES 2
   DEFINE LCD_BITS 4
   DEFINE ADC_BITS 10
```

```
'Variables
amplitude VAR word
prevamp VAR word
pwmv VAR byte
pwmmax VAR byte
ampmax VAR word
i VAR byte
pause 500
'Enable pull-up resistors
asm
    bsf 03,5
    bcf 01,7
endasm
pause 500
start:
lcdout $FE, 1, "Admittance locking"'
pause 500
'set up adc
adcon1 = adcon1 | %10000000
'clear variables
pwmv = 0
prevamp = 0
ampmax = 0
pwmmax = 0
amplitude = 0
'sweep bandwidth to find currrent peak
for pwmv = 0 to 255
    LCDOUT $FE,1,"PWM ",#pwmv," A2D ",#amplitude,$FE,$c0,"Amax ",#amp-
max,"Pmax",#pwmmax
    pause 70
```

```
        hpwm 1,pwmv,20000
        adcin porta.0, amplitude          'Read current
        if amplitude > ampmax then        'find highest current, save frequency
            pwmmax = pwmv
            ampmax = amplitude
        endif
        next pwmv
    eloop:
    LCDOUT $FE,1,"Finished ",#pwmmax," ",#ampmax, $FE,$c0,"Going... ",#am-
plitude
    hpwm 1,pwmmax,20000
    adcin porta.0, amplitude
    pause 2000
    prevamp = amplitude
    pwmmax = pwmmax + 50
    follow:
    'track current peak
    for i = 0 to 250
        hpwm 1,pwmmax,20000
        prevamp = amplitude
        adcin porta.0, amplitude
        if amplitude < prevamp then
            pwmmax = pwmmax - 1
        endif
        if amplitude > prevamp then
            pwmmax = pwmmax + 1
        endif
    next i
    lcdout $FE,1,"Tracking ",#pwmmax," ",#ampmax, $FE,$c0,#amplitude
    goto follow
```

Appendix F

Calculating transducer models

```
% Programme: Asks the user for the series and parallel resonant frequencies
    % of a PZT transducer as well as the admittance (Y) at
    % those points and calculates the R,L,C and Co of the BVD equiv.
    % Plots simulation as well as a measured transducer in the same graphs.
    % ENTER INFO FOR PZT (read off Y measurement graph)
    %=========================================
    Fm=input('Enter Fm: ');
    if isempty(Fm)
    Fm=40090
    end
    Fn=input('Enter Fn: ');
    if isempty(Fn)
    Fn=42000
    end
    YFm=input('Enter YFm: ');
    if isempty(YFm)
    YFm=0.066
    end
    YFn=input('Enter YFn: ');
    if isempty(YFn)
```

```
YFn=0.0005
end
CoMultfactor=2.05;
Ro=460;
%==========================================
%CALCULATIONS
%==========================================
w=2*pi;
Qm=((w*Fm)/(2*(w*Fn-w*Fm)))*(YFm/YFn);
Keff=(1-(Fm^2/Fn^2))^0.5;
R=1/(abs(YFm)-abs(YFn));
L=(Qm*R)/(w*Fm);
C=1/(w*Fm*Qm*R);
Co=C*((1/Keff^2)-1);
Co=Co*CoMultfactor
%==========================================
%DISPLAYVALUES
%==========================================
disp(['R=',num2str(R)])
disp(['L=',num2str(L)])
disp(['C=',num2str(C)])
disp(['Co=',num2str(Co)])
disp(['Ro=',num2str(Ro)])
%==========================================
%INPUT MEASURED TRANSDUCER
%==========================================
TXdata=input('Enter file name of measured TX data .txt : ');
if isempty(TXdata)
TXdata='TR.txt';
end
```

```
load(TXdata);
Ymeas=TR(:,1);
PH_DMeas=TR(:,2);
FRmeas=TR(:,3);
%=================================================
%CALCULATING MEASURED TX PARAMETERS
%=================================================
frequency_range = FRmeas(1):(FRmeas(2)-FRmeas(1)):max(FRmeas);
frequency_range_sim = FRmeas(1):0.05:max(FRmeas);
PH_RMeas=PH_DMeas.*(pi/180);
Gmeas=Ymeas.*cos(PH_RMeas);
Bmeas=Ymeas.*sin(PH_RMeas);
%=================================================
%PLOTTING ALL
%=================================================
W = 2*pi.*frequency_range_sim;
f=1/(2*pi*sqrt(L*C))
Zs = R + (j.*W.*L) - (j./(C.*W));
Zp = -j./(Co.*W);
Ztot = (Zs.*Zp)./(Zs+Zp);
Ztotp = (1./Ro)+(1./Ztot); %static resistance
Ztotpar = (1./Ztotp);
Ytot = 1./Ztotpar;
%plot(frequency_range, abs(Ytot));
G=real(Ytot);
B=imag(Ytot);
%plot(G,B);
figure(1);
subplot(2,1,1);
plot(frequency_range_sim, abs(Ytot));
```

```
title('Admittance of measured PZT and simulated BDV')
xlabel('Frequency Hz')
ylabel('Admittance Y')
hold on
figure(2)
subplot(2,1,2);
plot(G,B);
title('Transadmittance circles of measured PZT and simulated BDV')
xlabel('Conductance G')
ylabel('Susceptance B')
hold on
figure(1)
subplot(2,1,1);
plot(FRmeas,Ymeas,'r');
figure(1)
subplot(2,1,2);
plot(Gmeas,Bmeas,'r');
figure(2);
plot(G,B);
title('Transadmittance circle comparison between measured and simulated transducer')
xlabel('Conductance G')
ylabel('Susceptance B')
hold on
plot(Gmeas,Bmeas,'r');
```

Appendix G

Transadmittance circles of the transducers and the test bath

G.1 The parallel transducer array

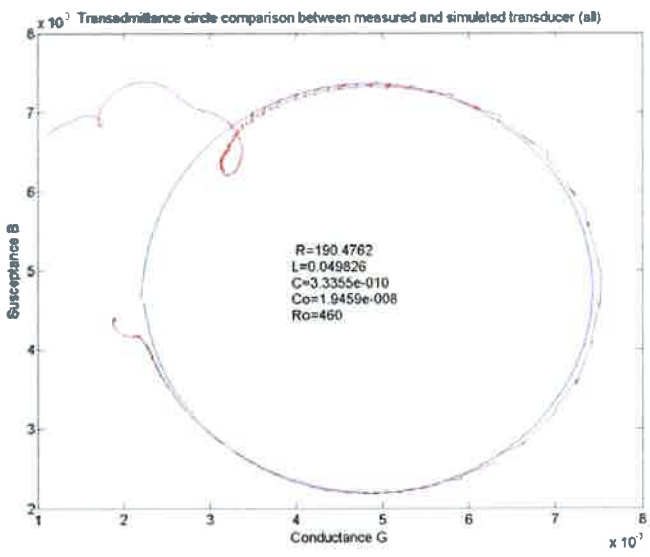

Figure G-1: The transadmittance circle of both the measured bath and the simulation of the measured bath. Note the close match confirming a realistic model

G.2 Transducer number 1

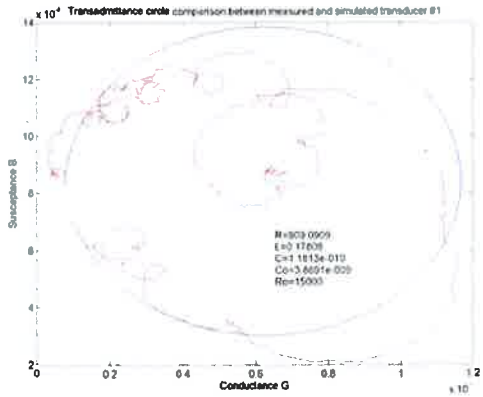

Figure G-2: Measured transadmittance circle of transducer number 1 and its BVD equivalent circuit model

G.3 Transducer number 2

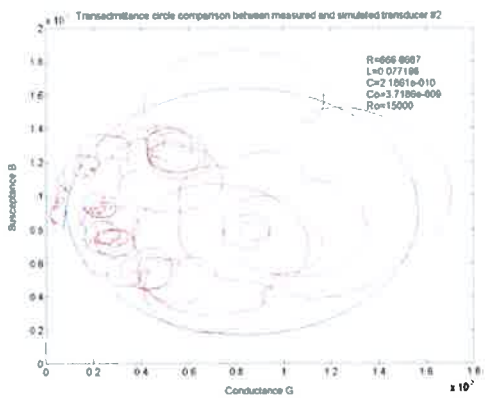

Figure G-3: Measured transadmittance circle of transducer number 2 and its model

G.4 Transducer number 3

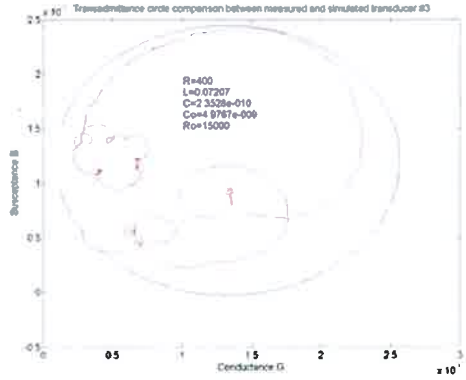

Figure G-4: Measured transadmittance circle of transducer number 3 and its model

G.5 Transducer number 4

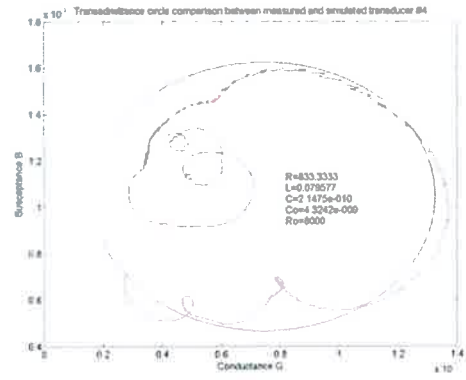

Figure G-5: Measured transadmittance circle of transducer number 4 and its model

G.6 Transducer number 5

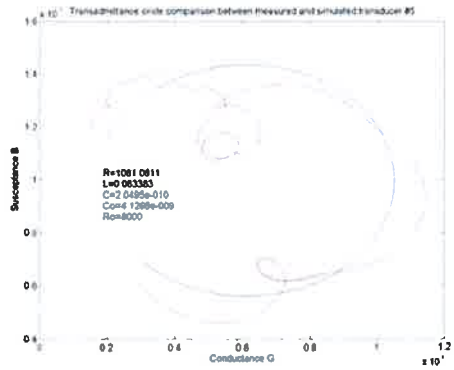

Figure G-6: Measured transadmittance circle of transducer number 5 and its model

G.7 Transducer number 6

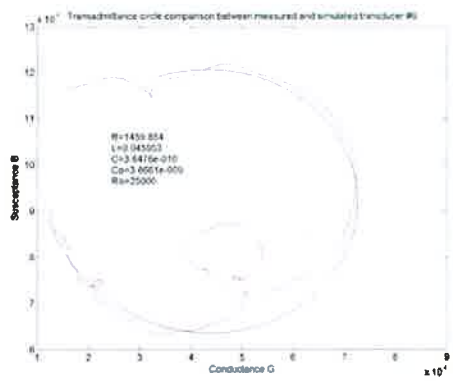

Figure G-7: Measured transadmittance circle of transducer number 6 and its model

Appendix H

Calculating static current through transducers

```
%Programme: To calculate static point-by-point current
    %through series LCR circuit==========================
    %Calulating v========================================
    A=10;            % Peak value of carrier wave
    fc=40000;            % carrier frequency
    fm=1;            % fm signal frequency
    fs=5000;       % max frequency shift of carrier one side of center eg fc=40k to
    % 50k=10k
    L=0.083963       % Physical RLC series branch values
    C=1.8771e-10
    R=15.2672
    t=[(0):0.000001:(1)];      %Time step array
    t_static=t;
    mf=(fs/fm);            % Modulation index
    %==================Make v array ======================
    vcarrier=A.*sin((2*pi*fc.*t));
    vmod=(mf.*cos(2*pi*fm.*t));
    vfm=A.*sin((2*pi*fc.*t)+(mf.*cos(2*pi*fm.*t)));
```

Appendix H

Calculating static current through transducers

```
%Programme: To calculate static point-by-point current
    %through series LCR circuit==========================
    %Calulating v=======================================
    A=10;            % Peak value of carrier wave
    fc=40000;            % carrier frequency
    fm=1;            % fm signal frequency
    fs=5000;       % max frequency shift of carrier one side of center eg fc=40k to
    % 50k=10k
    L=0.083963       % Physical RLC series branch values
    C=1.8771e-10
    R=15.2672
    t=[(0):0.000001:(1)];      %Time step array
    t_static=t;
    mf=(fs/fm);              % Modulation index
    %================Make v array ========================
    vcarrier=A.*sin((2*pi*fc.*t));
    vmod=(mf.*cos(2*pi*fm.*t));
    vfm=A.*sin((2*pi*fc.*t)+(mf.*cos(2*pi*fm.*t)));
```

```
Modsin=(vmod.*fm)+fc;
%================Plot the frequency at each time step point========
figure(1)
plot(t,vmod)
title('Frequency at points t driving the system')
xlabel('Time (s)')
ylabel('Amplitude')
%================Plot the carrier wave and modulation signal======
figure(2)
plot(t,vfm)
hold on
plot(t,vmod,'r')
hold on
title('Carrier wave and modulation wave')
xlabel('Time (s)')
ylabel('Amplitude')
%================Plot modulation voltage==================
figure(3)
plot(t,vfm)
title('Frequency modulated voltage signal')
xlabel('Time (s)')
ylabel('Amplitude')
frequency_range_sim = (fc-fs):0.1:(fc+fs); %select frequency bandwidth and step
size
period=1./frequency_range_sim;
plot(period)
%=================================================
%================Calulating I=====================
W = 2*pi.*Modsin;
f=1/(2*pi*sqrt(L*C));
```

```
Zs = R + (j.*W.*L) - (j./(C.*W));
i=(vfm./Zs);
figure(4);
hold on
plot(t,i,'r');
title('Current response')
ylabel('Amplitude')
xlabel('Time (s)')
```

Appendix I

RLC sinusoidal transient

I.1 Solving for i to get current envelope

The equation for a series resistor, inductor and capacitor circuit is as follows.

$$Ri + L\frac{di}{dt} + \frac{1}{C}\int i dt = V_{\max}\sin(\omega t + \phi) \tag{I.1}$$

where

R=Resistor

C=Capacitor

L=Inductor

V=Applied sinusoid

Differentiate (1) with respect to t :

$$L\frac{d^2i}{dt^2} + R\frac{di}{dt} + \frac{i}{C} = \omega.V_{\max}\cos(\omega t + \phi)$$

Using the method of undetermined coefficients:

let

$$i = A\cos(\omega t + \phi) + B\sin(\omega t + \phi) \tag{I.2}$$

$$\therefore \frac{di}{dt} = i' = -A\omega \sin(\omega t + \phi) + B\omega \cos(\omega t + \phi) \tag{I.3}$$

and

$$\int i dt = \frac{A}{\omega} \sin(\omega t + \phi) - \frac{B}{\omega} \cos(\omega t + \phi) \tag{I.4}$$

Substituting I.2, I.3, I.4 into I.1:

$$RA\cos(\omega t + \phi) + RB\sin(\omega t + \phi) - LA\omega \sin(\omega t + \phi) + LB\omega \cos(\omega t + \phi)$$

$$-\frac{A}{C\omega} \sin(\omega t + \phi) - \frac{B}{C\omega} \cos(\omega t + \phi) = V \max \sin(\omega t + \phi)$$

Equating coefficients of like terms:

$$RA - B[\frac{1}{C\omega} - L\omega] = 0 \tag{I.5}$$

and

$$RA - LA\omega - \frac{\beta}{C\omega} = V_{\max}$$

$$RB + A[\frac{1}{C\omega} - L\omega] = V_{\max} \tag{I.6}$$

From I.5:

$$B = \frac{RA}{\frac{1}{C\omega} - L\omega} \tag{I.7}$$

Substituting I.7 into I.6:

$$R[\frac{RA}{\frac{1}{C\omega} - L\omega}] + A[\frac{1}{C\omega} - L\omega] = V_{\max}$$

$$\therefore A = \frac{V_{\max}[\frac{1}{C\omega} - L\omega]}{R^2 + [\frac{1}{C\omega} - L\omega]^2}$$

and

$$B = \frac{R\frac{V_{\max}[\frac{1}{C\omega} - L\omega]}{R^2 + [\frac{1}{C\omega} - L\omega]^2}}{\frac{1}{C\omega} - L\omega}$$

$$B = \frac{RV_{\max}}{R^2 + [\frac{1}{C\omega} - L\omega]^2}$$

but

$$i = A\cos(\omega t + \phi) + B\sin(\omega t + \phi)$$

represented as a single sinusoid:

$$i = H\sin\{(\omega t + \phi) + \beta\} \tag{I.8}$$

$$= H\sin(\omega t + \phi)\cos\beta + H\cos(\omega t + \phi)\sin\beta$$

where

$$H = \sqrt{A^2 + B^2}$$

and

$$\beta = \tan^{-1}[\frac{\sin\beta}{\cos\beta}]$$

so

$$\beta = \tan^{-1}[\frac{A}{B}]$$

but

$$\phi = \tan^{-1}[\frac{A}{B}]$$

so

$$\phi = \tan^{-1}[\frac{\frac{1}{C\omega} - L\omega}{R}]$$

and

$$H = \sqrt{\frac{V_{\max}^2}{R^2 + [\frac{1}{C\omega} + L\omega]^2}[R^2 + [\frac{1}{C\omega} - L\omega]^2]}$$

$$= \frac{V_{\max}}{\sqrt{R^2 + [\frac{1}{C\omega} - L\omega]^2}}$$

Substituting H and β into I.8:

$$i = \frac{V_{\max}}{\sqrt{R^2 + [\frac{1}{C\omega} - L\omega]^2}} \times \sin(\omega t + \phi) + \tan^{-1}(\frac{\frac{1}{C\omega} - L\omega}{R})) \tag{I.9}$$

Appendix J

Calculating transient current through transducers

```
%----------Programme: Calculate the current through a ----------
    %----------series LCR circuit (BVD equiv of transducer)----------
    %----------Initiation: - clear screen, workspace----------
    clear all
    clc
    %----------Calculations----------
    fm=1;
    tf=1/fm                    % Input('Final time=');
    x0=[0; 0];
    [t,x]=ode45('LRC',[0 tf], x0);        % Do differentiation using function ODE45
    t=[0:(tf/(length(t)-1)):tf];
    x=x(:,2);
    xab=abs(x);
    mean(xab)
    %----------Plot Graph----------
    plot(t,x)
    title('Transducer array model, sweep freq = ')
    ylabel('Current amplitude (A)')
```

```
xlabel('Time (s)')
%----------Function: Used in above programme defining LCR system----------
function f=LRC(t,x)
%----------LCR constants----------
A=10;                    % Peak value of carrier wave
fc=40000;                % carrier frequency
fm=1;                    % fm signal frequency
fs=5000;      % max frequency shift of carrier one side of center
% eg fc=40k to 50k=10k
mf=(fs/fm);              % modulation index
L=0.083963;              % physical RLC series branch values
C=1.8771e-10;
R=15.2672;
%----------Defining equation----------
f=[x(2); -(R/L)*x(2)-(1/(L*C))*x(1)+A.*(sin(2*pi*fc.*t+(fs/fm).*sin(2*pi*fm*t)))];
```